

Design of walls with linear elastic finite element methods

Master Thesis Report

By Marc Romans

A thesis submitted in partial fulfillment for the degree of Master of Science
Faculty of Civil Engineering and Geosciences, Delft University of Technology

By Marc Romans

April 2010

Members of the thesis committee:

Prof. dr. ir. J.C. Walraven

Delft University of Technology, Faculty of Civil Engineering and Geosciences
Section Concrete Structures

Dr. ir. P.C.J. Hoogenboom

Delft University of Technology, Faculty of Civil Engineering and Geosciences
Section Structural Mechanics

Ir. J. A. den Uijl

Delft University of Technology, Faculty of Civil Engineering and Geosciences
Section Concrete Structures

Ir. F. H. Middelkoop

Corsmit Raadgevend Ingenieurs, a company of Royal Haskoning

Ir. L.J.M. Houben

Delft University of Technology, Faculty of Civil Engineering and Geosciences
Section Road and Railway Engineering

Preface

This thesis contains the results of a study into the design of reinforced concrete walls with linear elastic finite element methods. This study is part of obtaining the degree of Master of Science at the faculty of Civil Engineering of Delft University of Technology and was carried out in cooperation with Corsmit Raadgevend Ingenieurs, a company of Royal Haskoning. I would like to express my gratitude towards my supervisors, in particular mr. Middelkoop, for sharing their knowledge and their support during this study.

Finally I would like to thank my family and friends for their support.

Marc Romans
May 19th, 2010
Zoetermeer, The Netherlands

Abstract

This thesis focuses on the design of reinforced concrete walls with the use of linear elastic finite element methods. Since the introduction of Eurocode EN1992, the set of design standards in which design requirements related to concrete structures are committed to paper, it is allowed to derive the required amount of reinforcement directly from the membrane forces which follow from a linear elastic finite element analysis. This method deviates however at some points considerably from common design methods. Compared to the common design methods the moment diagram is for example no longer shifted over a specific distance during the design of beams to prevent failure due to the development of inclined bending cracks. In addition, the assumed linear elastic isotropic material behavior in the finite element analyses results in the computation of load transfer mechanisms which deviate considerably from mechanisms which are expected to develop in practice. These deviations gave rise to analyze this recently approved design method in further detail, indicated by the term linear elastic finite element method (LE-FEM) henceforth.

The linear elastic finite element method is verified by considering a large number of single- and several two-span beams. The required reinforcement of these beams is determined with LE-FEM by taking all relevant provisions of the Eurocodes into account. In a subsequent step the structural behavior of the considered beams was analyzed by means of a non-linear finite element analysis, in which a similar level of reliability was taken into account as during the design process. These non-linear analyses, which are performed in ATENA, are capable to predict the actual behavior of concrete.

Structural analyses of the considered specimen led to the following main conclusions:

- Assuming linear elastic material behavior of concrete for reinforcement design with LE-FEM of structures does not approximate concrete behavior in an accurate way.
- No direct relation is found between the limited amount of longitudinal reinforcement which reaches the supports and the observed failure mode. Concrete crushing in the compressive zone, caused by flexural deformations, turned out to be the normative failure mode.
- Reinforcement designs according to LE-FEM of the considered beams do not meet requirement related to crack control in the serviceability limit state. It is not possible to determine the stresses in the required distributed reinforcement without the application of advanced (non-linear) methods, since there is no direct relation between the applied load and stress development in individual reinforcement bars.
- Design of structures with LE-FEM which are loaded by a compressive force and contain symmetrical reinforcement, such as columns, results in an overestimation of the concrete compressive strength since eccentricities and second order effects are left out of consideration.
- Redistribution of considered two-span beams in case differential support settlements appear is insufficient to withstand settlements which are allowed by the codes.

Contents

1 Introduction	13
1.1 Background.....	13
1.2 Problem definition.....	13
1.3 Aim of this study.....	15
1.4 Thesis outline.....	15
2 Linear elastic finite element method - design process	17
2.1 Introduction.....	17
2.2 Design procedure.....	17
2.3 Tension reinforcement expressions.....	17
2.3 Eccentricities.....	20
3 Linear elastic finite element method – specifications	21
3.1 Introduction.....	21
3.2 Geometry of considered specimen.....	21
3.3 Material strength parameters.....	22
3.4 Loads and load combinations.....	23
3.4.1 Load combinations.....	23
3.4.2 Loads.....	24
3.5 Environmental conditions.....	25
3.6 Anchorage of reinforcement.....	25
4 Linear elastic finite element method – designs	27
4.1 Introduction.....	27
4.2 Numerical models.....	27
4.2.1 Mesh size.....	27
4.2.2 Supports and loads.....	28
4.3 Reinforcement configurations.....	29
4.3.1 Design of reinforcement.....	29
4.3.2 Reinforcement configuration of specimen S-2-1.....	30
4.3.3 Reinforcement configuration of specimen S-2-3.....	31
4.3.4 Reinforcement configuration of specimen S-2-5.....	32
4.4 Verification of reinforcement configurations.....	33
4.4.1 Considered specimen.....	33
4.4.2 Verification of moment capacity.....	34
4.4.3 Verification of crack width requirements.....	36
5 Non-linear finite element analyses - principles	43
5.1 Introduction.....	43
5.2 Material models.....	43
5.2.1 Concrete.....	43
5.2.2 Reinforcement Steel.....	44
5.3 Geometry and model properties.....	45
5.3.1 Overall geometry.....	45
5.3.2 Supports and loading point.....	45
5.3.3 Reinforcement bond slip.....	46
5.3.4 Anchorage of reinforcement mesh.....	47
5.4 Load path.....	47
5.5 Solver properties.....	48
5.5.1 Mesh size.....	48
5.5.2 Solver.....	49
6 Non-linear finite element analyses – safety formats	51

6.1 Introduction	51
6.2 Safety format according to Eurocode EN1992-1-1	52
6.3 Safety format according to Eurocode EN1992-2	54
6.4 Probabilistic analysis.....	55
6.4.1 Introduction.....	55
6.4.2 Resistance to failure R.....	57
6.4.3 Load S	62
6.4.4 Design resistance.....	62
6.5 Comparison safety formats.....	63
6.6 Conclusion	65
7 Non-linear finite element analyses – results	67
7.1 Introduction	67
7.2 Analysis results	67
7.2 Overall behavior.....	68
7.3 Failure mode	70
7.3.1 Normative failure mode.....	70
7.3.2 Concrete compressive zone.....	71
7.3.3 Influence of the stress-strain relation on the failure mode	73
7.4 Redistribution of internal forces	80
8 Shrinkage and support settlements	83
8.1 Introduction	83
8.2 Shrinkage.....	83
8.3 Differential support settlements	85
8.3.1 Considered specimens.....	85
8.3.3 Reinforcement design with LE-FEM.....	87
8.3.4 Reinforcement designs	87
8.3.5 Non-linear analyses.....	90
9 Conclusions and recommendations	99
9.1 Introduction	99
9.2 Conclusions	99
9.3 Recommendations	101
Appendix A – Results survey	103
A.1 Introduction.....	103
A.2 Results of the survey	103
Appendix B - Reinforcement drawings	107
B.1 Introduction.....	107
B.2 Specimen S-1-1	107
B.3 Specimen S-1-2.....	107
B.4 Specimen S-1-3.....	108
B.5 Specimen S-1-4	109
B.6 Specimen S-1-5.....	109
B.7 Specimen S-2-2.....	110
B.8 Specimen S-2-4.....	110
B.9 Specimen S-3-1	111
B.10 Specimen S-3-2.....	112
B.11 Specimen S-3-3.....	112
B.12 Specimen S-3-4	113
B.13 Specimen S-3-5.....	113
B.14 Specimen S-4-1	114
B.15 Specimen S-4-2.....	115
B.16 Specimen S-4-3.....	115
B.17 Specimen S-4-4	116
B.18 Specimen S-4-5.....	117

B.19 Specimen S-5-1	117
B.20 Specimen S-5-2	118
B.21 Specimen S-5-3	119
B.22 Specimen S-5-4	119
B.23 Specimen S-5-5	120
Appendix C - Maple code	123

1 Introduction

1.1 Background

The use of linear elastic finite element methods as a tool for the design of reinforced concrete structures has shown a tremendous growth in the past years and is still under development. Increasing calculation capacity of personal computers provides current engineers the possibility to analyze simple, as well as more complex concrete structures with these methods within a limited amount of time. A small survey showed that the use of finite element analyses is nowadays a frequently used tool in the design of concrete structures. Appendix A discusses this survey in more detail.

The introduction of Eurocode EN1992, the set of design standards in which design requirements related to concrete structures are committed to paper, responds to the increasing use of linear elastic finite element analyses during the design process of reinforced concrete structures. Eurocode EN1992-1-1, which provides general rules and rules for buildings, gives in §5.1.1 (3) its explicit approval to the use of “simplified” design methods to determine the reinforcement for in plane stress fields. This implies that it is allowed to derive the required amount reinforcement for in plane stress fields directly from membrane forces which follow from a linear elastic finite element analysis. This can be done manually, but the great advantage is that some in engineering practice frequently used computer programs are capable to perform these calculations within a couple of seconds. Henceforth this method to determine reinforcement will in this thesis be indicated by the term “linear elastic finite element method” (LE-FEM).

One of the major advantages of this recently approved method is, as already stated above, its economical attractiveness. Computer programs are capable to analyze simple as well as more complicated structural elements within a very short timeframe compared to manual calculations. Besides, the required amount of reinforcement which follows from the linear elastic finite element method is more economical compared to the regular design methods. An earlier performed master thesis [1] which focused on the reinforcement of deep beams, showed a significant reduction in the amount of required reinforcement compared to the regular beam theory or strut-and-tie method.

Although at first glance the linear elastic finite element method seems to be very attractive, its reinforcement design process and underlying principles deviate at some essential points from common design methods. These deviations lead to questions about the overall applicability and correctness of this recently approved method, which gives reason for a further analysis.

1.2 Problem definition

Where common design methods are based on the assumption that concrete is only capable to transfer compressive forces in assumed load transfer mechanisms, reinforcement design with the linear elastic finite element method is initially based on isotropic, uncracked linear elastic material behavior. Not until the reinforcement is derived from the determined membrane forces, the assumption is made that concrete is not capable to transfer tensile stresses. This approach results in applied load transfer mechanisms which can be considered questionable. It can be elucidated by considering an elementary single-span wall element, loaded by a concentrated top load at midspan.

Common design methods show general agreement on the way loads are transferred in single-span walls. Figure 1.1 gives an example of two possible load transfer mechanisms in a single-span deep

beam in case the strut-and-tie method is applied to determine the required reinforcement. The left figure shows a tied-arch model, the right figure a truss mechanism. Which mechanism is applied in practice depends on the shear span-depth ratio (a/d). A tied arch model is predominantly used in design of short beams, which have a a/d equal to 1,0 or less, and is based on the assumption that load is transferred directly from the loading point into the support through the formation of concrete compressive struts. The horizontal component of each strut is set in equilibrium at the support by a horizontal tie which extends the full length of the beam. For longer beams, which have a a/d of 4,0 or above, load transfer occurs indirectly from the loading point into the supports through struts that form between diagonal cracks within the shear span of the beam. The vertical component of struts that reach the bottom longitudinal reinforcement is set in equilibrium by vertical tie forces generated in stirrups that enclose the longitudinal reinforcement. The bottom longitudinal reinforcement provides equilibrium between the horizontal components of strut forces at the bottom nodes. In beams of intermediate length a combination of both load transfer mechanisms can be assumed [2].

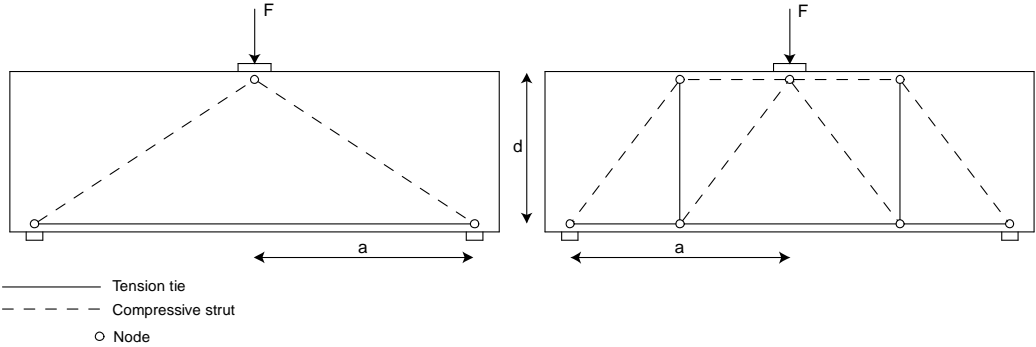


Figure 1.1: Load transfer mechanisms according to the strut-and-tie method: tied-arch (left) and truss mechanism (right).

Although the strut-and-tie method only gives a possible approach of the actual behavior, from the beginning of the design process load transfer mechanisms are taken into account which correspond to the typical strength properties of applied materials. Contrary, the linear elastic finite element method assumes during the derivation of the membrane forces that concrete behaves as a linear elastic isotropic material. As a consequence load transfer mechanism develop that deviate from the common design methods. This can be illustrated with the trajectory plot of a structure which is loaded in a similar way as the structures in figure 1.1.

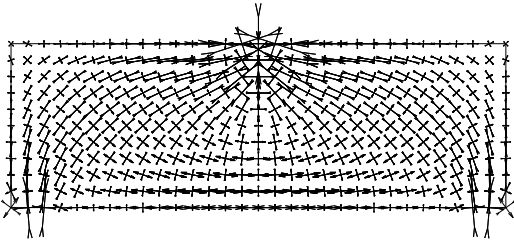


Figure 1.2: Stress trajectories which follow from a linear elastic finite element analysis.

Due to the top load the stress trajectories show the development of a compression arch, which shows similarities to the tied-arch mechanism of figure 1.1. However, besides the development of a compression arch, also the development of a tension arch can be observed. It is questionable if the applied orthogonal reinforcement, which is derived directly from the membrane forces in an in-plane stress field, in practice will transfer loads in a similar way as is assumed in the linear elastic analyses. Due to the anisotropic behavior of concrete it can be expected that in practice the tied-arch mechanism finally becomes the normative load transfer mechanism. However, the amount of reinforcement in the bottom tensile tie might be too limited to transfer the full load by tied-arch action, since the amount of applied reinforcement is during the design process based on the development of multiple load transfer mechanisms.

A second point at which the linear elastic finite element method deviates considerably from common design methods is that during the design process the moment diagram is no longer shifted over a specific distance d , equal to the effective height of a cross-section. The former Dutch Code NEN 6720 explicitly prescribed shifting of the moment line to prevent failure as a result of possible occurrence of diagonal cracks in the ultimate limit state. A similar approach is embedded in the strut-and-tie method.

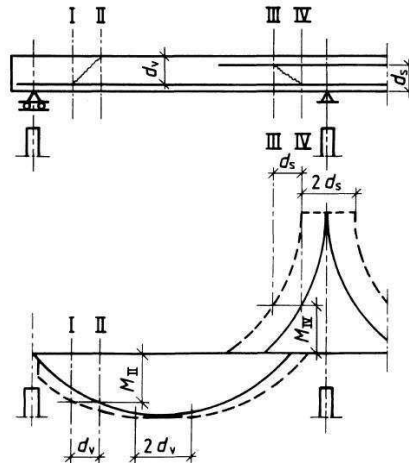


Figure 1.3: Shifting of the moment line for a continuous beam, as shown in NEN 6720 [3].

In combination with the relative limited amount of longitudinal reinforcement which according to the linear elastic finite element method is required to reach the supports, anchorage problems can be expected in the vicinity of the supports.

1.3 Aim of this study

As stated in the previous section, a short analysis of the reinforcement design process of a relative basic single-span deep beam with the linear elastic finite element method shows already some considerable deviations compared to common design methods. These deviations, in combination with the increasing use of the linear elastic finite element method in engineering practice, gave reason to examine this design method in further detail. The aim of this master thesis is to examine to what extent the discussed deviations have an influence on the structural behavior or resistance to failure of reinforced concrete deep beams.

Reinforcement of the considered beams is determined according to the linear elastic finite element method, taking all relevant provisions of the Eurocodes into account. For the design of reinforcement Scia Engineer 2009 is used, although every other finite element program can be applied which is capable to apply the in Eurocode EN1992-1-1 mentioned “simplified” design method. Subsequently their structural behavior is analyzed in the non-linear finite element program ATENA, which is capable to simulate the actual structural behavior of the considered beams numerically. On the basis of the non-linear analysis results conclusions can be drawn about the use of the linear elastic finite element method for reinforcement design of concrete structures.

1.4 Thesis outline

This thesis continues in chapter 2 with a more detailed introduction of the linear elastic finite element method. The backgrounds of this method, which are closely linked to continuum mechanics, will be

discussed in further detail. Chapter 3 will subsequently discuss the considered beams of which the reinforcement will be designed according to the linear elastic finite element method. Besides all relevant basic principles which are related to the reinforcement design process are discussed in this chapter, such as for example material properties, the design loads and the geometry of considered beams. The reinforcement configurations of the considered beams will be presented in chapter 4. In this chapter also code checks are discussed which are related to crack control in the serviceability limit state.

Chapter 5 continues with an overview of the assumed principles in non-linear analyses. Material models and model properties will be discussed in detail. Compared to the reinforcement design process a same level of reliability will be taken into account in these non-linear analyses. In chapter 6 the options are considered which are available to obtain a same level of reliability in the non-linear analyses. Based on this comparison analysis an optimal safety format is chosen which is applied in the non-linear analyses of the considered specimens. The results of the non-linear analyses will be discussed in chapter 7, which focuses on the structural behavior and the observed failure modes. In chapter 8 subsequently the unfavorable effect of shrinkage and unequal support settlements is discussed shortly. This thesis finishes in chapter 9 with an overview of the conclusions and recommendations.

References

- [1] Mahmoud, M.N., Design of deep beams, Nieuwegein, The Netherlands, October 2007
- [2] Breña, S.F., Roy, N.C., Evaluation of Load Transfer and Strut Strength of Deep Beams with Short Longitudinal Bar Anchorages, Massachusetts, United States, September 2008
- [3] NEN 6720, Voorschriften Beton – Constructieve eisen en rekenmethoden, Delft, The Netherlands, September 1995

2 Linear elastic finite element method - design process

2.1 Introduction

Finite element methods are a well known method in engineering practice to analyze the behavior and load transfer mechanisms of in-plane stress fields. The introduction of Eurocode EN1992-1-1, which gives its approval to the use of simplified design methods for determining of reinforcement in in-plane stress fields, provides the possibility to derive the required reinforcement directly from the membrane forces which are determined with finite element analyses. The amount of reinforcement is roughly determined by dividing appearing tensile stresses by the design strength of reinforcement. This chapter gives a global overview of the design procedure with this relatively new method.

2.2 Design procedure

The design procedure with the linear elastic finite element method can be subdivided into some general, chronological design steps. A step by step overview of the design procedure is given below.

- Definition of material strength parameters and normative load combinations. Similar to other common reinforcement design methods, material strength parameters and normative load combinations have to be specified according to relevant provisions, stated in the Eurocodes.
- Creation of an adequate finite element model of the considered structure, which is capable to take the assumed material parameters and load combinations into account.
- Calculation of the membrane forces in the in-plane stress field by means of a linear elastic finite element analyses. In each node of the finite element mesh the membrane forces σ_x , σ_y and τ_{xy} will be determined, which in a subsequent step will be used to derive the required amount of reinforcement.
- Derivation of the required reinforcement from the determined membrane forces σ_x , σ_y and τ_{xy} . This design step forms the basis of the linear elastic finite element method. Required reinforcement is given in an amount per element of the finite element mesh. Transformation to a reinforcement configuration which consists of discrete bars has to be done manually in a subsequent step.
- Transformation of the required amount of reinforcement into a reinforcement configuration consisting of discrete bars, taking all relevant code requirements with respect to proper anchoring and bar spacing into account

The theoretical background of the linear elastic finite element method will be discussed in further detail in the next section. Remaining design steps will be specified in more detail in chapter 3 and 4, where the principles and reinforcement designs of the considered specimen will be discussed.

2.3 Tension reinforcement expressions

The expressions given in this section to derive required reinforcement directly from known membrane forces are taken from Eurocode EN1992-1-1. They only take effect for in-plane stress fields and can be derived from elementary continuum mechanics. They are based on the assumptions that the tensile strength of concrete is ignored and that strain in bonded reinforcement is the same as that in the surrounding concrete.

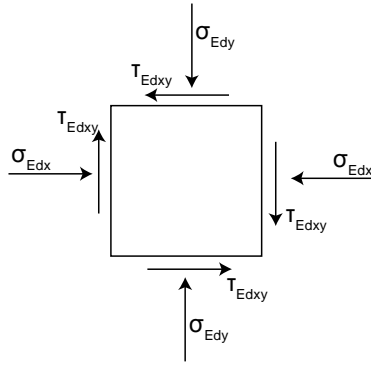


Figure 2.1: Forces in a membrane element and definition of the axes.

Required tension reinforcement in elements which are subjected to in-plane forces depends on the sign and size of the normal stresses σ_{Edx} , σ_{Edy} and shear stress T_{Edxy} , shown in figure 2.1. When compressive stresses are taken as positive, with $\sigma_{Edx} > \sigma_{Edy}$, and the direction of reinforcement coincides with the x and y axes, the tensile strength provided by reinforcement can be determined from:

$$f_{tdx} = \rho_x f_{yd} \quad \text{and} \quad f_{tdy} = \rho_y f_{yd} \quad (2.1)$$

In equation 2.1 f_{tdx} and f_{tdy} are the resolved stresses in an element along the x and y axes respectively, ρ_x and ρ_y are the corresponding geometric reinforcement ratios for each direction. The design yield strength f_{yd} of the reinforcement has to be determined according to:

$$f_{yd} = \frac{f_{yk}}{\gamma_s} \quad (2.2)$$

Where:

f_{yk} is the characteristic yield strength of reinforcement.
 γ_s is the partial safety factor for reinforcement.

In locations where σ_{Edx} and σ_{Edy} are both compressive and $\sigma_{Edx} \cdot \sigma_{Edy} > T_{Edxy}^2$, design reinforcement is not required. The maximum compressive stress should however not exceed the design compressive strength of concrete f_{cd} , which is prescribed by equation 2.3. The provisions in Eurocode EN1992-1-1 related to reinforcement design with simplified design methods do not include specific expressions for compression reinforcement.

$$f_{cd} = \frac{f_{ck}}{\gamma_c} \quad (2.3)$$

Where:

f_{ck} is the characteristic cylindrical compressive strength of concrete
 γ_c is the partial safety factor for concrete.

In locations where σ_{Edy} is in tension or $\sigma_{Edx} \cdot \sigma_{Edy} < T_{Edxy}^2$, reinforcement is required. Eurocode EN1992-1-1 distinguishes two separate sets of expressions which give provisions to determine the required amount of reinforcement. One set is based on the optimum amount of reinforcement, in which the directions of reinforcement are identical to the direction of the principal stresses. The optimum reinforcement, which is indicated by a subscript 'o', is determined by equations 2.4 up to 2.9.

For $\sigma_{Edx} < |\tau_{Edxy}|$:

$$f'_{tdx} = |\tau_{Edxy}| - \sigma_{Edx} \quad (2.4)$$

$$f'_{tdy} = |\tau_{Edxy}| - \sigma_{Edy} \quad (2.5)$$

$$\sigma_{cd} = 2|\tau_{Edxy}| \quad (2.6)$$

For $\sigma_{Edx} > |\tau_{Edxy}|$:

$$f'_{tdx} = 0 \quad (2.7)$$

$$f'_{tdy} = \frac{\tau_{Edxy}^2}{\sigma_{Edx}} - \sigma_{Edy} \quad (2.8)$$

$$\sigma_{cd} = \sigma_{Edx} \left(1 + \left(\frac{\tau_{Edxy}}{\sigma_{Edx}} \right)^2 \right) \quad (2.9)$$

Alternatively, Eurocode EN1992-1-1 provides also a general set of expressions to determine the reinforced concrete stresses f_{tdx} , f_{tdy} and σ_{cd} , expressed by equation 2.10 up to 2.12. The angle θ is the angle between the principal concrete compressive stress and the x-axis.

$$f_{tdx} = |\tau_{Edxy}| \cot(\theta) - \sigma_{Edx} \quad (2.10)$$

$$f_{tdy} = \frac{|\tau_{Edxy}|}{\cot(\theta)} - \sigma_{Edy} \quad (2.11)$$

$$\sigma_{cd} = |\tau_{Edxy}| \left(\cot \theta + \frac{1}{\cot \theta} \right) \quad (2.12)$$

Eurocode EN1992-1-1 requires the verification of the concrete stress σ_{cd} , which is expressed in equation 2.9 and 2.12, with a realistic model that describes the compressive strength of cracked concrete. Eurocode EN1992-2 §6.109 gives detailed expressions for concrete strength of cracked sections. However, the concrete stress σ_{cd} should at least meet the requirement stated in equation 2.13.

$$\sigma_{cd} \leq v f_{cd} \quad (2.13)$$

In equation 2.13 v is a strength reduction factor for concrete cracked in shear, expressed in Eurocode EN1992-1-1 §6.2.2 (6). Its recommended value follows from equation 2.14.

$$v = 0,6 \left[1 - \frac{f_{ck}}{250} \right] \quad (2.14)$$

In order to avoid unacceptable cracks in the serviceability limit state, and to ensure the required deformation capacity in the ultimate limit state, EC2-1-1 requires that the amount of reinforcement derived from expressions 2.10 and 2.11 for each direction should not be more than twice and not less than half of the reinforcement determined by expressions 2.4 and 2.5 or 2.7 and 2.8. These limitations can be expressed by equation 2.15.

$$\frac{1}{2}f'_{tdx} \leq f_{tdx} \leq 2f'_{tdx} \quad \text{and} \quad \frac{1}{2}f'_{tdy} \leq f_{tdy} \leq 2f'_{tdy} \quad (2.15)$$

2.3 Eccentricities

The tension reinforcement expressions which are discussed in the previous section derive the required reinforcement directly from the membrane forces in an in-plane stress field. Since the calculation of membrane forces in an in-plane stress fields is based on two-dimensional elements, all loads act centrally on the modeled structure. Possible eccentricities of the load are not taken into account, although for specific types of structures this is required according to Eurocode EN1992-1-1. In §6.1 (4) it is required that in cross sections with symmetrical reinforcement which are loaded by a centric compression force it is necessary to assume a minimal eccentricity equal to $e_0 = h/30$, but not less than 20 mm, where h is the depth of the considered section. For centrally loaded structures which show a direct load transfer from the point of loading to the supports, such as for example columns or walls, use of the linear elastic finite element method results therefore in underserved optimal reinforcement designs and an overestimation of the allowable concrete compressive strength. This is illustrated in figure 2.2.

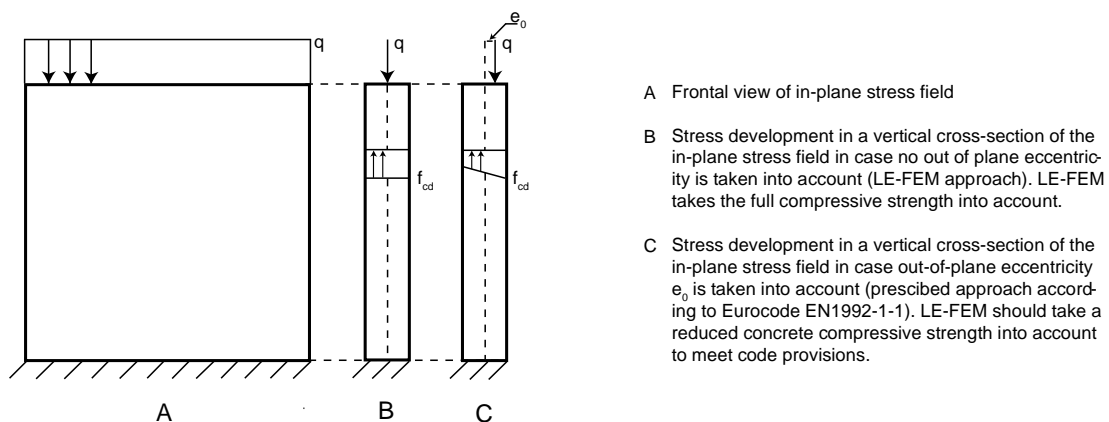


Figure 2.2: Stress development as assumed in a vertical cross-section of an in-plane stress field.

It must be emphasized that this inadequacy has no influence on the single-span specimens which are considered in this thesis, since for horizontal forces which develop in the compressive zone of a structure which is subjected to a flexural deformation eccentricities do not have to be taken into account.

References

- [1] NEN, NEN-EN 1992-1-1, Eurocode 2: Ontwerp en berekening van betonconstructies – Deel 1- 1: Algemene regels en regels voor gebouwen, Delft, The Netherlands, December 2007
- [2] NEN, NEN-EN 1992-2, Eurocode 2: Ontwerp en berekening van betonconstructies – bruggen, Delft, The Netherlands, November 2005

3 Linear elastic finite element method – specifications

3.1 Introduction

The linear elastic finite element method is evaluated by considering the structural behavior of reinforced, single-span beams. Their reinforcement is determined by taking all relevant provisions of the Eurocodes into account. In this chapter the normative design principles and geometry of the considered specimens are discussed.

3.2 Geometry of considered specimen

This study focuses on relative basic, statically determined single-span structures. In the introductory chapter it has already been discussed that reinforcement design of this type of structures based on the linear elastic finite element method shows considerable deviations from common design methods. The overall geometry of the considered specimens and the applied external load cases can be seen in figure 3.1.

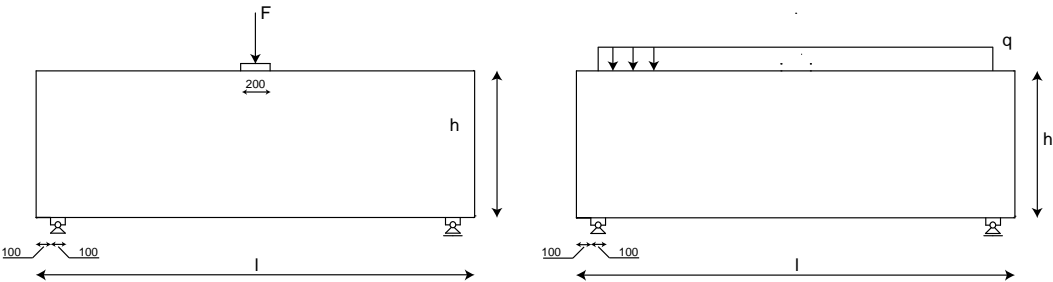


Figure 3.1: Overall geometry of considered specimen and applied external load cases.

In total five types of specimen with a varying length and height are considered. The width of all specimen is equal to 200 mm. An overview of their dimensions can be seen in table 3.1.

Specimen	Length l [mm]	Height h [mm]	Width t [mm]
S-1	2000	1000	200
S-2	3000	1000	200
S-3	4000	1000	200
S-4	6000	1000	200
S-5	2000	2000	200

Figure 3.1: Dimensions of considered specimens.

Concentrated loads are applied at midspan, since this will result in the greatest amount of locally required flexural reinforcement. The size of the supports and load introduction zone are chosen such that similar stress concentrations in vertical direction can be expected in the compressive zone and around the supports. A well distributed introduction of the concentrated load and support reaction is considered to be important to prevent local failure in these areas due to concrete crushing. Distributed loads are applied over the distance between the centre lines of the supports, to exclude the favorable effects of hogging moments on the bending moment at midspan which can appear if a load is applied at the overhangs directly near the supports.

3.3 Material strength parameters

Eurocode EN1992-1-1 prescribes for the design of concrete structures the use of simplified, idealized material models, which are subdivided into a number of strength classes. The applied concrete class for all test specimen is C30/37, the two numbers indicate the characteristic cylindrical and cubical compressive strength respectively. The strength and deformation characteristics of C30/37 according to EN1992-1-1 can be seen in table 3.2.

f_{ck} [N/mm ²]	f_{cm} [N/mm ²]	f_{ctm} [N/mm ²]	$f_{ctk,0,05}$ [N/mm ²]	$f_{ctk,0,95}$ [N/mm ²]	E_{cm} [N/mm ²]	ϵ_{cu} [%]
30	38	2,9	2,0	3,8	33000	3,5

Table 3.2: Material properties of concrete class C30/37.

The mean modulus of elasticity E_{cm} , the parameter on which the structural behavior is based in the linear finite element analyses, is defined as:

$$E_{cm} = 22 \left(\frac{f_{cm}}{10} \right)^{0,3} \quad (3.1)$$

Characteristic concrete strength parameters are based on the 5% fractile of their statistical distribution, defined through elaboration of compression tests on cylindrical specimens with a diameter and height of 150 mm, executed after 28 days of hardening. The relation between the characteristic cylindrical strength f_{ck} and mean cylindrical strength f_{cm} , both given in table 3.2, is defined as:

$$f_{cm} = f_{ck} + 8 \quad (3.2)$$

The mean cylindrical tensile strength is derived from the cylindrical compressive strength according to:

$$f_{ctm} = 0,30 f_{ck}^{2/3} \quad (3.3)$$

The characteristic cylindrical tensile strength is subsequently defined as:

$$f_{ctk,0,05} = 0,7 f_{ctm} \quad (3.4)$$

Design values of the compressive strength of f_{cd} and tensile strength f_{ctd} are derived from their characteristic values according to:

$$f_{cd} = \alpha_{cc} f_{ck} / \gamma_c \quad \text{and} \quad f_{ctd} = \alpha_{ct} f_{ctk} / \gamma_c \quad (3.5)$$

Where α_{cc} and α_{ct} are coefficients taking into account long term strength effects, having a value equal to 1,0, and γ_c is the partial material safety factor for concrete, which has a value of 1,5. For concrete class C30/37 this result in a design compressive strength of 20 N/mm² and design tensile strength of 1,33 N/mm². The tensile strength is however not taken into account during the reinforcement design process.

The applied idealized bilinear stress-strain relation can be seen in figure 3.2. Besides the uniaxial stress-strain relation is shown which would follow from laboratories tests.

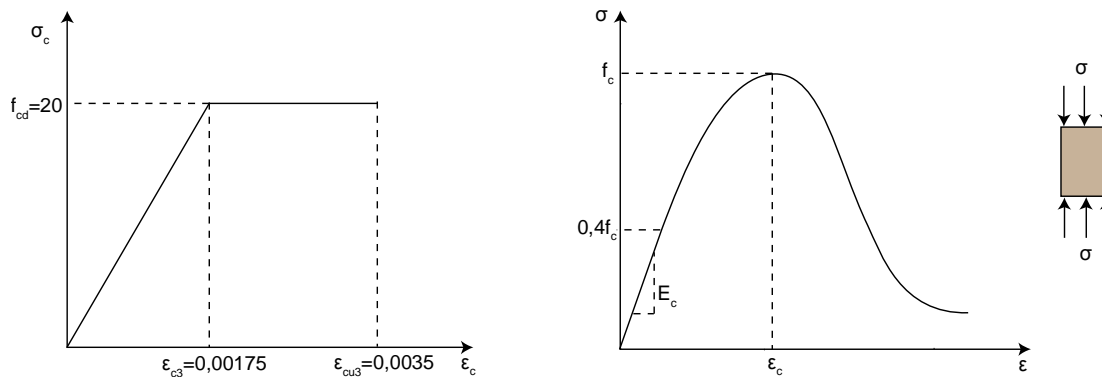


Figure 3.2: Prescribed quantitative material model according to Eurocode EN1992-1-1 (left figure) and the typical, global uniaxial behavior which follows from laboratory tests (right figure).

According to the right diagram of figure 3.2 the response of concrete under compression is linear-elastic to approximately 40% of the peak stress f_c . Beyond this point concrete behaves non-linear up to the peak stress with a decreasing stiffness, caused by micro cracking. When the maximum compressive strength has been reached, the compressive strength reduces into a softening region due to the development of macro cracks. According to the applied bilinear material model of Eurocode EN1992-1-1, this descending branch may be neglected.

Applied reinforcement quality is B500, which has a characteristic tensile strength of 500 N/mm^2 . The corresponding design strength is equal to 435 N/mm^2 . The idealized stress-strain diagram, which applies both for tensile as well as compression forces, can be seen in figure 3.3. Also the actual stress-strain relation which would follow from laboratory tests of hot rolled reinforcement under tension is shown.

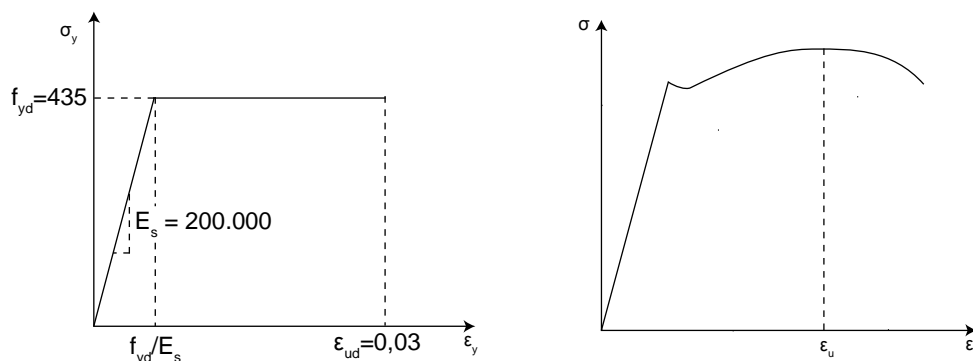


Figure 3.3: Prescribed quantitative material model according to Eurocode EN1992-1-1 (left figure) and the typical, global behavior which follows from laboratory tests (right figure).

3.4 Loads and load combinations

3.4.1 Load combinations

Reinforcement design of the considered specimen is based on a load combination which takes account for the specimen's dead weight, equal to 24 kN/m^3 , and a specific external top load. Table 3.2 gives an overview of the partial safety factors which are taken into account in the serviceability limit state (SLS) and ultimate limit state (ULS) for the considered load combination. The SLS concerns limits to the functioning of a structure under normal use, the comfort of people and the appearance of the structure, the ULS to the safety of people and structures. The external applied top

load is theoretically composed of a permanent and variable part, for which a load factor equal to respectively 1,2 and 1,5 should be taken into account. It is assumed that 2/3 of the external load consists of a permanent part, while the other 1/3 is variable. This results in an overall partial safety factor equal to 1,3.

Load case	Load factor [-]	
	SLS	ULS
Dead weight	1,0	1,2
Permanent and variable loads	1,0	1,3

Table 3.2: Applied load cases and corresponding safety factors.

3.4.2 Loads

To evaluate to what extent the amount of reinforcement influences the structural behavior of the considered specimen, reinforcement designs are based on several load sizes. It can be expected that a relative high load will result in a relative high amount of locally required longitudinal reinforcement bars at midspan that does not reach the supports, which could possibly result in failure at the supports. Contrary, a relative small design load will result in an overall limited amount of reinforcement, both at midspan as well as at the supports.

Initially the amount of reinforcement is based on an as large design load as possible, indicated as the limit load, which is limited by the maximum allowed concrete compressive strength f_{cd} of concrete. Scia Engineer verifies automatically if the design compressive strength of concrete is exceeded. In addition, for the specimen loaded by a concentrated load also the reinforcement configuration is evaluated which is based on a reduced load, equal to half and a quarter of this limit load.

All of above discussed reinforcement configurations will contain a basic reinforcement mesh with a bar diameter of 5 mm and a centre to centre distance of 150 mm, in both directions. For specimens loaded by the concentrated limit load also the reinforcement configuration is evaluated in which instead of a basic mesh an equivalent amount of additional reinforcement is applied.

Table 3.3 gives an overview of the applied design loads for the considered specimens. Beside the design load in the ultimate limit state (ULS), also the serviceability limit state (SLS) load is shown.

Specimen	Reinforcement mesh	Load type	Load size	ULS	SLS
S-1-1	yes	concentrated	limit load	651 kN	501 kN
S-1-2	yes	concentrated	$\frac{1}{2}$ · limit load	326 kN	251 kN
S-1-3	yes	concentrated	$\frac{1}{4}$ · limit load	163 kN	125 kN
S-1-4	no	concentrated	limit load	651 kN	501 kN
S-1-5	yes	distributed	limit load	382 kN/m	294 kN/m
S-2-1	yes	concentrated	limit load	646 kN	497 kN
S-2-2	yes	concentrated	$\frac{1}{2}$ · limit load	323 kN	248 kN
S-2-3	yes	concentrated	$\frac{1}{4}$ · limit load	162 kN	125 kN
S-2-4	no	concentrated	limit load	646 kN	497 kN
S-2-5	yes	distributed	limit load	239 kN/m	184 kN/m
S-3-1	yes	concentrated	limit load	640 kN	492 kN
S-3-2	yes	concentrated	$\frac{1}{2}$ · limit load	320 kN	246 kN
S-3-3	yes	concentrated	$\frac{1}{4}$ · limit load	160 kN	123 kN
S-3-4	no	concentrated	limit load	640 kN	492 kN
S-3-5	yes	distributed	limit load	172 kN/m	132 kN/m

Table 3.3: Applied design loads and considered specimen.

Specimen	Reinforcement mesh	Load type	Load size	ULS	SLS
S-4-1	yes	concentrated	limit load	628 kN	483 kN
S-4-2	yes	concentrated	$\frac{1}{2} \cdot$ limit load	314 kN	242 kN
S-4-3	yes	concentrated	$\frac{1}{4} \cdot$ limit load	157 kN	121 kN
S-4-4	no	concentrated	limit load	628 kN	483 kN
S-4-5	yes	distributed	limit load	110 kN/m	85 kN/m
S-5-1	yes	concentrated	limit load	696 kN	535 kN
S-5-2	yes	concentrated	$\frac{1}{2} \cdot$ limit load	348 kN	268 kN
S-5-3	yes	concentrated	$\frac{1}{4} \cdot$ limit load	174 kN	134 kN
S-5-4	no	concentrated	limit load	696 kN	535 kN
S-5-5	yes	distributed	limit load	409 kN/m	315 kN/m

Table 3.3 (continuation): Applied design loads and considered specimen.

3.5 Environmental conditions

Eurocode EN1992-1-1 classifies the influence of environmental conditions into exposure classes. It is assumed that none of the specimens will be exposed to severe chemical environmental conditions nor subjected to chloride attack. Since concrete walls can be located both at the relative dry inner side of a structure, as well as at its more humid façade, exposure class XC4 (cyclic wet and dry) is taken as a standard for all specimens. The design working life category is estimated to be S3 (design working life of 50 years). For specific code requirements related to this safety class one is referred to Eurocode EN1992-1-1 [2].

3.6 Anchorage of reinforcement

To safely transmit bond forces to the concrete and avoid longitudinal cracking or spalling, a minimum required anchorage length is added to all longitudinal reinforcement bars. A same length is added to all transversal bars that do not have to enclose longitudinal bars at the bottom or top of the specimens. The minimum applied anchorage length is equal to 100 mm or 10 times the diameter ϕ of the applied bar.

Bar diameter ϕ [mm]	Anchorage length [mm]
6	100
8	100
10	100
12	120
16	160
20	200

Table 4.4: Applied minimum anchorage lengths.

References

- [1] European Concrete Platform ASBL, Commentary Eurocode 2, Brussels, Belgium, June 2008
- [2] NEN, NEN-EN 1992-1-1, Eurocode 2: Ontwerp en berekening van betonconstructies – Deel 1- 1: Algemene regels en regels voor gebouwen, Delft, The Netherlands, December 2007

4 Linear elastic finite element method – designs

4.1 Introduction

This chapter focuses on the reinforcement design of the considered specimens. Its first part discusses the bottlenecks which came across during reinforcement design with the linear elastic finite element method. Special attention is paid here to the creation of an adequate finite element model, which is of importance to exclude singularities and obtain a reliable reinforcement configuration. Subsequently the reinforcement configurations of the considered specimens are discussed, which are determined by taking the design principles of the previous chapter into account. In the last section the reinforcement configurations are verified by some basic code checks, which are related to the moment capacity and crack control. Code provisions impose limits to the stress in reinforcement to control the width of cracks in the serviceability limit state. Cracking is a normal phenomenon in reinforced concrete structures, although it should be limited to an extent that will not impair the proper functioning or durability of a structure or cause its appearance to be unacceptable.

4.2 Numerical models

4.2.1 Mesh size

As an initial step, the models of the considered specimens are subdivided into a number of square four noded finite elements, in which the membrane forces and strains are calculated. An important step in finite element modeling is the selection of the mesh density. A convergence of results is obtained when an adequate number of elements is used in a model. This is practically achieved when an increase in the mesh density has a negligible effect on the results.

A convergence study is applied for each considered specimen. An overall finite element mesh which consists of square elements of 50 mm turned out to provide adequate analysis results. This is illustrated in figure 4.1, where the maximum applicable load is set out against the mesh size of for example specimen S-1-1, S-2-1 and S-3-1.

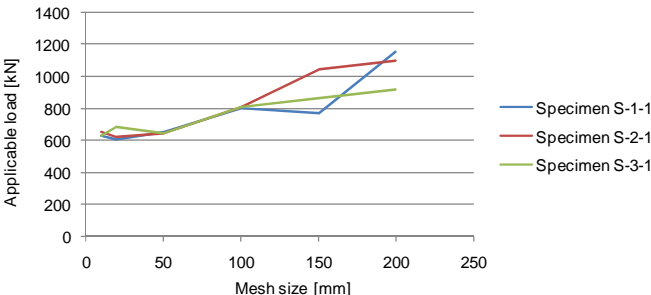


Figure 4.1 Mesh size versus applicable load for specimen S-1-1, S-2-1 and S-3-1.

For estimation of the membrane forces a calculation methodology is applied which is based on the theory of Reissner-Mindlin. This theory takes shear deformation into account, which can not be neglected given the depth of the considered specimen.

4.2.2 Supports and loads

Pin supports and loads which are applied at single nodes of the finite element mesh result in infinite stresses, indicated by the term singularities. Since the amount of reinforcement is directly derived from the determined stresses, singularities will result in an incorrect required amount of reinforcement. Therefore, applied finite element models are optimized to exclude any unfavorable influence of these numerical problems. They are avoided by taking the actual width of the supports and introduction zone of the concentrated load into account, similar as was depicted in figure 3.1. Singularities are also the reason that the supports are positioned 100 mm from the specimens' edges.

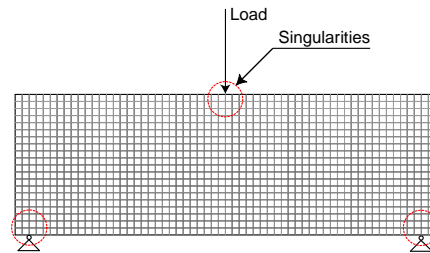


Figure 4.2: Regions in the finite element mesh which are sensitive to singularities and therefore are optimized to avoid numerical problems. These findings correspond to those found by Rombach [1].

For proper modeling of the supports two possibilities are considered to model distributed supports that do not prohibit rotation, one which is based on distributed springs and one which is based on a distributed reaction force equal to the concentrated support reaction. Both types of supports are illustrated in figure 4.3.

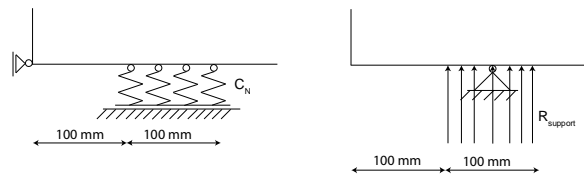


Figure 4.3: Considered types of supports: distributed springs (left) and distributed support reaction (right).

Modeling of supports with flexible springs is preferable, since still disturbances can be found near the pin supports which are connected to a single node. The spring stiffness is related to the stiffness of the material to which it is connected and the dimensions of the support. The axial stiffness C_n is obtained from equation 4.1.

$$C_n = \frac{E_{cm} t}{h} \quad (4.1)$$

Where:

- E_{cm} is the modulus of elasticity of concrete, for C30/37 equal to 33000 N/mm².
- t is the width of the specimen.
- h is the depth of the structure located above the flexible support.

For S-1 up to S-4, which have a depth equal to 1000 mm, a stiffness of 6,6 MN/m² is applied. For specimen S-5, which has a depth 2000 mm, the applied stiffness is equal to 3,3 MN/m².

Concentrated loads are modeled as a distributed load over a width of 200 mm. Modeling of a load introduction zone in Scia Engineer similar as was depicted in figure 3.1 turned out to be difficult, since the elements which should introduce the concentrated load become part of the load bearing mechanism. Scia Engineer did not provide the possibility to apply interface type elements to overcome

this problem. Figure 4.4 gives a global overview of the applied numerical model in the linear elastic finite element analyses.

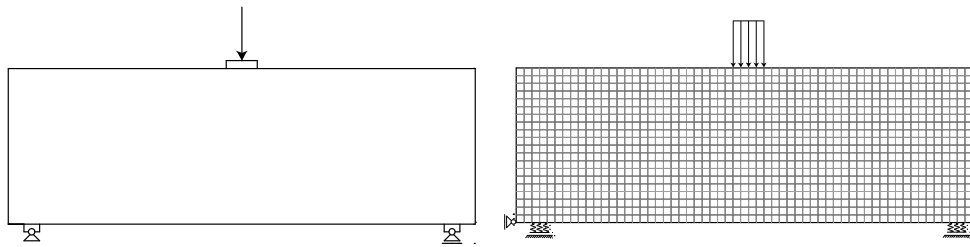


Figure 4.4: Original geometry of a specimen loaded by a concentrated load (left figure) and its numerical model which is applied to determine the required reinforcement (right figure).

4.3 Reinforcement configurations

4.3.1 Design of reinforcement

The linear elastic finite element method derives the required reinforcement directly from the membrane forces which are calculated in individual nodes of the finite element mesh. As a consequence, high concentrations of local reinforcement are required in regions where high concentrations of tensile stresses appear. Reinforcement bars are positioned according to this specific output of the linear elastic finite element method. Longitudinal reinforcement bars do not always reach the supports, while locally required transversal bars do not always enclose longitudinal reinforcement at the top or bottom of a specimen. Besides, reinforcement is distributed over the height of a specimen, similar to the distribution of the membrane forces. Also bars with different diameters are applied within a same specimen, all to approach the output of required reinforcement as close as possible. As a consequence, estimated reinforcement configurations deviate slightly from common design principles which are applied in engineering practice.

The average output of required reinforcement per finite element is used to determine the reinforcement configuration of the considered specimen. This average value is the mean of the values which are determined in the four individual nodes of a finite element. Scia Engineer gives its output per element in mm^2/m . To obtain the actual required reinforcement area A_s in longitudinal direction, the output must be multiplied by the height of the finite element. For the transversal direction the output must be multiplied by the width of the finite element. The output for each finite element is processed in the spreadsheet program Microsoft Excel to determine as accurately as possible a reinforcement configuration which corresponds to the output of the linear elastic finite element method.

To meet code requirements related to minimum reinforcement ratios, Scia Engineer requires a minimum reinforcement amount of $0,002A_{c,e}$ per element, where $A_{c,e}$ is the cross sectional area of a single finite element. For the considered specimens which are subjected to flexural deformations this approach results in a relative conservative amount of reinforcement, since provisions in Eurocode EN1992-1-1 §9.6 require a minimum amount of reinforcement equal to $0,002A_c$ over the whole cross sectional area A_c .

The next subsections contain the detailed reinforcement drawings of the considered specimen, based on the output of Scia Engineer and provisions given in Eurocode EN1992-1-1. To keep this chapter concise, only the reinforcement configurations of specimen and S-3-1, S-3-3 and S-3-5 are discussed in this section to give an impression of the design process and the effect of assumed linear elastic

uncracked material behavior on the required amount of reinforcement. Reinforcement drawings of the other considered specimens can be found in appendix B.

4.3.2 Reinforcement configuration of specimen S-2-1

Reinforcement design of specimen S-2-1 is based on a concentrated limit load of 646 kN. In figure 4.5 the reinforcement can be seen which is required according to the linear elastic finite element method. It must be emphasized that the output is given for one single side of the specimen only, and should be applied at both sides.

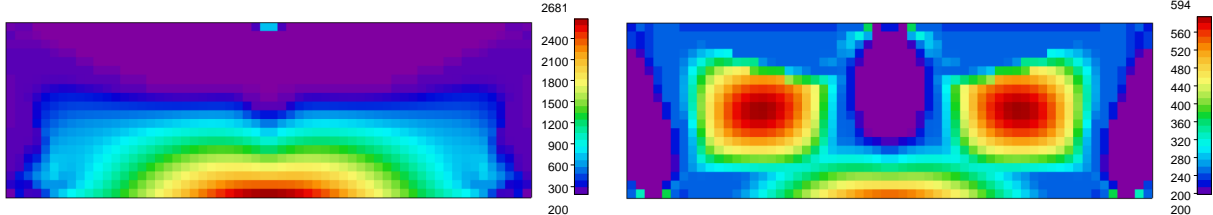


Figure 4.5: Required reinforcement in longitudinal (left figure) and transversal direction(right figure). Output is in mm²/m.

Figure 4.5 clearly shows that a relative high amount of longitudinal reinforcement is required at midspan, where the maximum tensile stresses appear as a result of flexural deformations. In the purple areas where an amount of reinforcement equal to 200 mm²/m is required, the minimum amount of required reinforcement is applied which is equal to 0,002A_{c,e}. A higher amount of reinforcement is required in these areas than would be derived from the membrane forces.

Compared to common methods where shear reinforcement is distributed equally over the span of a structure, the linear elastic finite element method requires transversal reinforcement mainly in concentrated areas between the loading points and supports. In addition, a considerable amount of transversal reinforcement does not have to enclose the longitudinal reinforcement at the top or bottom of the specimen. This is primarily caused by the development of a tension arch which can be seen in the stress trajectory plot of figure 4.6. As was already discussed in the introductory chapter, the approach of concrete as a linear elastic isotropic material results in the development load transfer mechanisms which deviate from common assumed mechanisms.

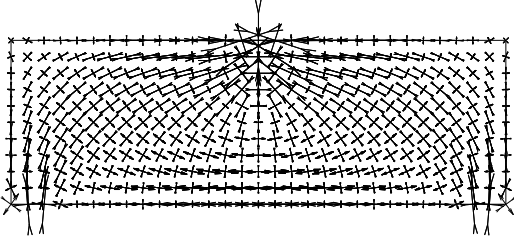


Figure 4.6: Development of load transfer mechanisms in case concrete is considered to behave as a linear elastic, isotropic material.

The reinforcement configuration which corresponds to the required amount of figure 4.5 is shown in figure 4.7. Except for the reinforcement mesh all individual bars are shown in this figure. Bars with a relative small diameter are applied to follow the distribution of reinforcement in figure 4.5 as close as possible. It must be emphasized that hairpins and other provisions to anchor the reinforcement mesh and stirrups properly have not been drawn.

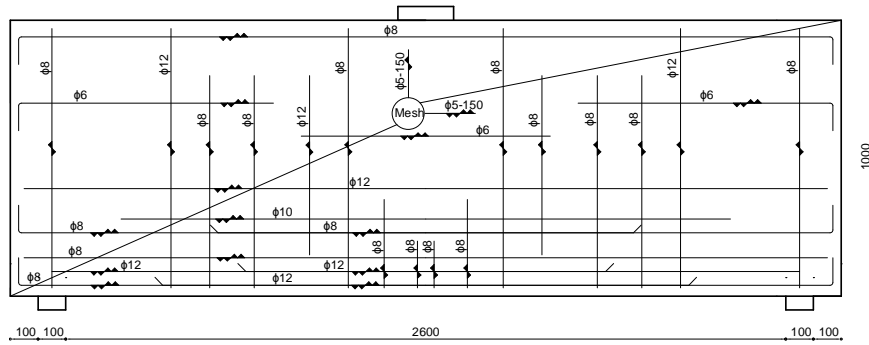


Figure 4.7: Reinforcement drawing of specimen S-2-1.

Figure 4.5 shows that a relative high amount of local longitudinal reinforcement is required directly below the loading area. To increase the capacity to sustain compressive stresses which exceed the assumed design compressive stress f_{cd} , in nodes of elements where both principal stresses are under compression, Scia Engineer applies compression reinforcement. This is illustrated in figure 4.8, where it can be seen that in the compressive zone directly below the concentrated load stresses develop which exceed the design strength f_{cd} .

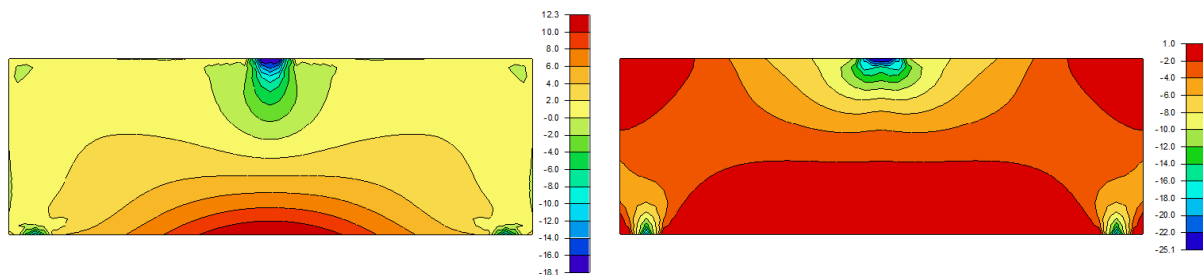


Figure 4.8: Principal stresses in specimen S-2-1 caused by a concentrated top load of 646 kN.

The cross sectional area of the two longitudinal bars with a diameter of 8 mm which are applied at the top of the specimen turned out to be sufficient to meet the amount of required compression reinforcement. However, when the slenderness of a specimen which is loaded by the maximum permissible load increases, an increasing amount of compression reinforcement is required. This can be seen in the required amount of reinforcement of specimens S-3-1 and S-4-1, which can be found in appendix B.

4.3.3 Reinforcement configuration of specimen S-2-3

Reinforcement design of specimen S-2-3 is based on a concentrated limit load of 162 kN, equal to a quarter of the design load of specimen S-2-1. Similar load transfer mechanisms develop as were shown in figure 4.6. The corresponding principal stresses and required reinforcement can be seen in figure 4.9 and 4.10. Due to the limited load size, no compressive reinforcement is required and only the minimum amount of required reinforcement is applied in longitudinal direction at the top of the specimen.

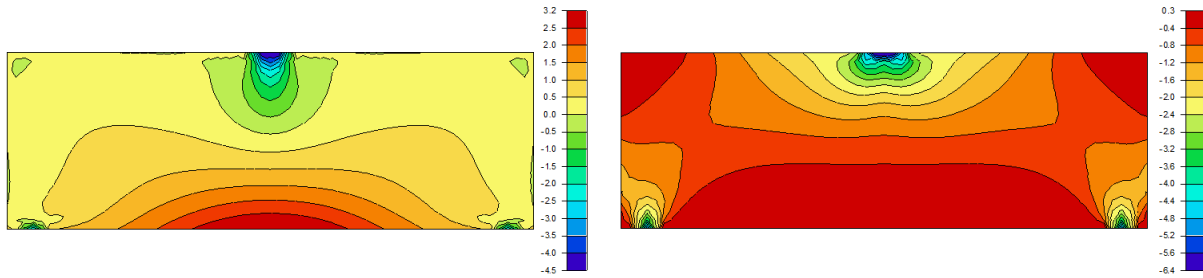


Figure 4.9: Principal stresses in specimen S-2-3 caused by a concentrated top load of 162 kN.

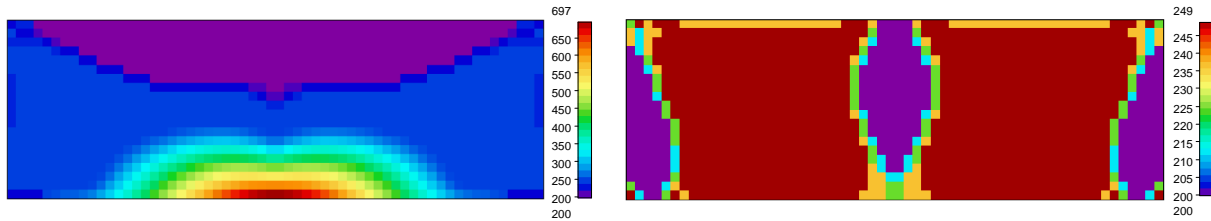


Figure 4.10: Required reinforcement in longitudinal (left figure) and transversal direction(right figure). Output in is in mm^2/m .

The reinforcement configuration which corresponds to the required reinforcement of figure 4.10 is shown in figure 4.11. Compared to specimen S-2-1 a relative limited amount of longitudinal bars reaches the supports, while transversal bars are more equally distributed over the length of the specimen and enclose longitudinal reinforcement bars at the top and bottom of the specimen.

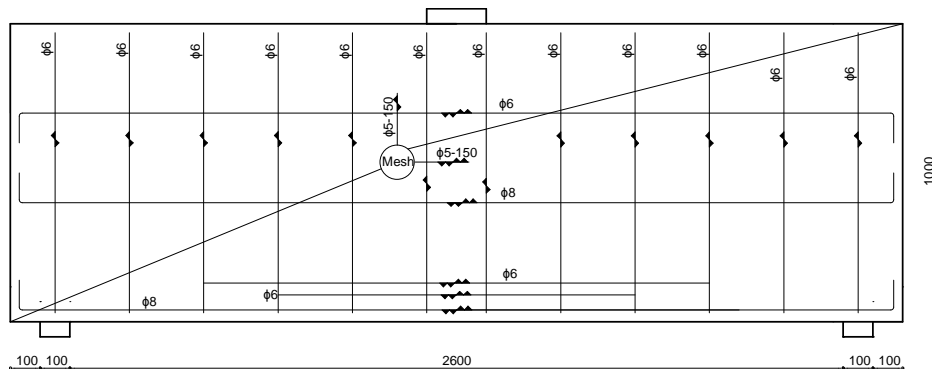


Figure 4.11: Reinforcement drawing of specimen S-2-3.

4.3.4 Reinforcement configuration of specimen S-2-5

Specimen S-2-5 differs from the previous discussed specimen because it is loaded by a distributed load. Compared to the concentrated loaded specimen, a considerable part of the applied load is transferred to the supports by a compression arch, while only a relative small part of the load is transferred by a tension arch. This is illustrated in figure 4.12, where the stress trajectories are plotted.

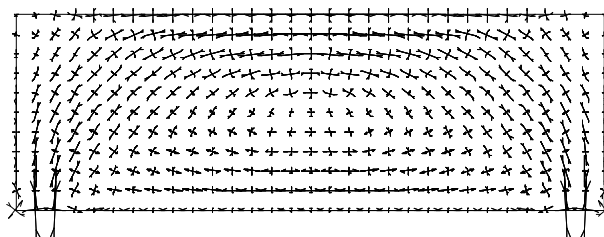


Figure 4.12: Development of load transfer mechanisms in case a distributed load is applied.

The distribution of principal stresses which follow from the linear elastic finite element analysis are shown in figure 4.13. The corresponding required amount of reinforcement can be seen in figure 4.14.

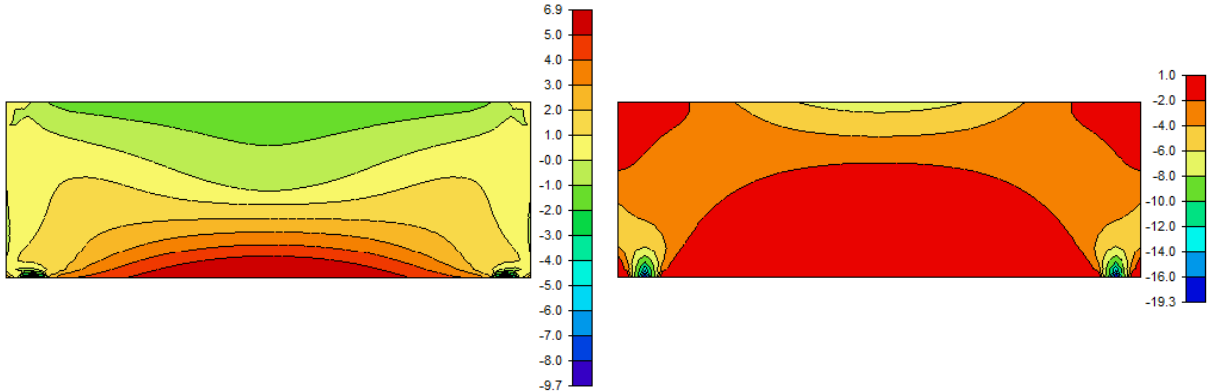


Figure 4.13: Principal stresses in specimen S-2-5 caused by a distributed top load of 239 kN/m.

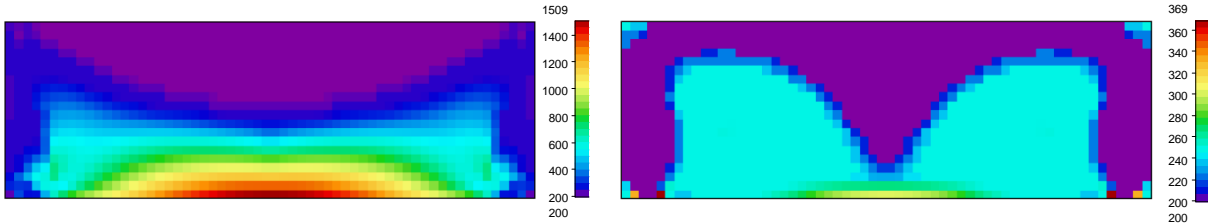


Figure 4.14: Required reinforcement in longitudinal (left figure) and transversal direction(right figure). Output in is in mm²/m.

In figure 4.15 the reinforcement configuration can be seen which corresponds to the required reinforcement of figure 4.14. Compared to the specimen loaded by a concentrated load a relative high amount of longitudinal bars reaches the supports.

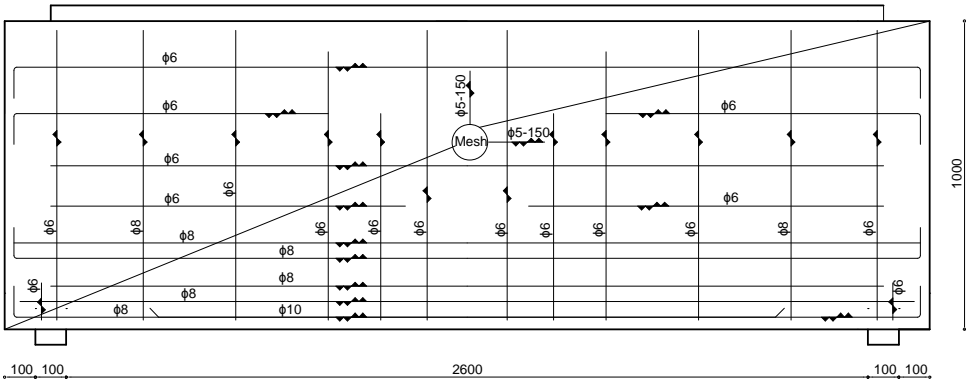


Figure 4.15: Reinforcement drawing of specimen S-2-5.

4.4 Verification of reinforcement configurations

4.4.1 Considered specimen

In advance of the non-linear analyses which will be applied to determine the specimens' actual structural behavior and resistance to failure, some basic code checks are applied to verify the reinforcement configuration of the considered specimen with code provisions. These code checks are related to the moment capacity in the ultimate limit state (ULS) and crack width requirements in the serviceability limit state (SLS).

The applied code checks are based on the conventional beam theory which assumes that plane sections remain plane in case of flexural deformations. Part of the considered specimens has however such a small span to depth ratio, that their behavior considerably differs from slender beams. In contrast to slender beams, the response is characterized by non-linear stress and strain distributions and a direct load transfer from the point of loading to the supports. As a consequence, only the different variants of specimens S-3 and S-4 are verified. The span of these specimens is more than three times the section depth. Structures of which this ratio is less than three must according to Eurocode EN1992-1-1 §5.3.1 (3) considered as deep beams, for which the conventional beam theory is no longer valid.

4.4.2 Verification of moment capacity

The moment capacity of the considered specimens is compared with the design bending moment which follows from its mechanical scheme. Since the amount of longitudinal reinforcement is not constant over the span, the moment capacity is verified at two sections, one at midspan and one in the vicinity of the supports. This last section must be capable to sustain a bending moment which is shifted over a distance d , where d is the effective height of the cross-section. It is assumed as the distance between the top of the compressive zone and the centre of the bottom longitudinal reinforcement bar. The procedure is illustrated in figure 4.16.

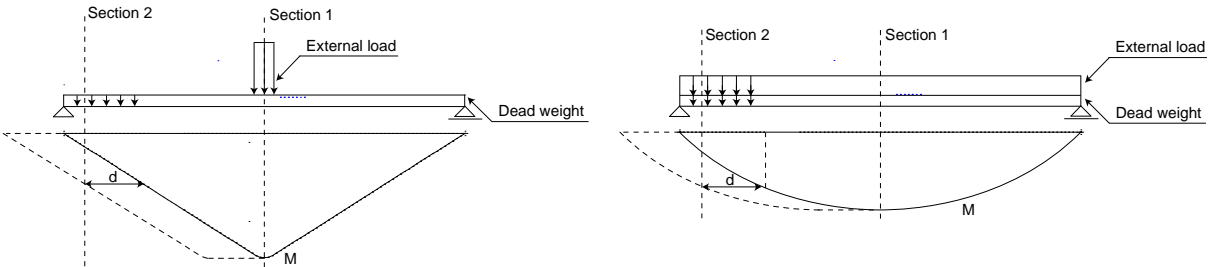


Figure 4.16: Global (shifted) moment diagrams of specimens which are loaded by a concentrated load and a distributed load. The span is defined as the distance between the centre lines of the supports.

The actual moment capacity at a specific cross-section depends on the distribution of longitudinal reinforcement bars which cross the considered section. If it is assumed that the concrete in the concrete compressive zone reaches its ultimate compressive strain ϵ_{cu} and a bilinear stress-strain relation is taken into account, the general distribution of internal forces can be seen in figure 4.17.

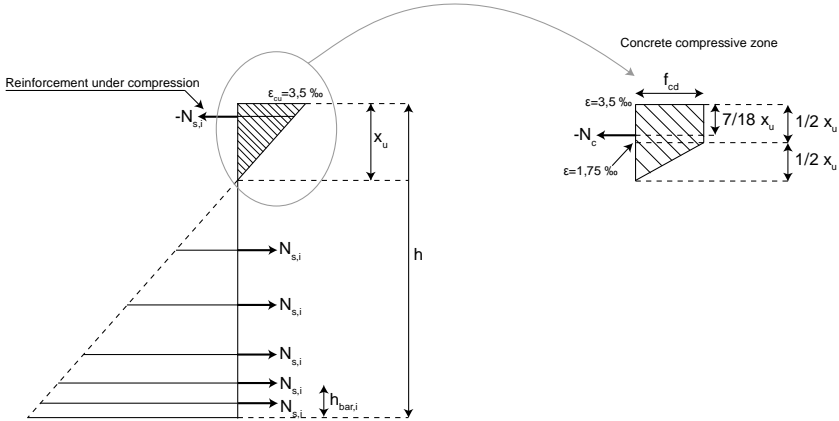


Figure 4.17: Internal forces at an arbitrary cross section which contribute to the moment capacity.

The forces in the reinforcement bars are related to the strain, which runs linearly over the height of the specimens since it is assumed that plane sections remain plane. The strain in an individual reinforcement bar can be expressed by equation 4.2.

$$\varepsilon_{y,i} = \left(\left(\frac{h}{x_u} \right) \varepsilon_{cu} - \varepsilon_{cu} \right) - \left(\left(\left(\frac{h}{x_u} \right) \varepsilon_{cu} \right) / h \right) h_{bar,i} = \varepsilon_{cu} \left(\frac{h - h_{bar,i}}{x_u} - 1 \right) \quad (4.2)$$

Where:

$\varepsilon_{y,i}$ is the strain in an individual reinforcement bar.

$h_{bar,i}$ is the distance between the centre of a reinforcement bar and the bottom edge of the specimen.

The force $N_{s,i}$ inside an individual bar follows from equation 4.3, where it must be emphasized that the maximum allowed stress is limited according to the assumed bilinear stress-strain diagram of reinforcement steel which was shown in figure 3.3.

$$N_{s,i} = A_{s,i} E_s \varepsilon_{y,i} = A_{s,i} E_s \varepsilon_{cu} \left(\frac{h - h_{bar,i}}{x_u} - 1 \right) \quad (4.3)$$

The height x_u of the concrete compressive zone, which is required to determine the moment capacity of a section, can be determined by solving equilibrium equation 4.4.

$$\sum_{i=1}^n N_{s,i} = N_c \quad \rightarrow \quad \sum_{i=1}^n A_{s,i} E_s \varepsilon_{cu} \left(\frac{h - h_{bar,i}}{x_u} - 1 \right) = \frac{3}{4} f_{cd} x_u t \quad (4.4)$$

With a known value of x_u the moment capacity can be determined in an arbitrary point on the considered section. Table 4.1 and 4.2 give an overview of the moment capacity and design moment at specific sections of the considered specimens. The fourth column shows the design moment M_d which follows from the mechanical scheme of figure 4.16, the fifth column the actual moment capacity M_c of the cross-section.

Specimen	Position section*	Design moment M_d [kNm]	Moment capacity M_c [kNm]	M_c/M_d [-]
S-3-1	2000	586	681	1,16
	300	50	284	5,56
	300	365 (shifted)	284	0,78
S-3-2	2000	298	375	1,27
	300	26	136	5,26
	300	187 (shifted)	136	0,73
S-3-3	2000	154	222	1,45
	300	14	130	9,29
	300	97 (shifted)	130	1,34
S-3-4	2000	586	672	1,15
	300	50	280	5,56
	300	365 (shifted)	280	0,77
S-3-5	2000	304	396	1,30
	300	47	293	6,23
	300	256 (shifted)	293	1,14

Table 4.1: Verification of the moment capacity of specimen S-3 according to Eurocode EN1992-1-1. *Position from left edge of specimen.

Specimen	Position section*	Design moment M_d [kNm]	Moment capacity M_c [kNm]	M_d/M_c [-]
S-4-1	3000	901	993	1,10
	300	49	336	6,67
	300	355 (shifted)	336	0,95
S-4-2	3000	462	558	1,20
	300	26	199	7,65
	300	185 (shifted)	199	1,07
S-4-3	3000	243	332	1,37
	300	14	130	9,29
	300	99 (shifted)	130	1,32
S-4-4	3000	901	1039	1,15
	300	49	365	8,11
	300	355 (shifted)	365	1,03
S-4-5	3000	470	543	1,16
	300	48	280	6,22
	300	290 (shifted)	280	0,97

Table 4.2: Verification of the moment capacity of specimen S-4 according to Eurocode EN1992-1-1. *Position from left edge of specimen.

The last column of table 4.1 and 4.2 shows that in a considerable amount of cases where the moment line is shifted over a distance d , reinforcement which is required according to the linear elastic finite element method provides insufficient moment capacity. Therefore it is preferable to apply longitudinal reinforcement bars which run over the full length of the span, also when this is not strictly necessary according to the output of the linear elastic finite element method. Required reinforcement at midspan turns out to meet the required design capacity in the ultimate limit state.

4.4.3 Verification of crack width requirements

As was discussed in chapter 2, the linear elastic finite element method determines the required reinforcement by dividing the membrane forces by the assumed yield strength of reinforcement. This approach is based on the assumption that in the ultimate limit state the strain in all nodes is such that the yield strength f_{yd} of reinforcement is reached.

However, in the considered specimens which are subjected to flexural deformations no yield strain is reached in bars which are required in the vicinity of the neutral axis, or just after considerable yielding of bars in the bottom part of the tension zone. The unjust assumption that these bars reach the full yield strength f_{yd} results in a too limited amount of longitudinal reinforcement to meet requirements related to crack control in the serviceability limit state. This is illustrated in figure 4.18.

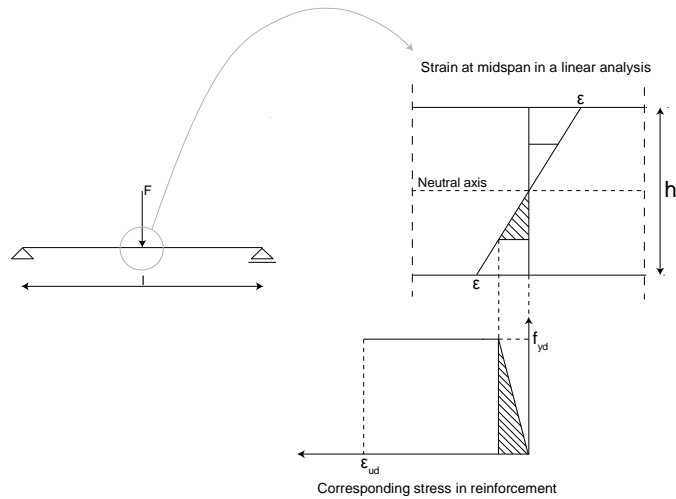


Figure 4.18: Strain in horizontal direction which will follow from a linear elastic analysis of a beam which is subjected to pure bending, assuming that the beam's geometry is such that plane sections remain plane. According to the strain distribution, which develops linearly, the yield strain of reinforcement will not be reached in the vicinity of the neutral axis, although this is assumed during the design process.

As a consequence, bars which are positioned at the bottom side of the tension zone in figure 4.18 have to yield considerably before the bars, which according to the linear elastic analyses are required in the vicinity of the neutral axis, are capable to transfer any load and equilibrium of internal forces is reached. In the serviceability limit state this results in stresses in reinforcement bars at the bottom part of the tension zone which do not longer satisfy code requirements related to crack control. This can be elucidated by a manual verification of the stresses in the individual bars.

In a similar way as the moment capacity was verified in section 4.4.2, the stresses in the individual reinforcement bars in the SLS are determined for those specimens of which the span is not less than three times the overall section depth. Based on the known bending moment and the assumption that plane sections remain plane the stress in each individual bar at midspan is determined.

Figure 4.19 shows the strain distribution and distribution of internal forces when a specimen is subjected to a known bending moment which is the result of a combination of loads in the SLS. The height of the concrete compressive zone x_u and the concrete strain ϵ_c are two unknown variables, which can be determined on basis of the known bending moment M_d in the SLS and horizontal equilibrium of forces. The general form of these two equations is given by equation 4.5 and 4.6.

$$\sum_{i=1}^n N_{s,i} + N_c = 0 \quad (4.5)$$

$$\sum_{i=1}^n M_{s,i} + M_c = M \quad (4.6)$$

Where:

- $N_{s,i}$ is the force in an individual reinforcement bar in horizontal direction.
- N_c is the resultant horizontal force in the concrete compressive zone.
- $M_{s,i}$ is the contribution to the bending moment of an individual reinforcement bar.
- M_c is the contribution to the bending moment of the concrete compressive zone.

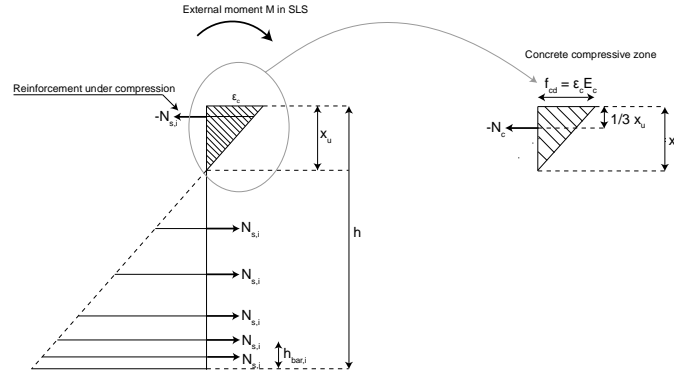


Figure 4.19: Strain and corresponding distribution of internal forces at midspan of an arbitrary specimen, as a result of a known bending moment.

Since the SLS is considered, it is initially assumed that the strain in the concrete compressive zone does not exceed a value of 1,75‰ and N_c can be expressed by equation 4.7.

$$N_c = \frac{1}{2} \varepsilon_c E_c x_u t \quad (4.7)$$

In above equation E_c is equal to the long-term value for the modulus of elasticity, which corresponds to the applied stress-strain diagram for concrete which was shown in figure 3.2 and can be expressed by equation (4.8)

$$E_c = \frac{f_{cd}}{\varepsilon_{c3}} \quad (4.8)$$

The force $N_{s,i}$ in an individual bar depends on the cross-sectional area $A_{s,i}$ and the strain $\varepsilon_{y,i}$, and can be expressed by equation 4.9.

$$N_{s,i} = \left(\frac{(h - h_{bar,i})}{x_u} - 1 \right) \varepsilon_c E_s A_s \quad (4.9)$$

Substitution of equations 4.7 and 4.8 in equation 4.6 results in:

$$\sum_{i=1}^n \left[\left(\frac{(h - h_{bar,i})}{x_u} - 1 \right) \varepsilon_c E_s A_{s,i} h_{bar,i} \right] + \frac{1}{2} \varepsilon_c E_c x_u t \left(h - \frac{1}{3} x_u \right) = M \quad (4.10)$$

As discussed above, ε_c and x_u can be derived by solving equations 4.5 and 4.6. To solve above system of equations efficiently for multiple specimens, the computer algebra system Maple is applied. The applied maple code can be found in appendix C. Table 4.3 gives an overview of the moment at midspan in the SLS for the considered specimens and the values of x_u and ε_c which follow from above system of equations.

Specimen	moment in SLS [kNm]	x_u [mm]	ε_c [-]	σ_s [N/mm ²]	ϕ [mm]
S-3-1	451	390	0,00127	374	12
S-3-2	230	310	0,00084	353	10
S-3-3	119	248	0,00054	311	8
S-3-4	451	390	0,00128	377	12
S-3-5	234	318	0,00083	336	12
S-4-1	695	435	0,00089	377	20
S-4-2	357	369	0,00111	357	12
S-4-3	239	294	0,00089	406	8
S-4-4	695	455	0,00151	338	16
S-4-5	363	365	0,00115	378	12

Table 4.3: Design moment at midspan,

With the known values of ε_c and x_u , the stress $\sigma_{s,i}$ in the individual bars can subsequently be derived from equation 4.11. The last two columns of table 4.3 show the stresses in the longitudinal bars which are located closest to the bottom edge of the considered specimens and their diameter.

$$\sigma_{s,i} = \left(\frac{(h - h_{bar,i})}{x_u} - 1 \right) \varepsilon_c E_s \quad (4.11)$$

The stresses which follow from equation 4.11 are compared with the assumed maximum permissible stress in the serviceability limit state, which is expressed in equation 4.12.

$$\sigma_s = \frac{f_{yd}}{\gamma} \quad (4.12)$$

Assuming an average partial external load factor γ of 1,3, as was derived in chapter 3, this results in a limit stress σ_s of 335 N/mm². Based on the data of table 4.3 and the equation 4.11 the development of stresses in the reinforcement bars is plotted over the depth of the considered specimens in figure 4.20 and 4.21. The considered maximum allowed stress in the SLS is indicated by a vertical line. It can be observed that in the serviceability limit state stresses will develop in the reinforcement bars which are located at the bottom of the tension zone which exceed the maximum stress of 335 N/mm². It is recommended to concentrate the longitudinal reinforcement in areas where the highest tension stresses appear, or to enlarge the required amount of reinforcement at the bottom side of the tension zone by a specific factor to reduce the stresses in reinforcement steel in the serviceability limit state.

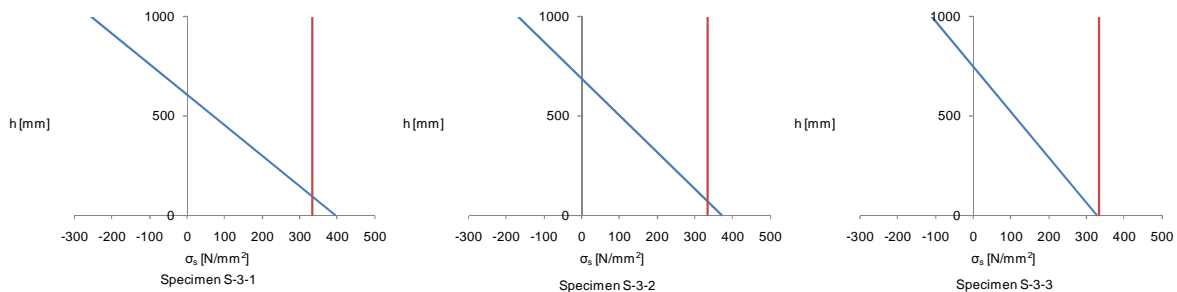


Figure 4.20: Development of stresses in reinforcement over the depth of the considered variants of specimen S-3. The vertical red line represents the maximum allowed tension stress in the SLS according to equation 4.12.

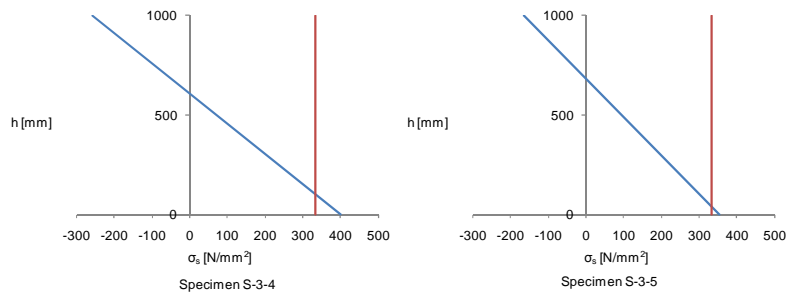


Figure 4.20 (continuation): Development of stresses in reinforcement over the depth of the considered variants of specimen S-3. The vertical red line represents the maximum allowed tension stress in the SLS according to equation 4.12.

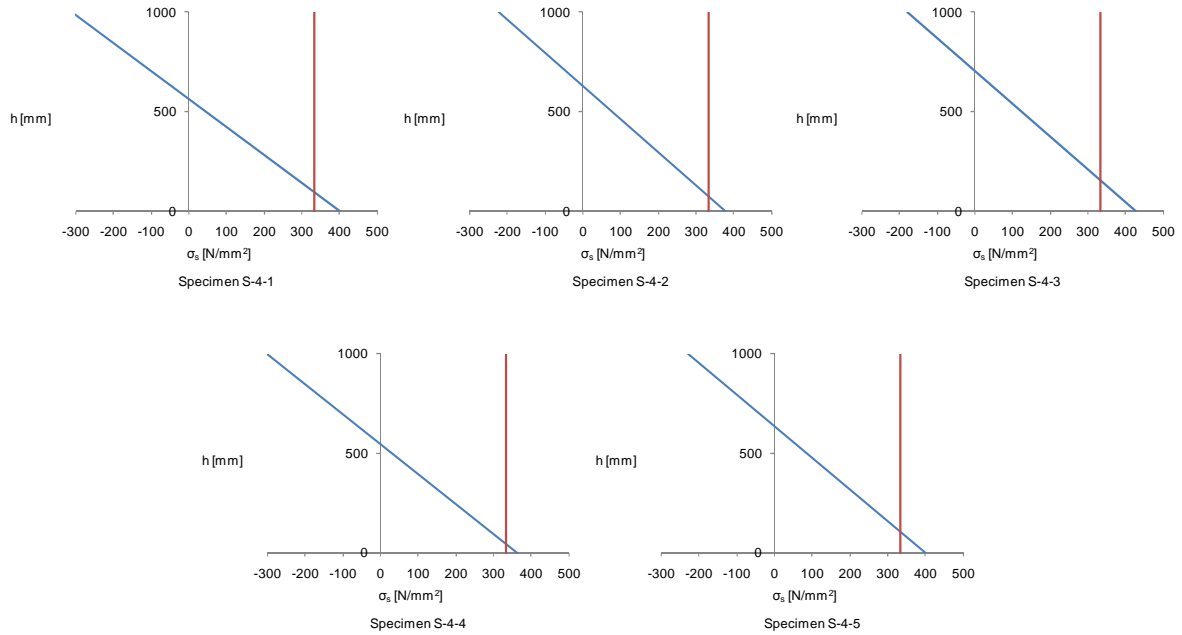


Figure 4.21: Development of stresses in reinforcement over the depth of the considered variants of specimen S-4. The vertical red line represents the maximum allowed tension in the SLS stress according to equation 4.12.

Also according to provisions in Eurocode EN1992-1-1 it can be shown that the determined stresses in reinforcement bars which are located at the bottom side of the tension zone will not meet the requirements which are related to crack control. Eurocode EN1992-1-1 provides an efficient and simplified method to verify by means of tabular data if, for a specific reinforcement stress, requirements which are related to crack control will be satisfied. Table 4.4 gives an overview of the allowed steel stresses for several bar diameters.

Steel stress σ_s [N/mm ²]	Maximum bar size [mm]		
	$w_k = 0,4$ mm	$w_k = 0,3$ mm	$w_k = 0,2$ mm
160	40	32	25
200	32	25	16
240	20	16	12
280	16	12	8
320	12	10	6
360	10	8	5
400	8	6	4
450	6	5	-

Table 4.4: Maximum bar diameters and steel stresses in the serviceability according to table 7.2N of Eurocode EN1992-1-1.

The third column of table 4.4, which is related to a maximum crack width w_k of 0,3 mm, corresponds to the exposure class which is assumed during the design of the considered specimens. If the maximum allowable steel stresses for specific bar diameters which are stated in table 4.4 are compared to the stresses which are determined in the serviceability limit state and are shown in the last two columns of table 4.3, again the conclusion can be drawn that in a major part of the considered specimens higher stresses develop than according to the tabular data of Eurocode EN1992-1-1 is allowed.

References

- [1] Rombach, G.A., Finite element design of concrete structures, London, United Kingdom, 2004
- [2] NEN, NEN-EN 1992-1-1, Eurocode 2: Ontwerp en berekening van betonconstructies – Deel 1- 1: Algemene regels en regels voor gebouwen, Delft, The Netherlands, December 2007

5 Non-linear finite element analyses - principles

5.1 Introduction

As discussed in the introductory chapter of this report, non-linear finite element analyses form an important part of this Master thesis. Non-linear numerical analyses are performed to simulate the failure behavior and to determine the ultimate load bearing capacity of the considered specimens. Contrary to the linear analyses which are applied during the reinforcement design, the non-linear analyses take the actual interaction between all structural elements into account, including the effect of for example concrete cracking, concrete crushing, tension stiffening, reinforcement bond slip and reinforcement yielding.

Before the results of non-linear analyses will be discussed in further detail, this chapter focuses on the basic principles which are taken into account during the non-linear analyses. Correct modeling is of great importance, since it can have a considerable influence on the analysis results.

The non-linear finite element program which is used to verify the reinforcement design and structural behavior of the considered specimens is ATENA 2D, version 4.2.2.0. ATENA's ability to simulate real concrete behavior has been proven numerous times in the preceding years, when results of non-linear analyses with ATENA showed great similarities with the structural behavior and failure loads which were found by real laboratory tests. Although ATENA's proven ability to simulate the behavior of concrete structures accurately, it must be emphasized that the results of non-linear analyses which will be discussed in following chapters always remain a numerical approach of the specimens' actual behavior.

This chapter starts with a description of the applied material models. Subsequently other analysis parameters are discussed, such as specific model details, the loading path and mesh properties.

5.2 Material models

5.2.1 Concrete

Concrete is modeled by using ATENA's default pre-programmed SBETA material model, which is largely based on guidelines of CEB-FIB Model Code 1990 [5]. This model adequately describes the behavior of concrete and meets the provisions of Eurocode EN1992-1-1 with respect to non-linear finite element analyses. The SBETA material model adopts a smeared crack approach for modeling of cracks. Rather than representing a single discrete crack, the smeared crack model represents an area of the concrete that is cracked. Within the smeared crack concept a fixed crack model is applied. In a fixed crack model the crack direction is given by the principal stress direction at the moment of the crack initiation.

A global overview of the uniaxial stress-strain relation which describes the non-linear behaviour of concrete can be seen in figure 5.1. Besides the biaxial failure function is shown. For a detailed description and the mathematical backgrounds of these diagrams and the applied SBETA material model in general, one is referred to ATENA's theoretical manual [2].

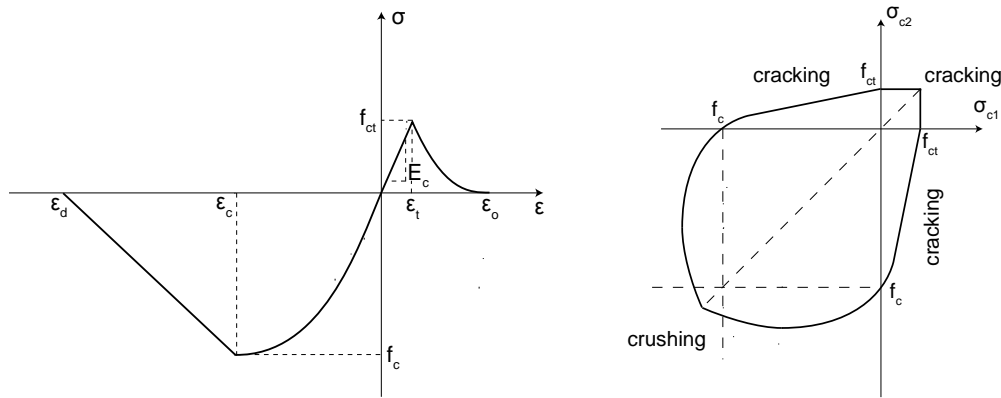


Figure 5.1: Stress strain diagram (left figure) and the bilinear failure function (right figure) of concrete in the considered SBETA model.

In compression, the stress-strain curve for concrete is linear elastic up to approximately 40% of the maximum compressive strength. Above this point the strength increases gradually up to the maximum compressive strength. After it reaches the maximum compressive strength f_c , the curve descends linearly into a softening region, and eventually crushing failure occurs at the ultimate strain ϵ_d . In tension, the stress-strain curve for concrete is linear elastic up to the maximum tensile strength. After this point, concrete cracks and the strength gradually decreases to zero.

In the plane stress analyses, cracking of concrete occurs when the principle stress in any direction lies outside the failure surface of the biaxial failure function. Crushing occurs when all principal stresses are compressive and lie outside the failure surface.

An overview of the derivation of the most important parameters in the SBETA material model can be seen in table 5.4. The SBETA material model calculates all parameters as functions of the entered concrete cubic strength f_{cu} . Values of concrete material parameters for C30/37 which according to the safety formats of Eurocode EN1992-1-1 and Eurocode EN1992-2 have to be used in non-linear analyses are shown in respectively the third and fourth column of table 5.1. Chapter 6 will discuss the backgrounds of these safety formats in more detail.

Parameter	Formula / notation	EN1992-1-1	EN1992-2
Nominal cubic strength [N/mm ²]	f_{cu}	23,53	29,76
Cylinder strength [N/mm ²]	$f_c = -0,85f_{cu}$	20	25,3
Tensile strength [N/mm ²]	$f_{ct} = 0,24f_{cu}^{\frac{2}{3}}$	2,09	2,305
Initial elastic modulus [N/mm ²]	$E_c = (6000 - 15,5f_{cu})\sqrt{f_{cu}}$	27340	30220
Fracture energy [MN/m]	$G_f = 0,000025f_{ct}$	$4,927 \cdot 10^{-5}$	$5,762 \cdot 10^{-5}$
Poisson's ratio [-]	ν	0,2	0,2
Softening compression [mm]	w_d	$-5 \cdot 10^{-4}$	$-5 \cdot 10^{-4}$
Compressive strain [-]	ϵ_c	$-1,463 \cdot 10^{-3}$	$-1,674 \cdot 10^{-3}$

Table 5.1: Properties of concrete in ATENA according to the SBETA material model. The fracture energy G_f is the required energy to propagate a tensile crack.

5.2.2 Reinforcement Steel

Reinforcement steel is modelled by a bilinear stress-strain relation. Its behavior is assumed to be perfectly elastic-plastic and identical in tension and compression. Hardening of reinforcement steel in the plastic stage is left out of consideration. The maximum allowable strain ϵ_{uk} at which rupture of the

reinforcement steel occurs is set at 3 percent. Figure 5.2 shows the applied uniaxial stress-strain diagram. Quantitative properties of reinforcement steel can be seen in table 5.2.

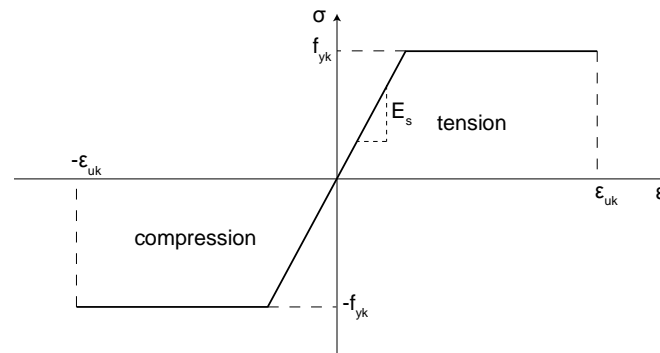


Figure 5.2: Assumed stress-strain diagram of reinforcement steel.

Parameter	Notation	EN1992-1-1	EN1992-2
Elastic modulus [N/mm ²]	E_s	200000	200000
Yield strength [N/mm ²]	f_{yk}	435	550
Ultimate strain [-]	ϵ_{uk}	0,03	0,03
Yield strain [-]	ϵ_y	0,002175	0,00275

Table 5.2: Reinforcement steel properties.

5.3 Geometry and model properties

5.3.1 Overall geometry

The in chapter 3 discussed specimens, including their reinforcement configuration which was determined in chapter 4, are transformed into two dimensional finite element models. Although due to symmetry of the considered single-span specimens it is possible to model only half of the specimens, the full geometry is taken into account in the non-linear analyses. It increases the computational expense, but any possible influence on the analysis results is excluded.

The concrete specimens are modeled by two-dimensional macro elements, which have a length and height similar to that of the considered specimens. A thickness is assigned to the macro-element, which represents its third dimension. The macro elements are subdivided into a specific amount of finite elements, such that accurate analysis results are obtained. All reinforcement bars are modeled as discrete elements.

5.3.2 Supports and loading point

Steel plates with a thickness of 50 mm are modelled below the loading point and above the pin supports to avoid local concrete crushing or stress concentration problems. If the support conditions or loads are applied at single nodes, this may create strong stress concentrations affecting the analysis results. The applied steel plates provide a more even stress distribution over the supports and load point. To obtain similar conditions, the width of these steel plates is set equal to the width of the supports and concentrated loads which are applied during the reinforcement design with linear elastic finite element methods. The behaviour of the steel plates is considered to be perfectly elastic, the considered stress-strain relation can be seen in figure 5.3. A pin support is placed under the centre line of the steel plates to allow rotation of the specimens.

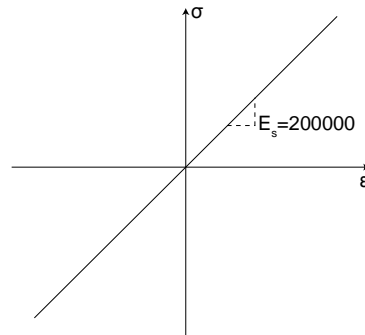


Figure 5.3: Uniaxial stress-strain relation for steel plates which are located at the supports and at the loading point.

To prevent that the steel plates become part of the concrete structure and contribute to a specimens load bearing capacity, gap type interface elements are modelled between the concrete and steel plates. Interface elements describe the physical properties of the contact between two surfaces, its behaviour is based on the criteria of Mohr-Coulomb. Properties of the interface material model can be seen in table 5.3.

Parameter	Notation	Value
Normal stiffness [MN/m ³]	K_{nn}	$3 \cdot 10^6$
Tangential stiffness [MN/m ³]	K_{tt}	$3 \cdot 10^6$
Tensile strength [N/mm ²]	f_t	0
Cohesion [N/mm ²]	C	0
Friction coefficient [-]	ϕ	0,1
Minimal normal stiffness [MN/m ³]	K_{nnmin}	$3 \cdot 10^3$
Minimal tangential stiffness [MN/m ³]	K_{ttmin}	$3 \cdot 10^3$

Table 5.3: Properties of the interface material model.

5.3.3 Reinforcement bond slip

Bond slip between the reinforcement steel and concrete is modelled by a reinforcement bond model according to default settings based on CEB-FIB Model code 1990. It defines the relationship between bond stress and slip between bar and concrete. Ribbed reinforcement, confined concrete and a good bond quality are assumed in the reinforcement bond model. The relation between bond strength and reinforcement slip can be seen in table 5.4. In all numerical analyses the settings of the reinforcement bond model are kept constant.

Slip [m]	Bond stress [N/mm ²]
0,00000	4,8425
0,00025	6,3582
0,00050	9,1766
0,00100	12,106
0,00300	12,106
0,01500	4,8425
1,00000	4,8425

Table 5.4: Relation between bond strength and reinforcement slip.

5.3.4 Anchorage of reinforcement mesh

Bars of the reinforcement mesh which are located at both faces of the specimens are in practice connected to each other by hairpins. Since a two dimensional numerical model is applied, it is not possible to take hairpins and their favorable effect on the resistance to failure into account in the numerical analyses. The effect of hairpins is therefore approached by the assumption that bond slip is disabled at the beginning and end of those bars that are part of the reinforcement mesh. The same setting is applied for additional vertical bars that enclose longitudinal bars at the top or bottom of the specimens.

5.4 Load path

In the non-linear analyses specimens are loaded up to failure to trace down their resistance to failure and corresponding failure mode. In a first load step the dead weight is taken into account, in subsequent steps the external load is applied.

The solution procedure of a non linear analyses is based on an incremental-iterative formulation. This implies that an external load is divided into a number of increments, which are then imposed on the finite element model. Within each increment an iterative procedure is applied to obtain the equilibrium solution. In case of a incremental-iterative analysis, there are two methods of imposing an external load and achieving convergence within each load step. The first method consists of applying a load into a number of increments, the load controlled method. The second method is based on applying a prescribed displacement divided into increments, the displacement controlled method. Except for the analyses of specimens which are loaded by distributed load over the full span, the displacement controlled method is applied in all numerical analyses. Use of the displacement controlled method for specimens loaded by a distributed load would result in immediate compressive failure of concrete that is located between the supports and the distributed load.

At the same node to which the prescribed displacement is applied, the specimens' resistance is monitored by a monitoring point, as shown in figure 5.4. Since it is not possible to monitor the size of an distributed load by a single monitoring point, for these specimens the reaction forces are monitored at the supports. Based on the found resistance at the support, the dead weight and the distance over which the load is distributed the distributed failure load can be determined.

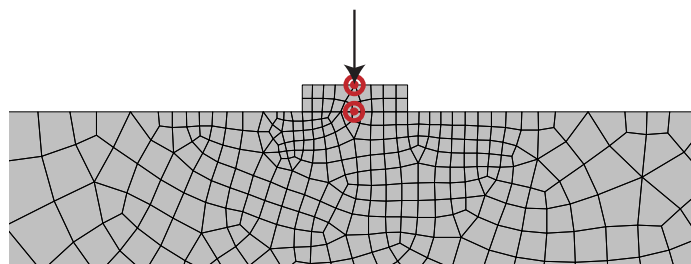


Figure 5.4: Monitoring points which monitor the reaction force (upper one) and displacement (lower one).

Although it results in a larger computational expense, a small increment size is desirable. It will provide a more stable and convergent numerical process, since the degree of non-linear response per increment is smaller and therefore the iterative procedure converges more easily. Besides, a smaller increment size will provide more accurate results. In figure 5.5 the effect of the increment size on the analysis results of specimen S-1-1 can be seen. Although the increment size does not seem to influence the found resistance to failure much, less information is available about the structural

behavior before failure occurs when a relative large increment size is applied. An average increment size of 0,1 mm turned out to result in accurate analyses results for all considered specimens. Only for specimens with a length of 6000 mm an increment size of 0,5 mm is applied. Due to the increasing flexural behavior of slender specimens an increment size of 0,1 mm would require too much computational expense, without providing more accurate analysis results.

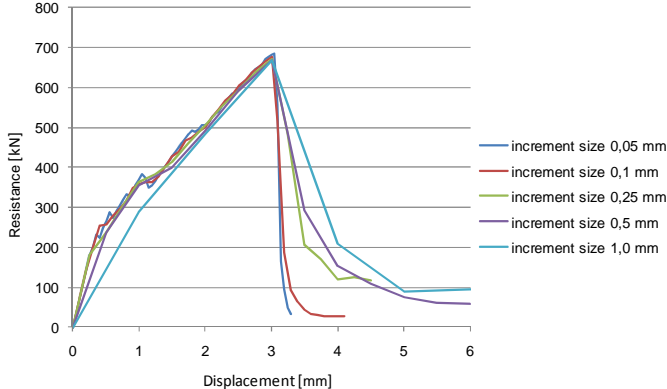


Figure 5.5: Effect of increment size on the load-displacement diagram of specimen S-1-1.

The applied increment size of the load controlled non linear analyses of specimen S-2-5, S-3-5 and S-4-5 is equal to 10 kN/m. To reduce the computational expense for specimen S-1-5 and S-5-5, which due to their limited slenderness show a relative high resistance to failure, a somewhat higher load increment size of 20 kN/m is applied.

5.5 Solver properties

5.5.1 Mesh size

An important step in the finite element modeling is the selection of the mesh density. An adequate number of finite elements has to be used to obtain accurate analysis results. The consequence of a too course mesh is that the accuracy requirements are not met. Although selecting of a very small element size will increase the accuracy, the calculation process may become computationally expensive since the corresponding stiffness matrix increases and more computations are required to solve the system of equilibrium equations. An overall finite element mesh with quadrilateral elements sized 100 by 100 mm, combined with mesh refinement in areas where high stress gradients can be expected, provided the most optimal analysis results with respect to computational expense and accuracy. The minimum size of elements in refined areas is equal to 20 by 20 mm. In figure 5.6 an example can be seen of meshing of specimen S-1-1 and S-2-1.

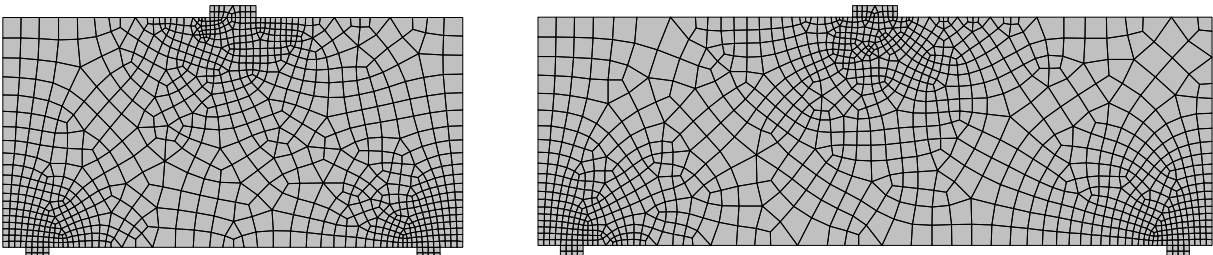


Figure 5.6: Example of the applied mesh for specimen S-1-1 and S-2-1.

5.5.2 Solver

Although ATENA provides the possibility to apply the more advanced and efficient arc-length solution method, the Newton Raphson method is applied since it showed more robust results. The Newton Raphson equilibrium iterations provide convergence at the end of each load increment within tolerance limits. The default pre-programmed tolerance limits in ATENA are applied in all numerical non-linear analyses.

References

- [1] Cervenka, V et. al., ATENA Program documentation Part 2-1: User's Manual for ATENA 2D, Prague, Czech Republic, November 2006
- [2] Cervenka, V et. al., ATENA Program documentation Part 1: Theory, Prague, Czech Republic, October 2009
- [3] Claus, T. T. B., Non-Linear Finite Element Analysis of Shear Critical Reinforced Concrete Beams, Delft, The Netherlands, April 2009
- [4] Kachlakev, D et. al., Finite element modeling of reinforced concrete structures strengthened with FRP laminates, Washington DC, United States, May 2001
- [5] Comité Euro-International du Béton, CEB-FIB Model Code 1990, London, United Kingdom, 1993
- [6] NEN, NEN-EN 1992-1-1, Eurocode 2: Ontwerp en berekening van betonconstructies – Deel 1- 1: Algemene regels en regels voor gebouwen, Delft, The Netherlands, December 2007
- [7] NEN, NEN-EN 1992-2, Eurocode 2: Ontwerp en berekening van betonconstructies – bruggen, Delft, The Netherlands, November 2005

6 Non-linear finite element analyses – safety formats

6.1 Introduction

Uncertainties which affect the structural performance of a structure must be taken into account during its design process. To account for possible uncertainties related to material and structural imperfections, Eurocode EN1992-1-1 prescribes the reduction of material strength parameters of concrete and reinforcing steel by specific partial safety factors. In practice this results in structures with a design resistance which is lower than their actual resistance which would follow from laboratory tests, all to meet a sufficient level of reliability. A similar procedure is prescribed for applied loads, which have to be multiplied by a specific partial load factor.

Reinforcement design according to the linear elastic finite element method is, similar to the other common design methods, based on these prescribed partial safety factors. A same level of reliability as assumed during the design process should be taken into account in the non-linear analyses to fairly verify the design resistance. However, use of the same partial material safety factors in non-linear analyses can be called into question, since non-linear analyses differ at some essential points from their linear counterparts. The safety format which is based on partial material safety factors is tailored for classical design procedures, based on hand calculations or linear analyses and local safety checks of critical individual sections. On the other hand, non-linear analyses are a global type of assessment in which all structural parts and intersections interact. In case design values of material strength parameters are applied in non-linear analyses, an unrealistic degraded material is assumed. This can result in structural behavior which deviates from the actual behavior that would be found in case mean values for material strength parameters are applied. Therefore in non-linear analyses a safety check of the overall structural resistance can possibly be preferred to the safety format of partial material safety factors.

Eurocode EN1992-2, which is prescribed as a basis for the design of bridges in plain reinforced and prestressed concrete, introduces a separate safety format especially for non-linear analyses to overcome the difficulties which are discussed above. A second, more general, alternative for the application of the partial safety factor method is the execution of a full probabilistic analysis, although this is a rather time-consuming method.

In this chapter a comparison is made between the above mentioned safety formats which can be applied in non-linear analyses. The main objective is to extend the understanding of the influence of a specific safety format on the results of non-linear analyses, the found resistance to failure. Based on this comparison analysis an optimal safety format can be chosen for the non-linear analyses which are discussed in the next two chapters. Specimen S-2-1 is chosen as the basis for the comparison analysis, its geometry and reinforcement configuration can be seen in figure 6.1.

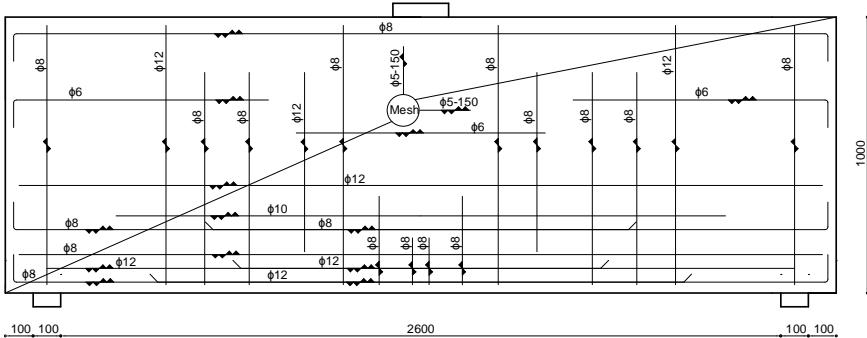


Figure 6.1: Geometry and reinforcement configuration of specimen S-2-1, based on an external design load of 646 kN.

This chapter starts with a concise explanation and some backgrounds of the prescribed safety formats in Eurocode EN1992-1-1 and Eurocode EN1992-2 which take account for uncertainties in material and model properties that can affect the structural performance. Subsequently the full probabilistic analysis is discussed, which is based on the principles of the Monte Carlo method. Preceding the Monte Carlo analysis the general backgrounds related to reliability analyses are introduced shortly. At the end of this chapter the analysis results which follow from the different safety formats are discussed.

6.2 Safety format according to Eurocode EN1992-1-1

The safety format which is prescribed in Eurocode EN1992-1-1 is completely based on partial safety factors [4,5]. Strength of materials is represented through a characteristic value, indicated as f_k . Eurocode EN1990 defines the characteristic value of a material property as the 5% fractile of its statistical distribution. To obtain the design value f_d , which has to be applied in design calculations, the characteristic value is reduced by a partial material safety factor γ_m to account for uncertainties in material and geometrical properties. This procedure is illustrated graphically in figure 6.2, where the normal probability density function of a random strength parameter is shown.

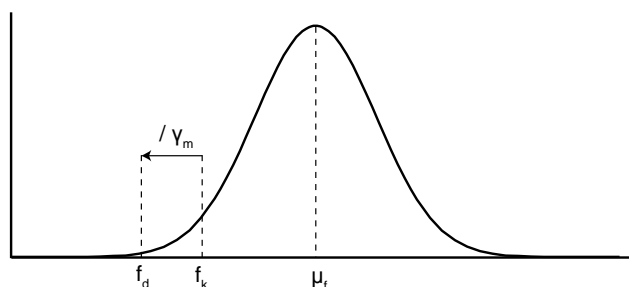


Figure 6.2: Procedure to determine the design value of a material strength parameter according to Eurocode EN1992-1-1 and Eurocode EN1990.

Eurocode EN1992-1-1 defines the design compressive concrete strength f_{cd} and tensile concrete strength f_{ctd} as:

$$f_{cd} = \alpha_{cc} f_{ck} / \gamma_c \quad (6.1)$$

$$f_{ctd} = \alpha_{ct} f_{tck,0,05} / \gamma_c \quad (6.2)$$

Where:

γ_c is the partial safety factor for concrete.

α_{cc} is a coefficient taking account of long term effects on the compressive strength and of unfavourable effects resulting from the way the load is applied.

α_{ct} is a coefficient taking account of long term effects on the tensile strength and of unfavourable effects resulting from the way the load is applied.

According to Eurocode EN1992-1-1 the recommended value of α_{cc} and α_{ct} is equal to 1,0. The prescribed design yield strength f_{yd} is determined in a similar way:

$$f_{yd} = f_{yk} / \gamma_s \quad (6.3)$$

Where:

γ_s is the partial safety factor for reinforcement steel.

An overview of the quantitative values given in Eurocode EN1992-1-1 for the above mentioned safety factors can be seen in table 6.1:

Design situation	γ_c for concrete [-]	γ_s for reinforcing steel [-]	γ_s for prestressing steel [-]
Persistent and transient	1,5	1,15	1,15
Accidental	1,2	1,0	1,0

Table 6.1: Partial safety factors for materials according to EC2-1-1. Partial safety factors related to accidental load will not be discussed further.

Partial safety factors related to persistent and transient design situations take account for variation in model uncertainty, geometry and material strength, which are all distributed according to a specific probability density function. The values of partial safety factors shown in table 6.1 are determined by:

$$\gamma_m = e^{3,04V_r - 1,64V_r} \quad (6.4)$$

Where:

$$V_r = \sqrt{V_m^2 + V_g^2 + V_f^2} \quad (6.5)$$

$$\alpha\beta = 0,8 \cdot 3,8 = 3,04 \quad (6.6)$$

$$\Phi(0,05) = 1,64 \quad (6.7)$$

V_r is the coefficient of variation of the resistance.

V_m is the coefficient of variation of the model uncertainty.

V_g is the coefficient of variation of the geometrical factor.

V_f is the coefficient of variation of the material strength.

α is the dominant FORM (First Order Reliability Method) sensitive factor for resistance.

β is the reliability index for a resistance class 2 structure with a reference period of 50 years.

$\Phi(0,05)$ is the 5% characteristic value corresponding to the Hasofer-Lind reliability index.

An overview of the coefficients of variation on which the partial safety factors are based can be seen in table 6.2:

Coefficient of variation	Concrete [-]	Steel [-]
V_m	0,05	0,025
V_g	0,05	0,05
V_f	0,15	0,04
γ_m	1,295	1,154

Table 6.2: Coefficients of variation for the different model uncertainties for concrete and reinforcement steel. The bottom row shows the resulting partial safety factor which follow from equation 6.4 and 6.5.

To cover the uncertainty arising from concrete being tested which is especially made and cured for this purpose, rather than from a random finished structure, the partial safety factor for concrete which is shown in table 6.2 is multiplied by a factor 1,15. This results in a final partial safety factor γ_c of 1,5, equal to the value shown in table 6.1.

$$\gamma_c = 1,15 \cdot 1,295 = 1,50 \quad (6.8)$$

6.3 Safety format according to Eurocode EN1992-2

Eurocode EN1992-2 gives in contrast to Eurocode EN1992-1-1 some clear provisions for material strength parameters which have to be used in non-linear analyses [6]. The prescribed safety format in Eurocode EN1992-2 is based on both partial, as well as global safety factors. The entered concrete compressive strength and reinforcement tensile strength have to be multiplied by a specific partial safety factor, the resistance which finally follows from the non-linear analysis has to be reduced by a global safety factor.

For reinforcing steel the required steel yield strength which has to be used in non-linear analyses is prescribed as:

$$f_y = 1,1f_{yk} \quad (6.9)$$

The concrete compressive strength which has to be used in non-linear analyses is prescribed by equation 6.10. No clear provisions are given for the other concrete strength parameters. However, all relevant material parameters in the default pre-programmed constitutive concrete model in ATENA are a function of the prescribed concrete compressive strength f_c , as was shown in table 5.1 of chapter 5.

$$f_c = \gamma_{cf} f_{ck} = 1,1 \frac{\gamma_s}{\gamma_c} f_{ck} \quad (6.10)$$

The structure has to be loaded by an increasing load, until one region of the structure attains the ultimate strength or there is global failure. The following inequality should be satisfied:

$$\gamma_{Rd} \gamma_{Sd} E(\gamma_g G + \gamma_Q Q) \leq R \left(\frac{q_{ud}}{\gamma_o} \right) \quad (6.11)$$

Where:

γ_{Rd} is the partial factor for model uncertainty for resistance, $\gamma_{Rd} = 1,06$.

γ_{Sd} is the partial safety factor for model uncertainty for action / action effort, $\gamma_{Sd} = 1,15$.

γ_o is the overall safety factor, $\gamma_o = 1,20$.

When model uncertainties γ_{Rd} and γ_{Sd} are not considered explicitly in the analysis, which is the case when $\gamma_{Rd} = \gamma_{Sd} = 1$, $\gamma_o = 1,27$ should be applied. It must be emphasized that in the hypothetical case in which a structure only exists of reinforcement steel or concrete, and thus no interaction between these materials in the non-linear analysis is present, the safety format prescribed in Eurocode EN1992-2 is equal to that of the partial safety factor format prescribed in Eurocode EN1992-1-1:

For concrete:

$$\left(\frac{1,1 \frac{\gamma_s}{\gamma_c}}{\gamma_o} \right) f_{ck} = \left(\frac{1,1 \frac{1,15}{1,5}}{1,27} \right) f_{ck} = 0,664 f_{ck} = \frac{f_{ck}}{1,51} \quad (6.12)$$

For reinforcement steel:

$$\left(\frac{1,1}{\gamma_o} \right) f_{yk} = \left(\frac{1,1}{1,27} \right) f_{yk} = 0,866 f_{yk} = \frac{f_{yk}}{1,15} \quad (6.13)$$

6.4 Probabilistic analysis

6.4.1 Introduction

A full probabilistic analysis is a suitable safety format for non-linear analyses. Probabilistic analyses are a general tool for safety assessment, and can therefore also be applied in case of non-linear analyses of reinforced concrete structures. Instead of the use of safety factors on which the other discussed safety formats are based, in probabilistic analyses the actual probability density functions of all relevant strength and load variables are taken into account.

The probabilistic analysis of the considered specimen is based on the general limit state function 6.14, which can also be denoted as the reliability function. The state just before failure occurs, which is the case when $Z=0$, is the limit state. The reliability is defined as the probability that this limit state will not be exceeded.

$$Z = R - S \quad (6.14)$$

Where:

- R is the strength or more generally the resistance to failure, which has an appropriate type of probability distribution.
- S is the load which is conducive to failure, which has an appropriate type of probability distribution.

The Monte Carlo method is applied to evaluate limit state function 6.14, a full probabilistic method which is based on repeated random sampling of variables. The resistance to failure R is represented by repeated non-linear numerical analyses, in which relevant strength parameters are assumed as random quantities having appropriate types of distribution function. Load S, which is conducive to failure, can be derived from the resistances which follow from the non-linear analyses and the assumed reliability index β .

The reliability index β is specified as the probability that failure occurs, which is the case when $Z < 0$. During the probabilistic analysis a reliability index β of 3,8 is assumed, which corresponds with the reliability index prescribed in Eurocode EN1990 for a class 2 structure with a reference time of 50 years. Besides, the safety formats provided by Eurocode EN1992-1-1 and Eurocode EN1992-2, discussed in the previous paragraphs, are based on a reliability index β of 3,8 too.

If it is assumed that the distribution of Z in equation 6.14 is normally distributed, the reliability index β can be expressed by equation 6.15:

$$\frac{\mu_z}{\sigma_z} = 3,8 \quad (6.15)$$

Where:

- μ_z is the mean value of the normal distribution of Z.
- σ_z is the standard deviation of the normal distribution of Z.

The failure probability P_f that corresponds to a reliability index of 3,8 of a normal distributed variable can be determined with the cumulative density function of the standard normal distribution. The

cumulative density function can be derived by integration of the probability density function of the standard normal distribution, shown by equation 6.16. The cumulative density function is expressed by equation 6.17.

$$\phi(x) = \frac{1}{\sqrt{2\pi}} e^{-\frac{1}{2}x^2} \quad (6.16)$$

$$\Phi(x) = \frac{1}{2} \left[1 + \operatorname{erf} \left(\frac{x}{\sqrt{2}} \right) \right] \quad (6.17)$$

Where erf is the error function, defined as:

$$\operatorname{erf}(x) = \frac{2}{\sqrt{\pi}} \int_0^x e^{-t^2} dt \quad (6.18)$$

The probability to failure P_f , which follows from equation 6.17 and corresponds to a reliability index β of 3,8, is equal to $7,23 \cdot 10^{-5}$. A graphical representation can be seen in figure 6.3. The probability to failure P_f subsequently follows from equation 6.19:

$$P_f = 1 - \Phi(x) \quad (6.19)$$

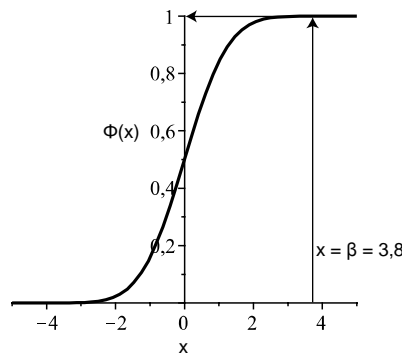


Figure 6.3: Graphical representation of the probability to failure P_f if it is assumed that the distribution of Z is normally distributed and a reliability index of 3,8 is taken into account.

In the next sections the probabilistic analysis will be discussed in more detail. It can roughly be divided into the following steps:

- Creation of a numerical model for the non-linear finite element analysis. This model describes the resistance function R and can perform deterministic analysis of the resistance for a given set of input variables. This step has already been discussed in detail in chapter 5.
- Randomization of the input variables. Random values are generated based on the statistical distribution of each input variable.
- Probabilistic analysis of the resistance and load. This is performed by a Monte Carlo analysis. Results of this analysis provide random parameters of the resistance R and load S .
- Evaluation of the reliability, based on the defined reliability index β .

6.4.2 Resistance to failure R

For the Monte Carlo analysis a total of hundred numerical analyses are applied to establish the resistance to failure. For each separate simulation the properties and circumstances which have the most significant influence on the resistance to failure are generated randomly according to their statistical distribution. Random numbers are drawn from a uniform probability density function between zero and one, which correspond to a specific non-exceedence value of the cumulative density function of the considered material property or circumstance. This can be formulated as:

$$F_x(X) = X_u \quad (6.20)$$

Where:

X_u is the value of the random drawn number from a uniform probability density function between zero and one.

$F_x(X)$ is the probability of non-exceedence of the corresponding cumulative density function of the considered material property or circumstance.

With a given random generated value of X_u the corresponding value of X is determined by:

$$X = F_x^{-1}(X_u) \quad (6.21)$$

Using this formula a random number X can be generated from an arbitrary distribution $F_x(X)$ by drawing a number X_u from the uniform distribution between zero and one. A graphical representation of this method can be seen in figure 6.4.

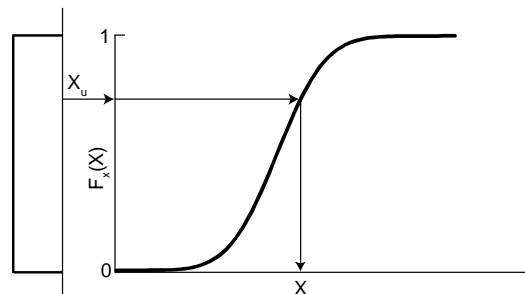


Figure 6.4: Randomization of the input variables.

Properties and circumstances which have a significant influence on the resistance to failure have to be taken into account in a probabilistic analysis and are listed below:

- Material strength properties.
- Model uncertainties caused by influence of the fabrication and execution procedures and uncertainties in geometrical parameters.
- Geometrical imperfections.

Two options are available to take the distribution of above properties and circumstances into account in the Monte Carlo analysis. The first option is to take the distribution of a property or circumstance into account in the actual numerical analysis which is applied to determine the resistance to failure. The second option is to leave the distribution out of the numerical analysis, and to multiply the resistance which follows from the numerical analyses by a multiplication factor. This multiplication

factor takes the effect of the distribution of a property or circumstance on the resistance to failure into account. The spreadsheet program Microsoft Excel is applied to generate all considered random variables and to process the data which follows from the non-linear analysis. Graphs are plotted with the computer algebra system Maple.

Model uncertainties and geometrical imperfections

The effect of geometrical imperfections and model uncertainties is modeled according to the second option, since it is extremely difficult to take their actual scatter into account in the numerical simulations. Their effect on the resistance to failure can be represented by:

$$R = k_m k_g R_{analysis} \quad (6.22)$$

Where:

k_m is a randomly generated multiplication factor which takes model uncertainties into account.

k_g is a randomly generated multiplication factor which takes geometrical imperfections into account.

$R_{analysis}$ is the resistance to failure which follows from the non-linear numerical simulation.

For each numerical analysis a random value for k_m and k_g is generated. Both the effect of geometrical imperfections as well as the effect of model uncertainties is assumed to have a lognormal distribution. Their parameters can be seen in table 6.3 and are taken from the Dutch CUR rapport titled "Probability in Civil Engineering" [3]. All other statistical data which will be discussed throughout this chapter is taken from this same rapport. The coefficient of variation V , which is shown in table 6.23, is defined as:

$$V = \frac{\sigma}{\mu} \quad (6.23)$$

Property or circumstance	Notation	Distribution	μ [-]	V [-]
Model uncertainty	k_m	lognormal	1	0,05
Geometrical imperfections	k_g	lognormal	1	0,05

Table 6.3: Parameters of the statistical distribution of k_m and k_g .

In figure 6.5 the probability density functions of k_m and k_g are plotted.

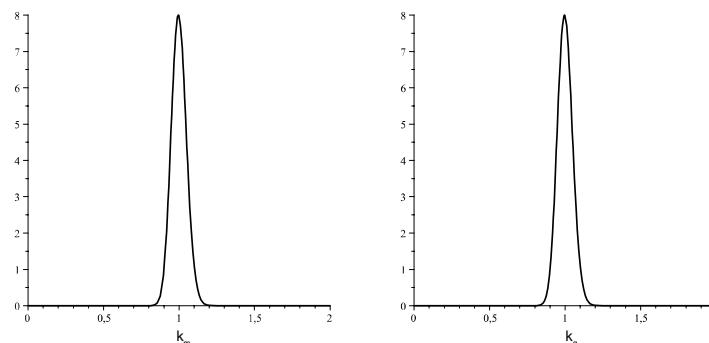


Figure 6.5: Probability density functions of k_m and k_g .

Material strength properties

Scatter in material strength parameters is taken into account in the actual numerical analyses. Since in practice every material parameter is scattered according to a specific kind of distribution, only the material parameters are randomly generated that have a significant influence on the resistance to failure. These considered material strength parameters are:

- The concrete compressive strength f_c .
- The concrete tensile strength f_{ct} .
- The reinforcement steel yield strength f_y .

All other material properties, such as for example the modulus of elasticity of reinforcing steel, are considered as deterministic values during the repeated simulations. Concrete properties are for each repeated simulation derived from the random generated concrete compressive strength by the formulas given in table 5.1 of chapter 5. Only the concrete tensile strength is replaced by a random generated value. Table 6.4 shows the assumed properties of the distribution functions which describe the scatter of above listed material strength parameters. The accompanying probability density functions can be seen in figure 6.6.

Strength parameter	Notation	Distribution	μ [N/mm ²]	V [-]
Concrete compressive strength	f_c	lognormal	38	0,15
Concrete tensile strength	f_{ct}	lognormal	2,9	0,20
Steel yield strength	f_y	lognormal	500	0,10

Table 6.4: Material properties used in numerical simulations.

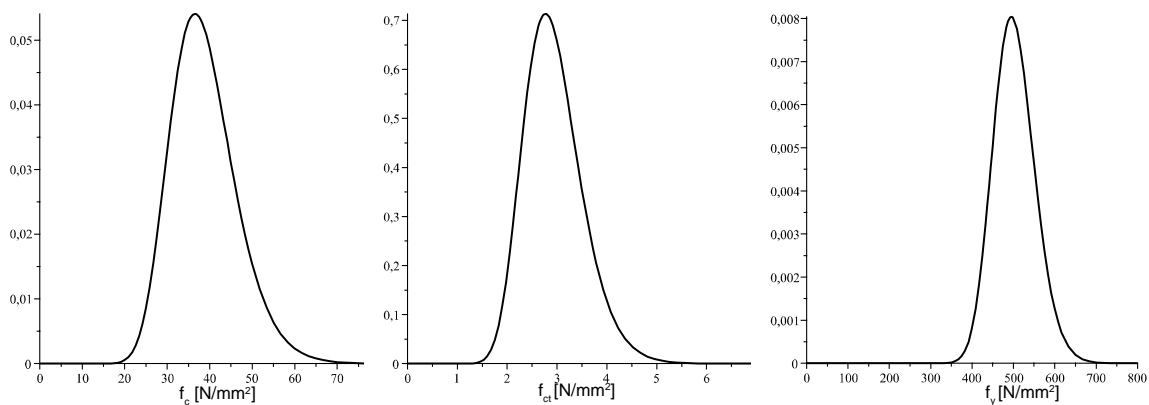


Figure 6.6: Statistical distribution of f_c , f_{ct} and f_y . It must be emphasized that the scale of the axes differs in each graph.

Mean concrete strength parameters provided in Eurocode EN1992-1-1 are related to the short-duration strength of concrete, estimated with tests of cubic specimens at an age of 28 days after casting. Long-term effects, which already appear during real laboratory tests of specimens, have significant influence on the considered concrete strength parameters and are taken into account in the numerical simulations. The diagram in figure 6.7 shows a representation of concrete strains as a function of the applied stresses for several loading times, nailed down in an extensive long-term effect study by Rüschi in the 1960's.

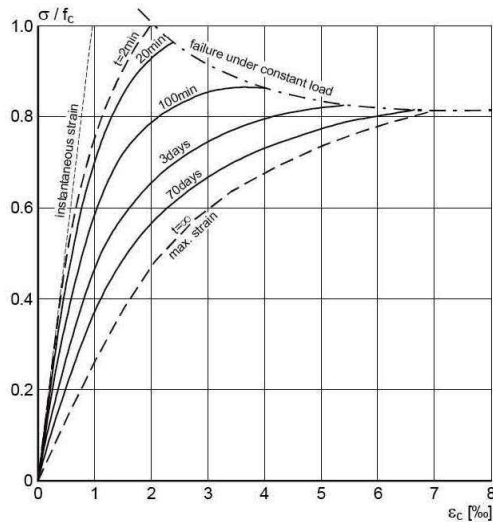


Figure 6.7: Stress strain relations for several time durations of axial compressive loads [4].

On basis of the ultimate compressive strain ϵ_{cu1} of C30/37, which is equal to 3,5‰, and an assumed duration of a real laboratory failure test which takes between 20 to 100 minutes, a reduction factor of approximately 0,85 for the short-term concrete compressive strength can be derived from the diagram in figure 6.7. A reduction factor for the effect of long-term loading on the concrete tensile strength is taken from the former Dutch concrete code NEN 6720, which charges the long-term effects with a reduction coefficient of 0,7. Random generated values of the concrete compressive and tensile strength are multiplied by these reduction factors before they are imported in the numerical analyses.

Since both the concrete compressive strength as well as the concrete tensile strength are generated randomly, both material properties are considered to be fully independent. In practice however a certain correlation between these two variables can be expected, a concrete specimen which has an above average compressive strength would probably also has an above average tensile strength. Closer examination on the influence of the concrete tensile strength on the resistance to failure of the considered specimen, which was performed to verify if disregarding of the correlation would have an unfavorable influence on the analysis results, shows however that its size has almost no influence. In the left diagram of figure 6.8 the concrete tensile strength is kept constant at a value corresponding to a non-exceedence probability of 0,5, while that of the concrete compressive strength varies between 0,01 and 0,99. In the right diagram the compressive strength is kept constant, while the tensile strength varies. From the right diagram in figure 6.8 it comes clear that the size of the concrete tensile strength has almost no influence on the analysis results, and that disregarding of the correlation would probably not influence the analysis results.

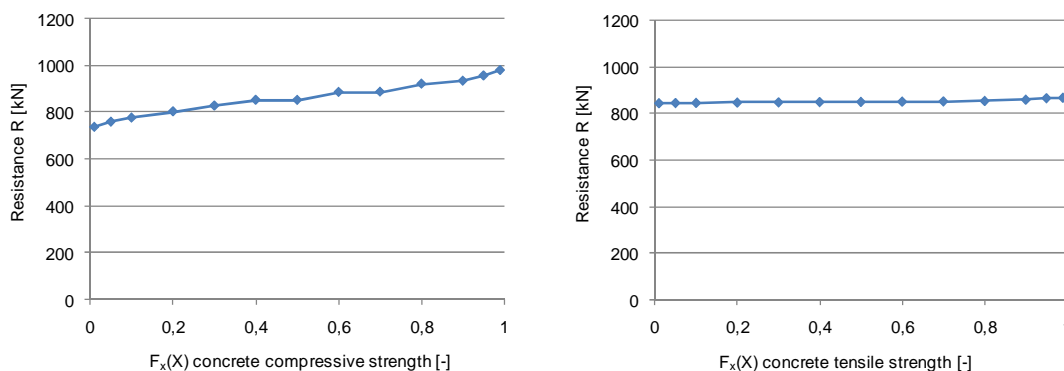


Figure 6.8: Influence of the concrete compressive strength (left diagram) and concrete tensile strength (right diagram) on the resistance to failure which follows from a non-linear analysis.

Results of non-linear analyses

Numerical simulation of the hundred test specimens which are based on random generated material properties and affected by random generated circumstances results in a dataset with a mean resistance to failure μ_R of 850 kN and a standard deviation σ_R of 83 kN. These values are determined according to equation 6.24 and 6.25.

$$\mu_R = \frac{1}{n} \sum_{i=1}^n R_i \quad (6.24)$$

$$\sigma_R = \sqrt{\frac{1}{n} \sum_{i=1}^n (R_i - \mu)^2} \quad (6.25)$$

The histogram in figure 6.9 shows the distribution of the found resistances. Three frequently appearing types of distribution functions in the field of probabilistic analyses are plotted manually through the histogram. In table 6.5 the corresponding probability density functions and scale parameters can be seen. The green graph corresponds to the normal distribution, the red graph to the lognormal distribution and the blue graph to the Gumbel distribution. The curve which corresponds to the lognormal distribution appears to describe as accurate as possible the scatter which is found in the analyses results, and has the advantage that it cannot assume negative values which on physical grounds are not possible. The correctness of the approximation of the resistance to failure by a lognormal distribution can be proven by the Kolmogorov-Smirnov-test, which compares the chosen distribution function with the statistical material.

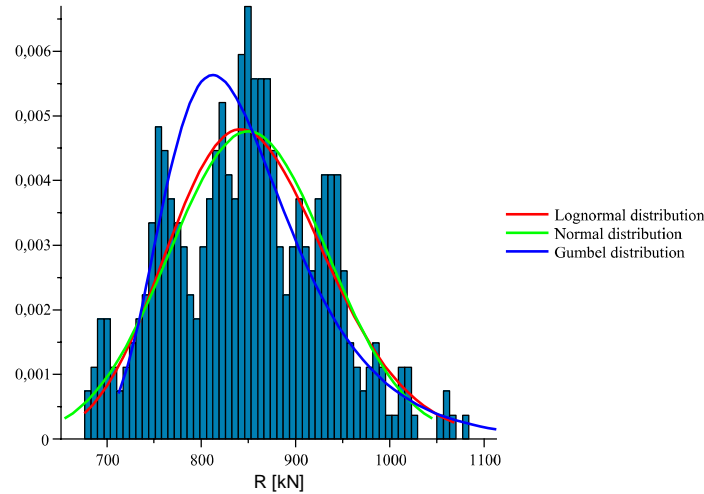


Figure 6.9: Statistical distribution of the resistance R which is found after 100 numerical analyses. Based on the available data different distribution functions are plotted.

Distribution	Probability density function	Scale parameters	
Normal	$f(R) = \frac{1}{\sqrt{2\pi}\sigma_R} e^{-\frac{(R-\mu_R)^2}{2\sigma_R^2}}$	See equation 6.24	See equation 6.25
Lognormal	$f(R) = \frac{1}{R\sqrt{2\pi}\sigma} e^{-\frac{(\ln(R)-\mu)^2}{2\sigma^2}}$	$\sigma = \sqrt{\ln\left(1 + \left(\frac{\sigma_R}{\mu_R}\right)^2\right)}$	$\mu = \ln\left(\mu_R - \frac{1}{2}\sigma^2\right)$
Gumbel	$f(R) = e^{-e^{-(R-u)/\beta}}$	$u = \mu_R - \gamma\beta$	$\beta = \frac{\sqrt{6}\sigma_R}{\pi}$

Table 6.5: Probability density functions and scale parameters of three frequently appearing distribution functions in the field of probabilistic analysis.

The histogram in figure 6.9 also shows one limitation of the performed Monte Carlo analysis. The amount of hundred repeated non-linear analyses is actually too limited to accurately determine a type of distribution function which describes the distribution in the lower and higher ends, since less analysis results are available in these regions. To obtain more accurate results the amount of non-linear analyses should be increased considerably, which due to the required computational time for a single non-linear analysis was not attainable.

6.4.3 Load S

The scale parameters that describe the distribution of the permissible load S, which is assumed to be lognormal, can be derived by an iterative process from reliability function 6.14 and the determined reliability index β of 3,8. Since only a single reliability function is available to solve the two unknown scale parameters that describe the distribution function of S, which are μ_s and σ_s , four separate analyses are performed. Each analysis is based on a different value for the coefficient of variation V_s of load S, so that μ_s remains as the only unknown variable. The values of V_s are chosen such that they represent the range in variation which can be found in practice. Table 6.6 gives an overview, inclusive the corresponding scale parameters.

Analysis	Distribution	μ_s [kN]	V_s [-]	σ_s [kN]
1	lognormal	515	0,05	26
2	lognormal	481	0,10	48
3	lognormal	443	0,15	66
4	lognormal	407	0,20	81

Table 6.6: Properties which describe the distribution functions of S for different coefficients of variation.

The four corresponding distribution functions can be seen in figure 6.10. The red graph corresponds to distribution function of the resistance.

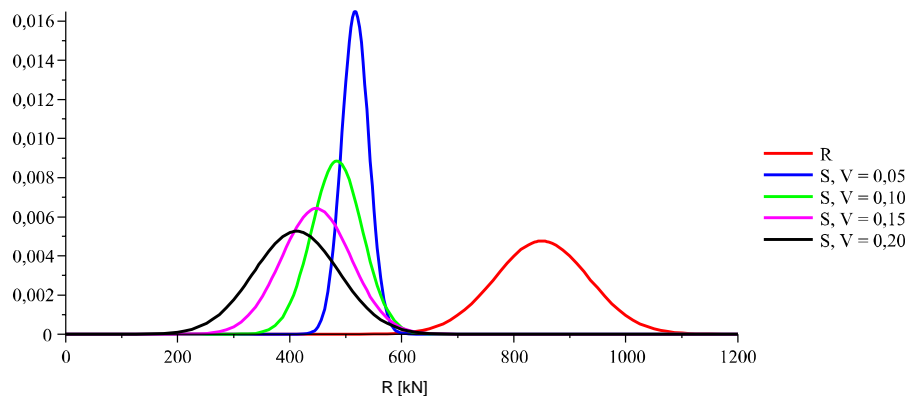


Figure 6.10: Probability density functions of R and S.

6.4.4 Design resistance

With the known statistical distributions of the resistance and each separate load case a level II FORM (First Order Reliability Method) analysis can be applied to determine the design points, which are defined as the points in the failure space with the greatest joint probability. The distribution functions which are shown in figure 6.10 are transformed to normally distributed variables to approximate the resistance R_d and load S_d which correspond to the design point. It is assumed that R and S are fully uncorrelated.

Figure 6.11 gives a graphical representation of the determination of the design point which belongs to a load with a coefficient of variation of 0,10. Design points which correspond to the other load cases are indicated at the graph which corresponds to the reliability function Z.

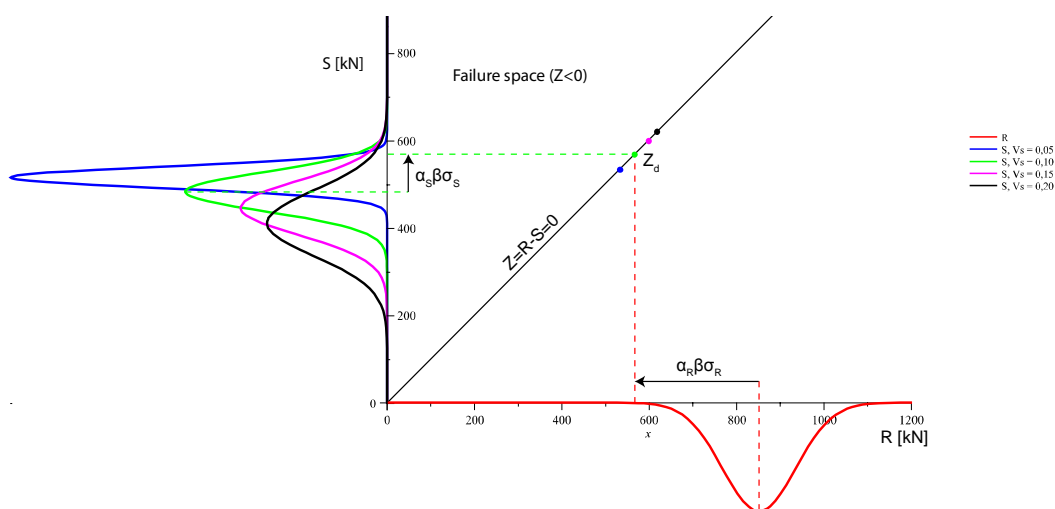


Figure 6.11: Failure space and determination of design points with the greatest joint probability.

The corresponding resistance R_d and load S_d for each considered load case can be determined by:

$$R_d = \mu_R - \alpha_R \beta \sigma_R \quad (6.26)$$

$$S_d = \mu_S + \alpha_S \beta \sigma_S \quad (6.27)$$

The α -values are a measure for the sensitivity of the reliability function Z to the resistance R and load S, and are specified by:

$$\alpha_R = \frac{\sigma_R}{\sqrt{\sigma_R^2 + \sigma_S^2}} \quad \alpha_S = \frac{\sigma_S}{\sqrt{\sigma_R^2 + \sigma_S^2}} \quad (6.28)$$

In table 6.7 an overview can be seen of the resistance and load which correspond to the design point of each considered load case.

Analysis	R [kN]	S [kN]	β [-]	α_R [-]	α_S [-]	R_d [kN]	S_d [kN]
1	850	515	3,84	0,955	0,295	544	544
2	850	481	3,83	0,867	0,499	570	570
3	850	443	3,82	0,782	0,623	601	601
4	850	407	3,80	0,716	0,698	623	623

Table 6.7: Design values of R_d which follow from the probabilistic analysis and meet a reliability index β of 3,8.

6.5 Comparison safety formats

Table 6.7 of the previous section already shows the design resistances which follow from a full probabilistic analysis which meets a reliability index of 3,8. The resistances to failure which are found when the safety formats of Eurocode EN1992-1-1 and Eurocode EN1992-2 are applied can be seen in table 6.8.

Safety format	f_{cd} [N/mm ²]	f_{yd} [N/mm ²]	$R_{analysis}$ [kN]	R_d [kN]
Eurocode EN1992-1-1	20	435	610,0	610,0
Eurocode EN1992-2	25,3	550	709,5	558,7

Table 6.8: Resistances which follow from a non-linear analysis in case the discussed safety formats of the Eurocodes are applied.

At first glance no significant differences can be seen between the results which follow from the different safety formats. All applied safety formats finally result in a similar type of failure mechanism, results which corresponds to earlier found observations by Cervenka [1]. The first load steps result in flexural cracks at the mid-span of the specimen. By an increasing prescribed displacement the amount of cracks in the compressive struts increase considerably. Failure is finally caused by flexural deformation. Due to yielding of the tensile reinforcement concrete in the compressive strain reaches its ultimate strain, whereupon the concrete fails in compression. In chapter 7 the observed failure mode will be discussed in more detail and it will be explained why, considering a same level of reliability, the non-linear analyses show a lower resistance to failure compared to the design load.

Figure 6.12 shows the load-displacement diagram of the analyses which are based on the safety format of Eurocode EN1992-1-1 and Eurocode EN1992-2. It must be emphasized that the resistance which follows from the non-linear analysis which corresponds to the Eurocode EN1992-2 method must be reduced by a factor γ_o of 1,27, as was discussed in section 6.3. The design resistances which follow from the full probabilistic analyses are indicated by a horizontal line.

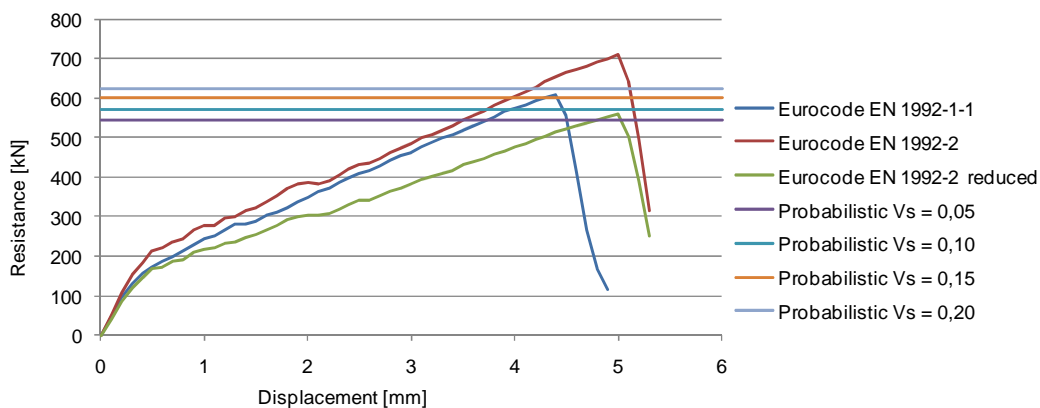


Figure 6.12: Resistances which follow from the different safety formats plotted in a load-displacement diagram. After the normative failure mode appeared the non-linear analyses were interrupted.

The small difference in resistance to failure between the two safety formats which are prescribed in the codes can be explained by a difference in the modulus of elasticity of concrete which is applied in the non-linear analyses. As discussed in chapter 5, the modulus of elasticity in the applied concrete material model in non-linear analyses is a function of the applied concrete compressive strength. Since the safety format of Eurocode EN1992-2 is based on a higher initial concrete compressive strength, the stiffness of concrete which is applied in the non-linear analyses is also higher compared to that of analyses which are based the safety format of Eurocode EN1992-1-1. Because the modulus of elasticity of reinforcement steel is kept constant in both safety formats, concrete in a non-linear analysis which is based on the safety format of Eurocode EN1992-2 will carry relatively more load due to its higher stiffness. Since exceeding of the ultimate compressive strain of concrete is the governing failure criteria, a relative lower resistance to failure is found in the analysis in which the safety format of Eurocode EN1992-2 is applied.

The design resistances which follow from the full probabilistic analyses do not deviate considerably from the results that follow from analyses which are based on safety formats of the codes. For the greater part this can be explained by the fact that the full probabilistic analysis is largely based on the

same assumptions as the ones on which the safety factors of the codes are based. The small deviation can be explained because code prescriptions deviate to a limited extent from the assumed reliability index of 3,8, mostly because of economical reasons. Furthermore it depends on the type of load, permanent or variable, which value for the coefficient of V_s should be applied.

6.6 Conclusion

The resistances which follow from the comparison analysis of the different safety formats all lie in approximately the same range. Although the full probabilistic analyses can be considered as the most exact method to determine the resistance to failure that meets a reliability index of 3,8, it has the disadvantage that it is too time-consuming to apply it on all considered specimens. Therefore preference is given to the safety format of Eurocode EN1992-2, which is exclusively derived for non-linear analyses.

References

- [1] Cervenka, C. et. al., Probabilistic Estimate of Global Safety Factor – Comparison of Safety Formats for Design based on Non-linear Analysis, Prague, Czech Republic, October 2006
- [2] Dekking, F.M et. al., A Modern Introduction to Probability and Statistics: Understanding Why and How, Delft, The Netherlands, February 2007
- [3] Civiel Technisch Centrum Uitvoering Research en Regelgeving, Kansen in de civiele techniek. Deel 1: probabilistisch ontwerpen in theorie, Gouda, The Netherlands, March 1997
- [4] European Concrete Platform ASBL, Commentary Eurocode 2, Brussels, Belgium, June 2008
- [5] NEN, NEN-EN 1992-1-1, Eurocode 2: Ontwerp en berekening van betonconstructies – Deel 1- 1: Algemene regels en regels voor gebouwen, Delft, The Netherlands, December 2007
- [6] NEN, NEN-EN 1992-2, Eurocode 2: Ontwerp en berekening van betonconstructies – bruggen, Delft, The Netherlands, November 2005
- [7] NEN, NEN-EN 1990: Eurocode – Grondslagen van het constructief ontwerp, Delft, The Netherlands, December 2002
- [8] NEN 6720, Voorschriften Beton – Constructieve eisen en rekenmethoden, Delft, The Netherlands, September 1995

7 Non-linear finite element analyses – results

7.1 Introduction

This chapter discusses the results which follow from non-linear analyses in ATENA of the considered specimens. The non-linear numerical analyses are applied to evaluate if the applied reinforcement is sufficient to meet the required load bearing capacity. In addition attention is paid to the appearing failure modes. As was already discussed extensively in the previous chapter, a same level of reliability is taken into account in the non-linear analyses as was applied during the reinforcement design process to make a clear comparison between the design load and resistance to failure. The safety format of Eurocode EN1992-2 is applied to meet the considered level of reliability, equal to 3,8.

7.2 Analysis results

Non-linear finite element analyses show a similar type of failure mode for the considered specimens. At the load increment which results in a regression of the monitored load bearing capacity, concrete in the compressive zone fails in compression, caused by bending of the specimens. Only the considered variants of specimen S-5, which have a dimension of 2000 by 2000 mm, fail due to shear. Rupture of the reinforcement steel due to exceeding of the limit strain or significant bond slip of the reinforcement in the vicinity of the supports, as was expected to be one of the possible normative failure modes, did not be normative.

An overview of the resistances to failure which follow from the non-linear analyses can be seen in the fourth column of table 7.1.

Specimen	Dimensions [mm]	Design load	Resistance	Displacement	Resistance / design load
S-1-1	2000 x 1000 x 200	651 kN	676 kN	3,0 mm	1,04
S-1-2	2000 x 1000 x 200	326 kN	498 kN	3,8 mm	1,53
S-1-3	2000 x 1000 x 200	163 kN	375 kN	4,1 mm	2,30
S-1-4	2000 x 1000 x 200	651 kN	706 kN	3,2 mm	1,08
S-1-5	2000 x 1000 x 200	382 kN/m	572 kN/m	-	1,50
S-2-1	3000 x 1000 x 200	646 kN	559 kN	5,0 mm	0,86
S-2-2	3000 x 1000 x 200	323 kN	428 kN	6,3 mm	1,33
S-2-3	3000 x 1000 x 200	162 kN	273 kN	6,5 mm	1,69
S-2-4	3000 x 1000 x 200	646 kN	536 kN	5,0 mm	0,83
S-2-5	3000 x 1000 x 200	239 kN/m	354 kN/m	-	1,48
S-3-1	4000 x 1000 x 200	640 kN	545 kN	8,5 mm	0,85
S-3-2	4000 x 1000 x 200	320 kN	421 kN	10,7 mm	1,32
S-3-3	4000 x 1000 x 200	160 kN	252 kN	5,8 mm	1,56
S-3-4	4000 x 1000 x 200	640 kN	548 kN	8,3 mm	0,86
S-3-5	4000 x 1000 x 200	172 kN/m	292 kN/m	-	1,70
S-4-1	6000 x 1000 x 200	628 kN	473 kN	16 mm	0,75
S-4-2	6000 x 1000 x 200	314 kN	342 kN	19,5 mm	1,09
S-4-3	6000 x 1000 x 200	157 kN	229 kN	21 mm	1,46
S-4-4	6000 x 1000 x 200	628 kN	489 kN	16,5 mm	0,79
S-4-5	6000 x 1000 x 200	110 kN/m	169 kN/m	-	1,54

Table 7.1: Resistances to failure which follow from non-linear analyses.

Specimen	Dimensions [mm]	Design load	Resistance	Displacement	Resistance / design load
S-5-1	2000 x 2000 x 200	696 kN	904 kN	1,4 mm	2,21
S-5-2	2000 x 2000 x 200	348 kN	852 kN	1,6 mm	2,45
S-5-3	2000 x 2000 x 200	174 kN	840 kN	2,1 mm	4,83
S-5-4	2000 x 2000 x 200	696 kN	918 kN	1,5 mm	1,32
S-5-5	2000 x 2000 x 200	409 kN/m	582 kN/m	-	1,42

Table 7.1 (continuation): Resistances to failure which follow from non-linear analyses.

As can be seen in table 7.1 it turned out that especially for slender, heavily loaded specimens the resistance to failure which follows from the non-linear analyses is lower than the assumed design strength. This is noticeable since a higher resistance to failure would be expected. Contrary to the design process, the non-linear analyses take the concrete tensile strength into account. In addition, ATENA also takes the favorable effect of confined concrete in the compressive zone into account, and the amount of reinforcement which is required according the linear elastic finite element method is rounded up. Section 7.3 will focus in more detail on the cause of the relatively low monitored resistances to failure of these specimens.

7.2 Overall behavior

Initial load steps result at all specimens in the development of flexural cracks at midspan. The development of cracks after subsequent load steps depends on the geometry of the specimens, corresponding load transfer mechanisms and the applied reinforcement. The relative less slender variants of specimens S-1 and S-5, which transfer a considerable part of their load by shear, show a relative direct load transfer from the loading area to the supports. During load increments up to failure the most significant cracks in the variants of specimens S-1 develop parallel to the compressive struts, while variants of specimens S-5 show primarily crack development at midspan. This is illustrated in figure 7.1. Besides the development of cracks, also the transfer of principle compressive stresses is plotted.

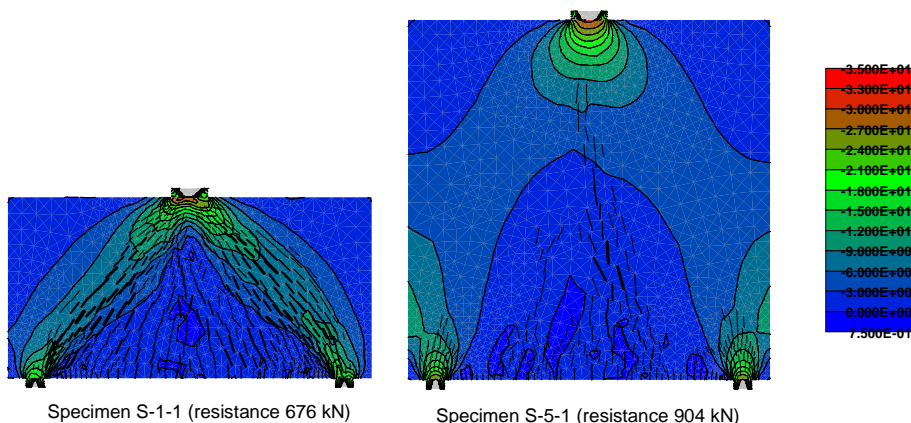


Figure 7.1: Crack development and direct load transfer before failure. Output is N/mm^2 .

The more slender variants of specimens S-2, S-3 and S-4 show a more distributed crack development after subsequent load increments. Normative cracks in specimens of which reinforcement is based on the limit load develop in compressive struts near the supports, while in specimens in which less reinforcement is applied normative cracks develop at midspan.

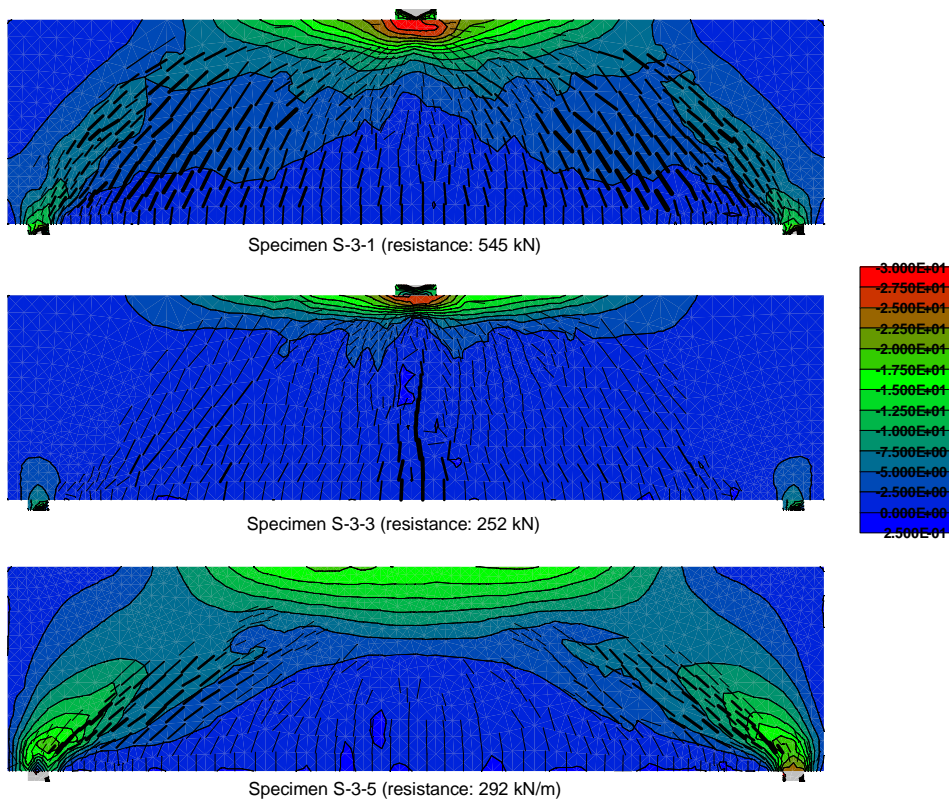


Figure 7.2: Example of crack development and principle compressive forces before failure. Output is in N/mm^2 .

Since the non-linear finite element analyses take the effect of redistribution due to cracking of the concrete into account, load transfer mechanisms develop which deviate from the mechanisms which were observed during the linear elastic analyses. Concrete loaded under compression behaves considerably stiffer compared to cracked, reinforced concrete in tension. Development of a tension arch to transfer loads to the supports as was observed in the linear analyses, is therefore not observed again in the non-linear analyses. Instead, all loads are, dependent on the span of the specimen, transferred to the supports by a tied arch or truss mechanism in which the outer struts transfer the highest compressive forces. As a consequence, to equilibrate the horizontal component of the strut forces, longitudinal reinforcement in the tension zone has to transfer higher loads than initially is assumed during the design process which was based on linear elastic analyses. This results in a considerable development of cracks and relative high compressive forces in the compressive zone, which will be discussed in more detail in section 7.4.

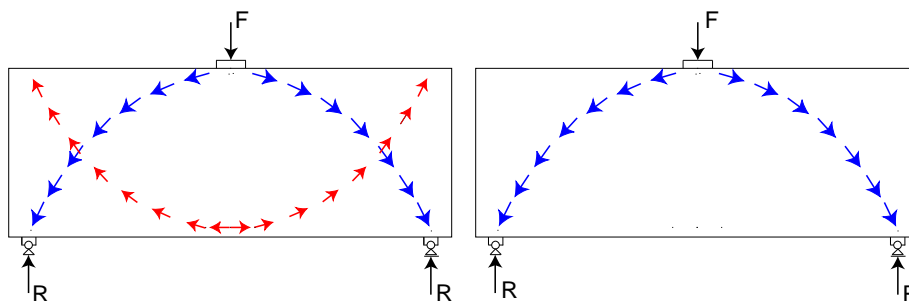


Figure 7.3: Development of normative load transfer mechanisms in linear analyses (left figure, development of both a compression and as well as a tension arch) and non-linear analyses (right figure, only the development of a compression arch).

In section 4.4.3 it has already been discussed that, based on the stresses in longitudinal bars at midspan, in the serviceability limit state (SLS) a significant number of considered specimens does not meet requirements related to crack control. Next to these flexural cracks at midspan, ATENA also

shows a significant development of inclined bending cracks near the supports in the SLS of heavily loaded specimen. Due to the concentrated forces in the compressive struts, lateral forces appear which results in the development of splitting cracks parallel to the load direction. Specimens of which the reinforcement is based on lower concentrated designs load or a distributed load show in the SLS primarily the development of flexural cracks at midspan.

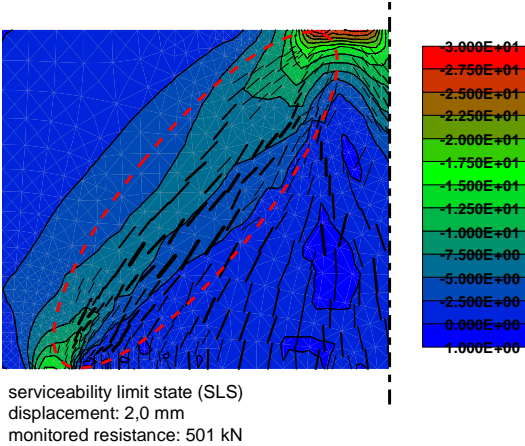


Figure 7.4: Development of shear- and splitting cracks in the compressive strut between the point of loading and support of specimen S-1-1. Output is in N/mm².

ATENA gives for each load increment a prediction of the crack width per element. A small element size of the finite element mesh will result in the development of many small cracks. In reality these small cracks will represent one or more big cracks. To obtain the actual crack width, the individual cracks have to be summed up over a specific distance. Table 7.2 gives an overview of the expected crack widths near the supports of three specimens loaded by the limit load. It can be seen that according to ATENA in each specimen in the SLS cracks develop which exceed the allowable crack width of 0,3 mm that according to Eurocode EN1992-1-1 §7.3.1 corresponds to the considered exposure class XC4.

Specimen	Dimensions [mm]	SLS Load [kN]	Crack width [mm]
S-1-1	2000 x 1000 x 200	501	0,78
S-2-1	3000 x 1000 x 200	497	0,69
S-3-1	4000 x 1000 x 200	492	1,27

Table 7.2: Crack width in the SLS near the support of four heavily loaded specimens.

The linear elastic finite element method does not explicitly require provisions to prevent or limit the development of these types of cracks. Due to the considered isotropic material behavior in linear elastic finite element analyses less load is transferred directly through the compressive struts, and the effect of lateral forces which causes the development of splitting cracks is underestimated. Therefore, additional code checks are recommended during the design process of structures with the linear elastic finite element method in which a load transfer trough compressive struts can be expected.

7.3 Failure mode

7.3.1 Normative failure mode

As was discussed shortly in the previous section, failure of the concrete compressive zone due to bending of the specimens turned out to be the normative failure mode. Rupture of the reinforcement steel due to exceeding of the limit strain or significant bond slip of the reinforcement in the vicinity of

the supports, as was in the introductory chapter expected to be one of the possible normative failure modes due to the limited amount of longitudinal reinforcement that reaches the supports, turned out not to be normative. Also the lack of shifting of the moment diagram, prescribed to prevent failure in the ultimate limit state due to the development inclined bending cracks, did not have a significant influence on the normative failure mode. The beam method, the design method in which it is required to shift the moment line over a specific distance, assumes that in case of the development of such a crack only the concentrated longitudinal reinforcement in the tension zone contributes to the load transfer mechanism, as was illustrated in figure 1.3. The non-linear analyses take however also the contribution of remaining reinforcement bars which cross the diagonal crack into account, which explains why lack of shifting of the moment diagram has no direct significant influence on the observed failure mode, although inclined bending cracks develop. This is illustrated in figure 7.5.

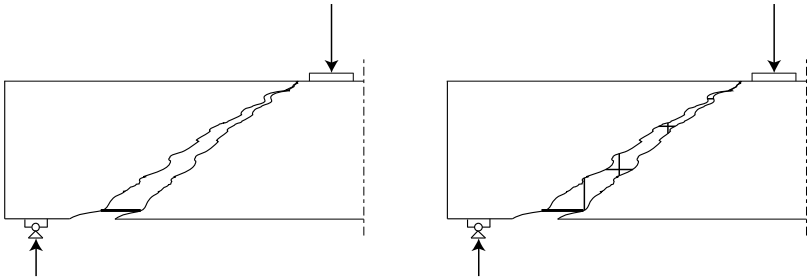


Figure 7.5: Contribution of reinforcement in case a diagonal crack develops in the ultimate limit state.

7.3.2 Concrete compressive zone

The increasing prescribed displacement on top of the specimens forces the longitudinal reinforcement bars in the tension zone to yield, which causes an increasing compressive strain in the concrete compressive zone. After concrete located at the top of the compressive zone has crushed, redistribution of forces occurs such that still a limited load bearing capacity is monitored, although considerably less than the initial resistance. Figure 7.6 gives an example of the development of horizontal stresses during several phases of the non-linear analyses of specimen S-3-1.

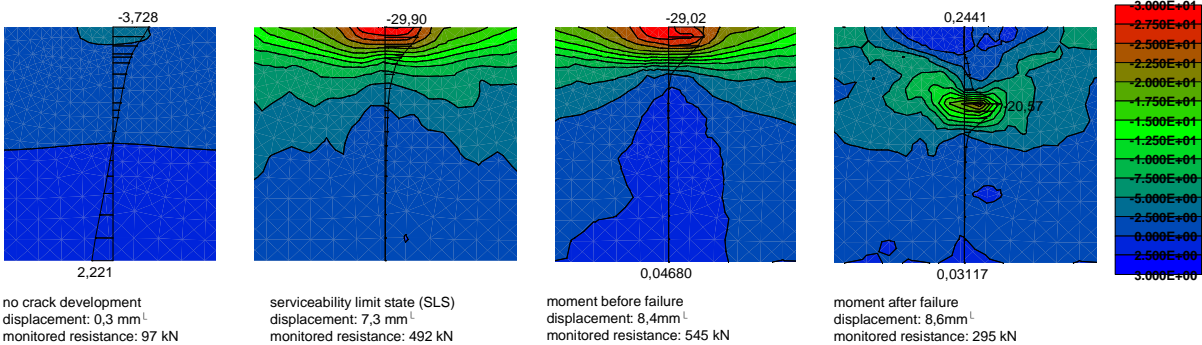


Figure 7.6: Development of horizontal stresses in specimen S-3-1 directly below the loading point at midspan. Output is in N/mm².

A similar global stress development as depicted in figure 7.6 is observed in the analyses of other considered specimens. Until the development of initial cracks, concrete behaves as a linear elastic material. In subsequent load increments, concrete cracks, loses its capacity to transfer tensile stresses and finally reaches its maximum compressive strength at the top of the concrete compressive zone.

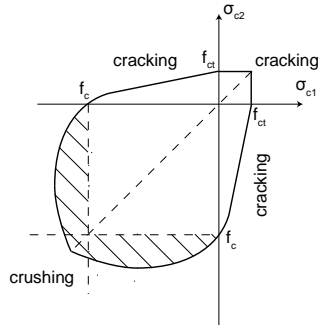


Figure 7.7: According to the biaxial failure function in the applied SBETA material model confined concrete in the compressive zone is capable to withstand higher stresses than the assumed uniaxial compressive strength f_c (dashed area).

In the second and third stress plot of figure 7.6 it can be seen that the maximum monitored compressive stress before failure is equal to $29,90 \text{ N/mm}^2$, which is 18% higher than the applied compressive strength in ATENA of $25,3 \text{ N/mm}^2$. Concrete located in the compressive zone is confined by the applied load in vertical direction and reaction forces caused by bending in horizontal direction. According to the applied bilinear failure function, shown in figure 7.7, confined concrete can withstand higher compressive forces than the assumed compressive strength f_c .

A noticeable result follows from the non-linear analyses of specimens in which reinforcement design is based on the relative high limit load. As was discussed in chapter 4, except for specimen S-1 and S-5, compressive reinforcement is required in the concrete compressive zone of these specimens. In none of the non-linear analyses of specimens in which compressive reinforcement is applied the design strength is reached. Non-linear analyses also show that at the moment of failure the compression reinforcement does not fully function. In table 7.3 the stresses σ_s are shown which are monitored in the compression reinforcement at the load increment before the normative failure mode appeared.

Specimen	$\sigma_s \text{ [N/mm}^2\text{]}$	f_{yd}	σ_s / f_{yd}
S-2-1	217,9	550	0,40
S-2-4	292,8	550	0,53
S-3-1	267,6	550	0,49
S-3-4	290,6	550	0,53
S-4-1	492,9	550	0,90
S-4-4	442,3	550	0,80

Table 7.3: Maximum monitored stresses in compression reinforcement.

The found resistances to failure are expressed as a percentage of their design load in the diagrams figure 7.8. The left diagram shows the specimens which reinforcement is based on the limit load and in which a basic reinforcement mesh is applied, the right one the specimens in which the reinforcement mesh is replaced by an equivalent amount of additional reinforcement.

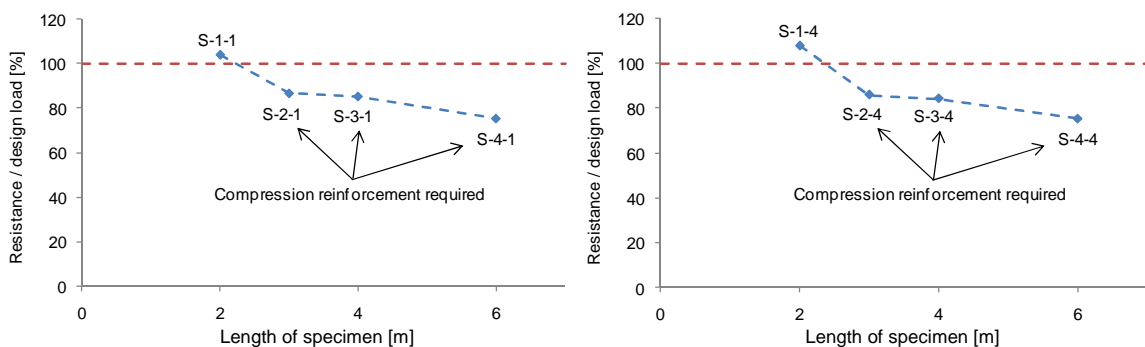


Figure 7.8: Resistance to failure of specimens of which reinforcement is based on the limit load, with a basic reinforcement mesh (left diagram) and without (right diagram).

It can be observed from figure 7.8 and table 7.1 that no significant differences in the resistance to failure can be seen between specimens in which a standard reinforcement mesh is applied and specimens in which instead of a reinforcement mesh a similar amount of additional reinforcement is applied. In both specimens a similar amount of reinforcement is required, which is distributed over the depth of the specimens similar to the output of the linear elastic finite element method. This explains the almost equal analysis results.

7.3.3 Influence of the stress-strain relation on the failure mode

The relative low resistance to failure of the heavily loaded specimens in which compression reinforcement is required can be explained by the relative conservative shape of the stress-strain diagram which is applied in the non-linear analyses. The applied vertical deflection at the top of the specimens is accompanied by a rotation of the specimens' cross section, which results in the development of a concrete compressive zone directly below the loading point. The horizontal compressive forces that can be transferred to this zone are related to the compressive strain and the applied stress-strain relation. According to the idealized stress-strain relations which are provided by the codes and have to be used during the design of concrete cross-sections, concrete preserves its full compressive strength up to the ultimate compressive strain is reached. In the non-linear analyses however a stress-strain relation is applied in which the compressive strength of concrete linearly decreases to zero as the ultimate limit strain is reached, which has a considerable influence on the moment capacity and corresponding utilized reinforcement. The influence on the resistance to failure of the differing stress-strain relations which are applied during the design and the verification of the specimens can be elucidated by considering an elementary beam element which is subjected to a flexural deformation.

Elementary beam element

In figure 7.9 the cross-section of an elementary single-span beam element can be seen which has a arbitrary width b and depth h . All longitudinal reinforcement, which surface is indicated by A_s , is concentrated in the tension zone at a distance equal to $0,1h$ from the bottom side of the beam. The presence of other reinforcement bars is not taken into account. The effective height d is equal to $0,9h$.

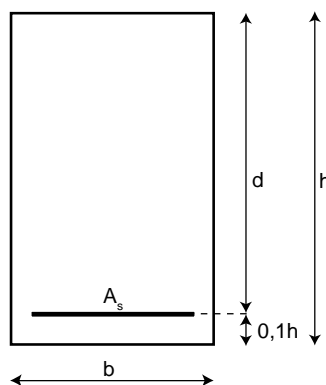


Figure 7.9: Geometry of cross-section of the considered beam element.

The ultimate moment capacity M_u of the considered section and corresponding reinforcement ratio ω depend on the applied stress-strain relation of concrete and the distribution of strain over the height of the beam. The relation between the reinforcement ratio ω and A_s is defined by:

$$A_s = \omega bd = 0,9\omega bh \quad (7.1)$$

In case a stress-strain diagram is applied which assumes that concrete preserves its full compressive strength up to the ultimate yield strain, the maximum reinforcement ratio ω is required when at the top of the beam the ultimate compressive strain ϵ_{cu} is reached and at the location where the concentrated reinforcement is positioned the yield strain ϵ_y . This is illustrated in figure 7.10, where the idealized linear strain distribution can be seen. The strain distribution is based on the assumption that plane sections remain plane and that the strain in the reinforcement is the same as that in the surrounding concrete. Besides, the tensile strength of concrete is not taken into account.

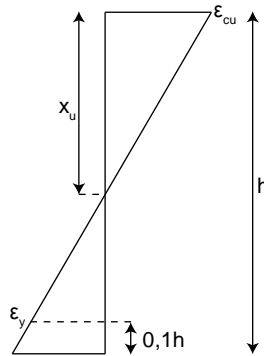


Figure 7.10: Idealized strain distribution over the depth of the considered section.

The depth of the concrete compressive zone, in figure 7.10 indicated by x_u , can be expressed by:

$$x_u = \frac{\epsilon_{cu}}{\epsilon_{cu} + \epsilon_y} d = 0,9 \frac{\epsilon_{cu}}{\epsilon_{cu} + \epsilon_y} h \quad (7.2)$$

Stress-strain relations of Eurocode EN1992-1-1

Eurocode EN1992-1-1 prescribes a parabola-rectangle stress-strain relation for the design of concrete under compression, which is based on the assumption that concrete preserves its full compressive strength up to the ultimate compressive strain ϵ_{cu} is reached. Other similar simplified stress-strain relations may be applied if they are equivalent or more conservative, as for example the bilinear stress-strain relation which has already been discussed in the previous chapters.

The mentioned parabola-rectangle stress-strain relation can be seen in figure 7.11. Besides the corresponding development of stresses in the concrete compressive zone is shown in case the elementary beam element of figure 7.9 is considered and the ultimate compressive strain is reached.

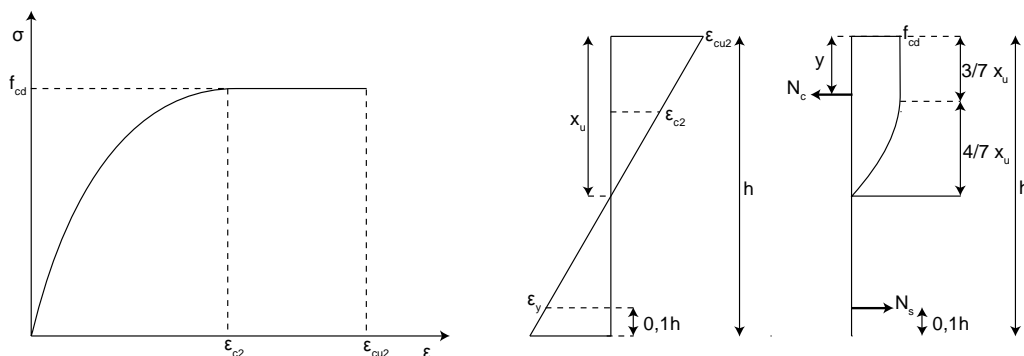


Figure 7.11: Parabola-rectangle stress-strain relation and development of compressive stresses in the concrete compressive zone.

For normal strength concrete ε_{c2} and ε_{cu2} are equal to 0,002 and 0,0035 respectively. The stress-strain relation for $0 \leq \varepsilon_c \leq \varepsilon_{c2}$ is expressed by equation 7.3, for $\varepsilon_{c2} \leq \varepsilon_c \leq \varepsilon_{cu2}$ by equation 7.4. The parameter n in equation 7.3 is equal to 2.

$$\sigma_c = f_{cd} \left[1 - \left(1 - \frac{\varepsilon_c}{\varepsilon_{c2}} \right)^n \right] \quad (7.3)$$

$$\sigma_c = f_{cd} \quad (7.4)$$

The reinforcement ratio ω , which expresses the required reinforcement, follows from horizontal equilibrium of forces.

$$N_s = N_c \quad (7.5)$$

The resultant forces N_s and N_c are defined as:

$$N_s = A_s f_y = 0,9 \omega b h f_y \quad (7.6)$$

$$N_c = \beta x_u b f_{cd} = \beta \frac{\varepsilon_{cu2}}{\varepsilon_{cu2} + \varepsilon_y} h b f_{cd} \quad (7.7)$$

The parameter β is a shape factor which takes account for the shape of the concrete compressive zone and can be derived by numerical integration of equation 7.3 and 7.4.

$$\beta = \frac{\int_0^{\varepsilon_c} \sigma_c d\varepsilon_c}{f_{cd} \varepsilon_c} \quad (7.8)$$

In case the ultimate compressive strain ε_{cu2} is reached, for the parabola-rectangle stress-strain relation of figure 7.11 β is equal to 0,810. After substitution of equation 7.6 and 7.7 into equation 7.5 the required reinforcement ratio ω can be expressed as:

$$\omega = \beta \frac{\varepsilon_{cu2}}{\varepsilon_{cu2} + \varepsilon_y} \frac{f_{cd}}{f_y} \quad (7.9)$$

The ultimate moment capacity can subsequently be determined according to equation 7.10.

$$M_u = A_s f_y (d - y) = 0,9 b h \beta \frac{\varepsilon_{cu2}}{\varepsilon_{cu2} + \varepsilon_y} f_{cd} (0,9 h - y) \quad (7.10)$$

In a similar way as discussed above the maximum effective reinforcement ratio can be derived in case the more conservative bilinear stress-strain relation is taken into account for the design of an arbitrary rectangular cross-section. The bilinear stress-strain relation, just like the development of stresses in the compressive zone, can be seen in figure 7.12. For normal strength concrete ε_{c3} and ε_{cu3} are equal to 0,00175 and 0,0035 respectively.

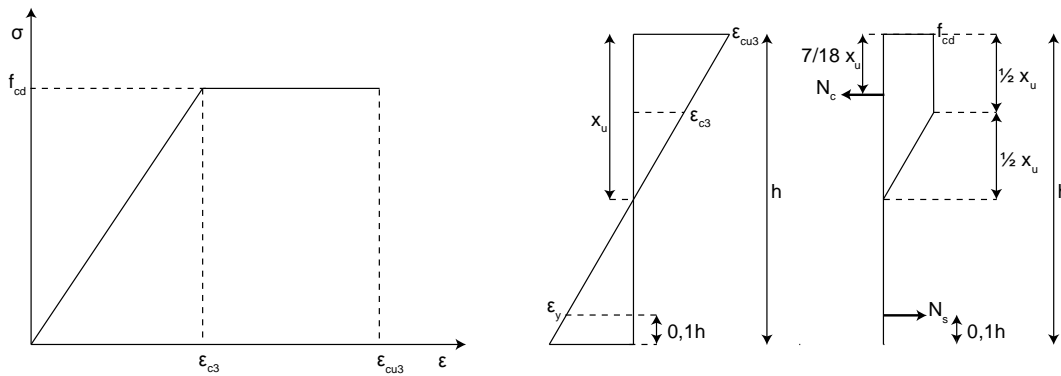


Figure 7.12: Bilinear stress-strain relation and development of compressive stresses in the concrete compressive zone.

Taking the material strength parameters into account which according to the safety format of Eurocode EN1992-2 are applied in the non-linear analyses and were discussed in chapter 5, the required reinforcement ratio ω and ultimate moment capacity M_u can be expressed in a quantitative way. Table 7.5 gives an overview of the required reinforcement ratio ω and moment capacity M_u at the moment that the ultimate compressive strain is reached. Figure 7.13 and 7.14 show the development of the required reinforcement ratio and moment capacity as a function of the compressive strain from the moment that, according to the stress-strain relation, the peak stress f_{cd} is reached.

Material	Strength parameter	Quantitative value
Concrete	f_{yd}	25,3 N/mm ²
Reinforcement	f_y	550 N/mm ²
	E_s	200000 N/mm ²
	ϵ_y	0,00275

Table 7.4: Summary of the relevant strength parameters according to the safety format for non-linear analyses described in Eurocode EN1992-2.

Relation	β [-]	x_u [mm]	y [mm]	ω [-]	M_u [Nmm]
Parabolic-rectangle	0,8095	0,5040h	0,2059h	0,0209	7,961bh ²
Bilinear	0,7500	0,5040h	0,1960h	0,0193	7,481bh ²

Table 7.5: Maximum reinforcement ratio and moment capacity for the parabolic-rectangle and bilinear stress-strain relation.

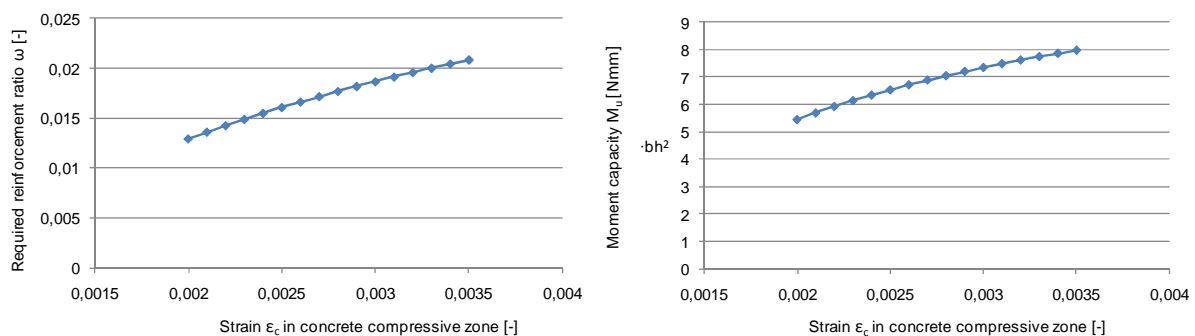


Figure 7.13: Development of the required reinforcement ratio and moment capacity after the peak stress f_{cd} is reached in case a parabola-rectangle stress-strain relation is assumed and the yield strain ϵ_y of reinforcement is reached.

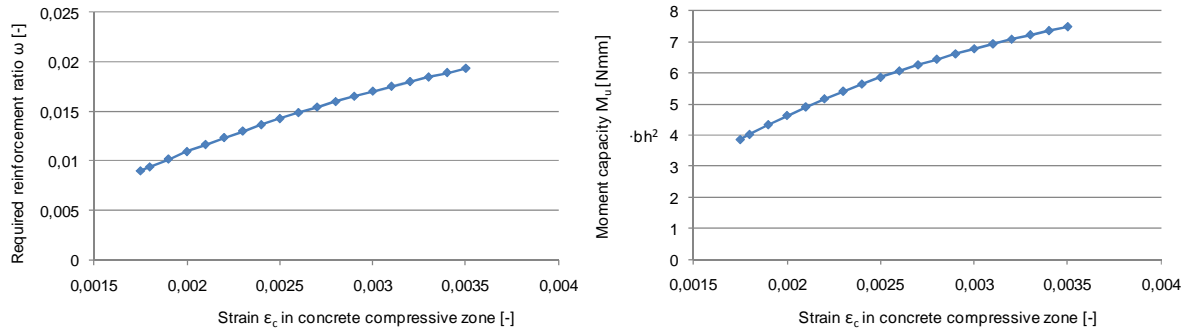


Figure 7.14: Development of the required reinforcement ratio and moment capacity after the peak stress f_{cd} is reached in case a bilinear stress-strain relation is assumed and the yield strain ϵ_y of reinforcement is reached.

Stress-strain relation ATENA

Above discussed stress-strain relations which according to Eurocode EN1992-1-1 are provided for the design of concrete cross-sections show an increasing moment capacity M_u and required reinforcement ratio ω up till the ultimate compressive strain is reached. Since in the applied stress-strain relation in the non-linear analyses the compressive strength linearly decreases to zero up to the ultimate compressive strain, a deviating behavior can be observed. Due to the descending compressive strength, the utilized reinforcement ratio ω and corresponding moment capacity M_u are lower than considered during the design process. This can be illustrated in a similar way as was done in the previous section.

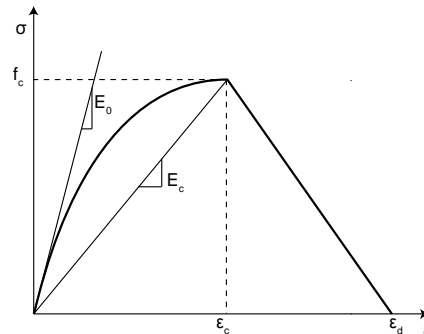


Figure 7.15: Stress-strain relation as applied in the non-linear analyses.

Figure 7.12 shows the applied stress strain-relation for concrete loaded under compression. Up to ϵ_c , which for a compressive strength f_c of $25,3 \text{ N/m}^2$ is equal to $0,001674$, the stress strain relation is defined by equation 7.11.

$$\sigma_c = f_c \frac{kx - x^2}{1 + (k-2)x} \quad x = \frac{\epsilon}{\epsilon_c} \quad k = \frac{E_0}{E_c} \quad (7.11)$$

After reaching the peak stress f_{cd} the compressive strength descends linearly into a softening region up to the limit compressive strain ϵ_d . This limit strain is calculated from a plastic displacement w_d and a band size L_d according to equation 7.12. For the backgrounds of this formula one is referred to ATENA's theoretical manual [1].

$$\epsilon_d = \epsilon_c + \frac{w_d}{L_d} \quad (7.12)$$

To make a clear comparison with the discussed parabolic-rectangle and bilinear stress-strain relations, ϵ_d is set to 0,0035. The development of stresses in the compressive zone at the moment that this strain is reached can be seen in figure 7.16, just like the stress development at a strain equal to ϵ_c .

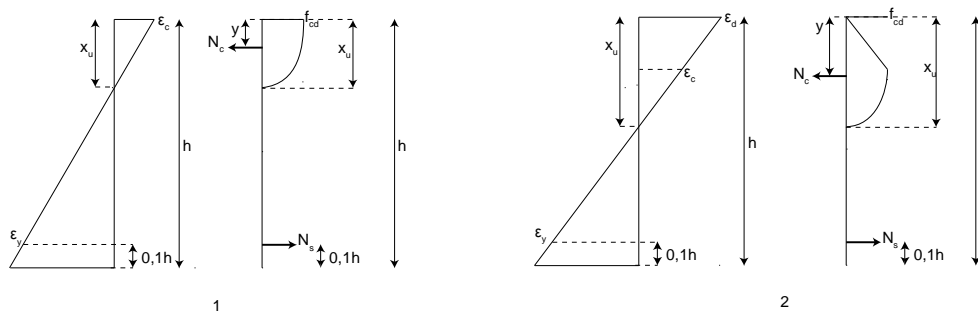


Figure 7.16: Stress development in the concrete compressive zone at a strain equal to ϵ_c and ϵ_d .

It follows clearly from above figure that according to the applied stress-strain relation the capacity to transfer compressive forces in the top of the compressive zone decreases. The influence of this descending capacity can be seen in figure 7.17, where the development of the utilized reinforcement ratio and moment capacity is set out against the compressive strain from the moment that the peak stress f_c is reached.

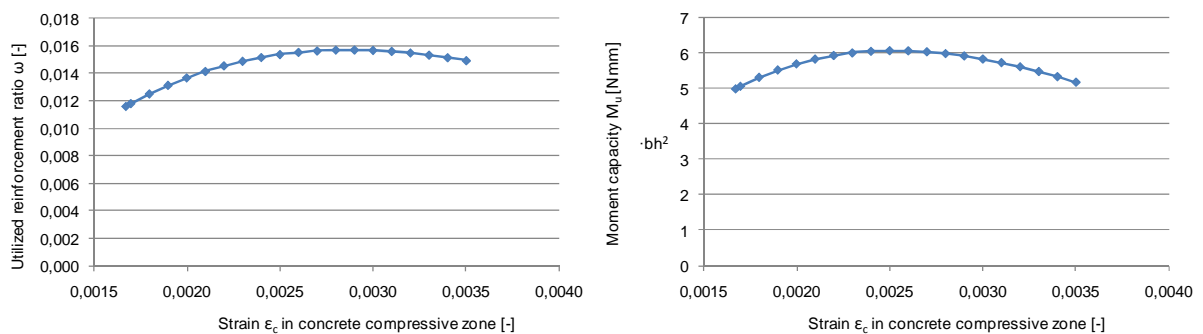


Figure 7.17: Development of the utilized reinforcement ratio and moment capacity after the peak stress f_{cd} is reached.

In figure 7.18 both the reinforcement ratio which is required according to reinforcement design based on a bilinear stress-strain relation, as well as the utilized reinforcement ratio when a descending stress-strain relation is applied in the non-linear analyses are plotted as a function of the compressive strain. The same is done in figure 7.19 for the moment capacity.

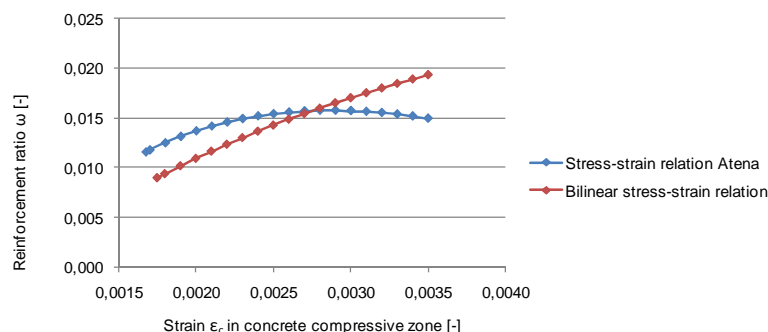


Figure 7.18: Required reinforcement ratio set out against the compressive strain, assuming that the yield strain ϵ_y of reinforcement is reached.

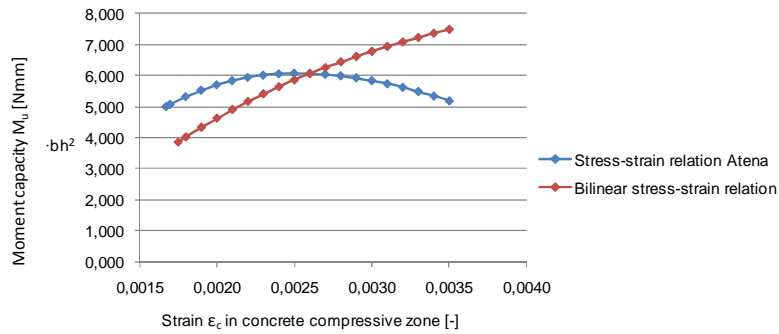


Figure 7.19: Moment capacity set out against the compressive strain, assuming that the yield strain ϵ_y of reinforcement is reached.

It follows from figure 7.18 and 7.19 that due to the descending compressive strength which is taken into account in the non-linear stress-strain relation the moment capacity decreases considerably. As a consequence a smaller amount of reinforcement is utilized to preserve horizontal equilibrium of forces than is initially assumed when for example the bilinear stress-strain relation is taken into account. In combination with the redistribution of internal forces at the top of the compressive zone, which goes hand in hand with the descending compressive strength, a resistance to failure is finally monitored which is lower than the initially assumed design strength. This phenomena will primarily appear in structures which transfer a significant part of their load by bending, since in these structures relative high concentrated compressive forces appear in combination with a significant compressive strain.

Although above analysis is based on an elementary reinforced concrete beam in which all reinforcement is located in the tension zone and reaches its plastic phase, the relative low resistances to failure which follow from the non linear analysis of the considered highly loaded slender specimens can be explained on the basis of the same principles. Also the relative limited stresses which are monitored in the compression reinforcement can be explained by the applied stress-strain relation of concrete in the non-linear analyses. Before the strain is reached in the concrete compressive zone at which the compression reinforcement reaches its full compressive strength, the strength of concrete in the concrete compressive zone has already decreased to such an extent that ATENA assumes that the concrete at the top of the compressive zone has failed in compression. This is illustrated in figure 7.20. It must be emphasized that the maximum stresses in concrete and reinforcement steel do not develop at the same rate.

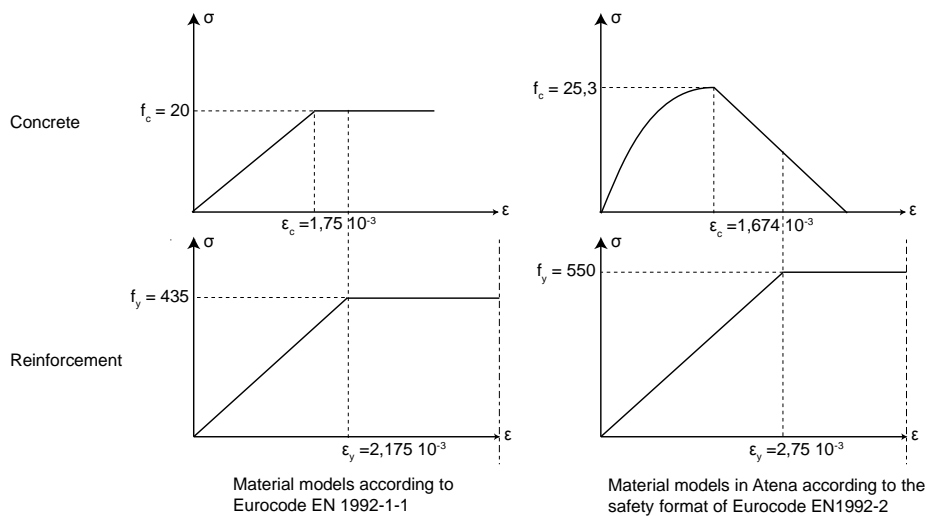


Figure 7.20: Development of compressive stresses in concrete and reinforcement as applied in the design process (left diagrams) and in the non-linear analyses (right diagrams).

Above explanation for the relatively low monitored resistances to failure of heavily loaded slender specimens raises the question if the stress-strain relation which is applied in the non-linear analyses is not too conservative, or on the other hand, if the parabola rectangle or bilinear stress-strain relations do not overestimate the capacity of concrete. A univocal answer to this question cannot be given and requires further research. Fact is that the uniaxial non-linear stress-strain relation which is applied in non-linear analyses gives a more realistic approach of the actual behavior which follows from laboratory tests, which never show a horizontal yield path which can be seen in the parabola-rectangle or bilinear stress-strain relation.

Moreover Eurocode EN1992-1-1 does not always allow the use of the full yield capacity of concrete as indicated in the idealized stress-strain relations. In §6.1 (5) it states that for cross sections in bending which are subjected to an approximately concentric loading, where $e/h < 0,1$, the compression strain should be limited to ϵ_{c2} or ϵ_{c3} . In case such a reduced stress-strain relation has to be taken into account during the design process, the deviation compared to the stress-strain relation which is applied in the non-linear analyses is reduced to a minimum.

7.4 Redistribution of internal forces

Evaluation of reinforcement designs which are based on a design load equal to half and a quarter of the limit load turn out to possess sufficient load bearing capacity, just like specimens which are loaded by a distributed load. Contrary to considered specimens of which reinforcement designs are based on concentrated limit loads, these specimens are during the design process not loaded up to the maximum compressive strength in the normative concrete compressive zone.

However, due to the redistribution of stresses in after crack development which is taken into account in the non-linear analyses, considerable higher compressive stresses in the concrete compressive zone will develop in practice than is assumed during the design process. This is illustrated in figures below for specimen S-3-2 and S-4-2, but a similar phenomenon is observed during linear and non-linear analyses the other considered specimens.

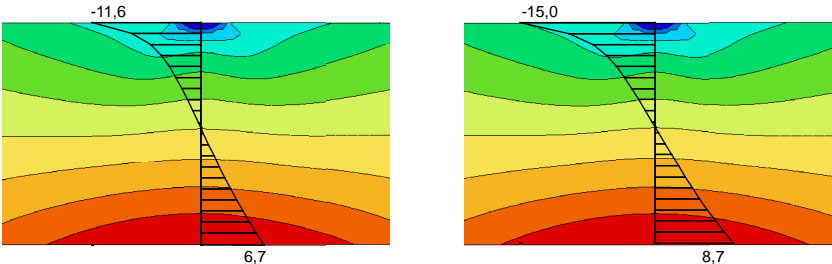


Figure 7.21: Distribution of horizontal stresses at midspan in a linear elastic analysis of specimen S-3-2 in the SLS (left figure, load 246 kN) and ULS (right figure, load 320 kN). Output is in N/mm².

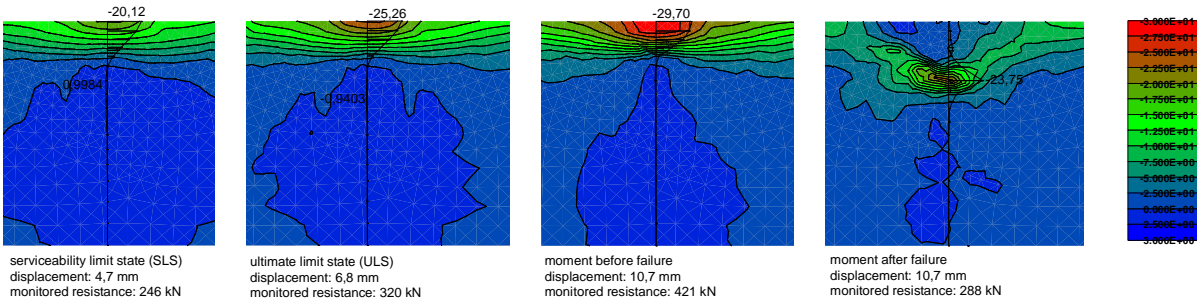


Figure 7.22: Development of horizontal stresses at midspan at several phases of the non-linear analysis of specimen S-3-2. Output is in N/mm².

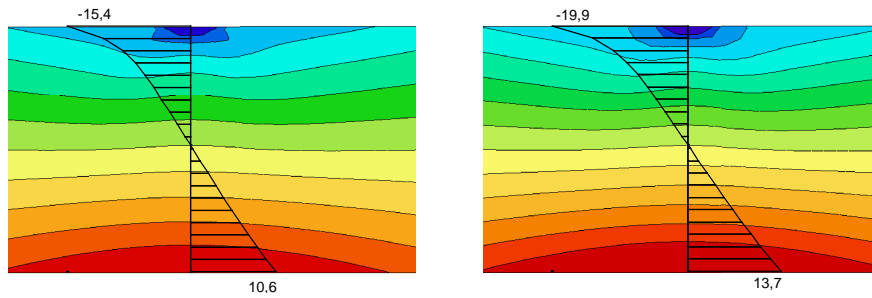


Figure 7.23: Distribution of horizontal stresses at midspan in a linear elastic analysis of specimen S-4-2 in the SLS (left figure, load 246 kN) and ULS (right figure, load 314 kN). Output is in N/mm^2 .

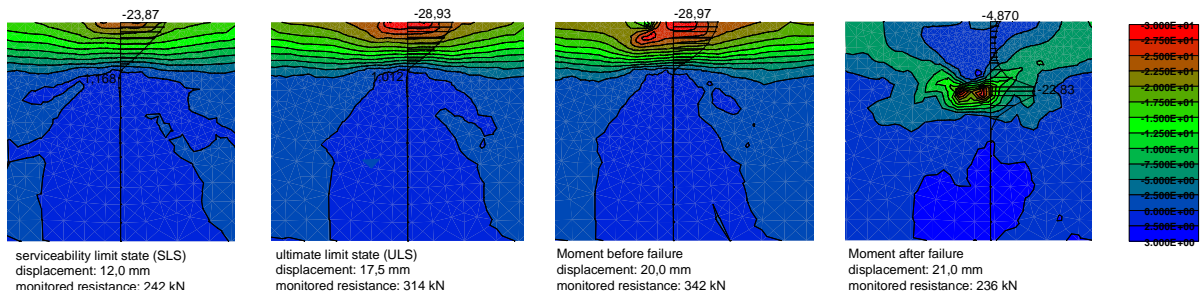


Figure 7.24: Development of horizontal stresses at midspan at several phases of the non-linear analysis of specimen S-4-2. Output is in N/mm^2 .

Since in the linear elastic finite element analyses during the design process a different safety format is applied compared to the non-linear analyses which are applied to evaluate the resistance to failure, values of above figures cannot be compared directly with each other. However, it is still possible to compare the relative stresses in the concrete compressive zone.

Specimen	Load	Linear analyses			Non-linear analyses		
		f_c uniaxial	f_c analysis	relative	f_c uniaxial	f_c analysis	relative
S-3-2	SLS	20	11,6	0,58	25,3	20,12	0,80
	ULS	20	15	0,75	25,3	25,26	1,00
S-4-2	SLS	20	15,4	0,77	25,3	23,87	0,95
	ULS	20	19,9	1,00	25,3	28,97	1,15

Table 7.6: Relative stresses in the concrete compressive zone of specimen S-3-2 and S-4-2 according linear and non-linear finite element analyses. Output is in N/mm^2 .

The fifth and eighth column of table 7.6 show the relative utilized compressive strength capacity in respectively the linear and non-linear analyses. It can be observed that in the non-linear analyses due to redistribution of internal forces considerable higher relative loads are transferred through the concrete compressive zone than was estimated in the linear analyses. Table 7.5 shows a relative increase in size of compressive stresses in the non-linear analyses up to 38% (specimen S-3-2, ULS). The conclusion can be drawn that for the considered specimens which are subjected to flexural deformations, the linear elastic finite element method underestimates the development of compressive stresses which will develop in practice.

References

- [1] Cervenka, V et. al., ATENA Program documentation Part 1: Theory, Prague, Czech Republic, October 2009
- [2] NEN, NEN-EN 1992-1-1, Eurocode 2: Ontwerp en berekening van betonconstructies – Deel 1- 1: Algemene regels en regels voor gebouwen, Delft, The Netherlands, December 2007

8 Shrinkage and support settlements

8.1 Introduction

To approach realistic concrete material behavior the tensile strength of concrete is taken into account in all non-linear analyses which are discussed in the previous chapter. According to code provisions however, the favorable effect of the concrete tensile strength was not taken into account during the design process of the required reinforcement. The resistance to failure which follows from a non-linear analysis of a specific specimen can therefore be seen as an upper-bound approximation.

Any unfavorable effect caused by thermal deformation, differential support settlements or shrinkage will result in the development of cracks, reducing the favorable contribution of the concrete tensile strength to the resistance to failure. This chapter focuses shortly on the influence of above phenomena on the resistance to failure which follows from non-linear analyses of specimen of which the reinforcement is determined on basis of the linear elastic finite element method. It is generally known that these phenomena result in the development of cracks, both during the hardening of concrete as well as during the lifetime of a structure. However, a specimen, or structure in general, should not immediately loose part of its load bearing capacity due to these cracks.

In this chapter the influence of shrinkage and differential support settlements are analyzed in two separate parts. The first part focuses on development and influence of cracks as a result of shrinkage in early aged concrete. The second part focuses on the developments and influence of differential support settlements during loading of a specimen.

8.2 Shrinkage

Shrinkage of concrete is a process which can develop during the hardening of early age concrete or during the lifetime of a structure due to changes in the environmental humidity. In this section primarily the first mentioned type of shrinkage is considered. The chemical processes which occur during hardening of young concrete are accompanied by volume and temperature changes. Hydration of cement is a highly exothermic process and thermally activated reaction. The exothermic nature of the chemical reaction leads to heat generation which may result in high temperature rises. As the rate of hydration slows down, the temperature decreases resulting in thermal shrinkage which induces significant tensile stresses. Furthermore this hydration process is accompanied by a volume reduction usually called autogeneous shrinkage, which develops during the hardening of concrete in the early days after casting and is caused by the internal consumption of water by hydration of cement. For the considered normal strength concrete C37/30 however, autogeneous shrinkage is small and is included with drying shrinkage [5].

If concrete is restrained, shrinkage can result in the development of cracks. In the last decades advanced finite element methods have been developed which link thermal mechanical to structural mechanical numerical analyses which are capable to take the time-dependent temperature effect that causes shrinkage into account. Also ATENA offers the possibility to apply advanced creep and shrinkage analyses, although this is only possible for three-dimensional models. Since a too limited amount of time was available to transform the in chapter 5 discussed two-dimensional models to a three dimensional model, a more fundamental approach is applied to analyze the effect of shrinkage on the resistance to failure.

As discussed above, shrinkage during the hardening of concrete can in the worst case result in the development of cracks which can affect the structural behavior or lead to a decay of structural performance. Therefore the effect of shrinkage is taken into account in the non-linear analyses by modeling an initial crack. The effect of such a crack is analyzed at two critical locations. One flexural vertical crack is modeled at midspan, a second diagonal crack is modeled near the supports. Since cracks which were modeled over the full depth of the specimens immediately resulted in a significant decay of the resistance to failure, the cracks are modeled up to 100 mm below the top side of the specimens.

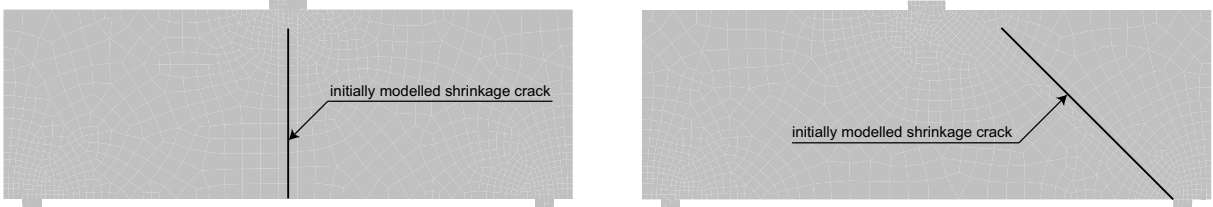


Figure 8.1: Deliberately modeled shrinkage cracks before appliance of the external top load. Left: flexural crack at midspan. Right: shear crack in the compressive strut.

The shrinkage cracks are modeled by interface elements. These elements, which are based on the theory of Mohr-Coulomb, are defined such that they possess a certain friction which represents the shear transfer mechanism by aggregate interlock.

Parameter	Notation	Value
Normal stiffness [MN/m ³]	K_{nn}	$3 \cdot 10^5$
Tangential stiffness [MN/m ³]	K_{tt}	$3 \cdot 10^5$
Tensile strength [N/mm ²]	f_t	0
Cohesion [N/mm ²]	C	0
Friction coefficient [-]	ϕ	0,1
Minimal normal stiffness [MN/m ³]	K_{nnmin}	$3 \cdot 10^2$
Minimal tangential stiffness [MN/m ³]	K_{ttmin}	$3 \cdot 10^2$

Table 8.1: Interface material properties for the modeled crack.

In the previous chapter it has already been discussed that the resistance of a number of specimens which followed from the non-linear analyses turned out to be lower than the actual design strength. These specimens are not considered furthermore. The analysis results of the remaining considered specimens can be seen in table 8.2. The third, fifth and seventh column show the monitored resistance in case no, a vertical and a diagonal crack are modeled respectively. Next to these columns the design strength is expressed as a ratio of the monitored resistance.

It can be observed that the overall effect of the modeled cracks is limited. The vertical modeled crack has only a significant influence in the slender specimen S-4-2, which already showed less overcapacity in the non-linear analysis in which no initial crack were modeled. Influence of diagonally modeled cracks can be observed in the heavily loaded deep specimens which show a relative direct load transfer to the supports. Due to the modeled diagonal crack, which runs parallel to the compressive strut, these specimens fail prematurely due to shear.

Specimen	Design load D	Resistance R without crack	R/D	Resistance R vertical crack	R/D	Resistance R diagonal crack	R/D
S-1-1	651 kN	676 kN	1,04	674 kN	1,04	564 kN	0,87
S-1-2	326 kN	498 kN	1,53	492 kN	1,51	492 kN	1,51
S-1-3	162 kN	375 kN	2,30	360 kN	2,22	370 kN	2,28
S-1-4	651 kN	706 kN	1,08	678 kN	1,04	575 kN	0,88
S-1-5	382 kN/m	572 kN/m	1,50	563 kN/m	1,47	538 kN/m	1,41
S-2-2	323 kN	428 kN	1,33	425 kN	1,32	417 kN	1,29
S-2-3	162 kN	273 kN	1,69	263 kN	1,62	271 kN	1,67
S-2-5	239 kN/m	354 kN/m	1,48	349 kN/m	1,46	356 kN/m	1,49
S-3-2	320 kN	421 kN	1,32	300 kN	1,07	279 kN	1,15
S-3-3	160 kN	252 kN	1,56	244 kN	1,53	250 kN	1,56
S-3-5	172 kN/m	292 kN/m	1,70	290 kN/m	1,69	279 kN/m	1,62
S-4-2	314 kN	342 kN	1,09	307 kN	0,98	342 kN	1,09
S-4-3	157 kN	229 kN	1,46	223 kN	1,42	228 kN	1,45
S-4-5	110 kN/m	169 kN/m	1,54	114 kN/m	1,04	137 kN/m	1,25
S-5-1	696 kN	904 kN	2,21	892 kN	1,28	583 kN	0,84
S-5-2	348 kN	852 kN	2,45	834 kN	2,40	592 kN	1,70
S-5-3	174 kN	840 kN	4,83	823 kN	4,73	591 kN	3,40
S-5-4	696 kN	918 kN	1,32	861 kN	1,24	524 kN	0,75
S-5-5	409 kN/m	582 kN/m	1,42	565 kN	1,38	574 kN	1,40

Table 8.2: Influence of shrinkage cracks on the resistance to failure.

8.3 Differential support settlements

8.3.1 Considered specimens

The so far considered single-span specimens are not sensitive to differential support settlements, since no significant redistribution of membrane forces will appear. To examine the influence of differential support settlements therefore two-span, statically undetermined, specimens are considered. It is generally known that, compared to their statically determined counterpart, statically undetermined deep beams are more sensitive to differential support settlements and do not possess a great amount of deformation capacity. The internal load distribution is very dependent on the stiffness of the supports. Differential support settlements can therefore result in a considerable development of cracks and in the worse case even result in loss of load bearing capacity.

In the past extensive research has already been performed to improve the understanding of the structural behavior of continuous deep beams and their load transfer mechanisms, for example by Asin [1]. Load transfer in two-span specimens can generally be simplified by three equilibrium systems, which can be seen in figure 8.2. These systems are interdependent and their individual contribution to the resistance to failure depends on their stiffness.

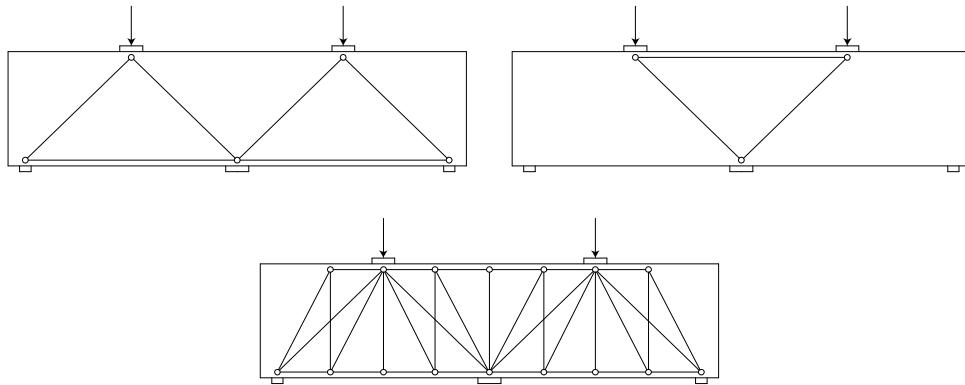


Figure 8.2: Load bearing systems in two span specimens: strut-and-tie action with bottom reinforcement (top, left), strut-and-tie action with top reinforcement (top, right), combination of strut-and-tie action with truss-action (bottom, middle) [1].

Reinforcement design with LE-FEM is based on a single, very specific linear elastic distribution of membrane forces in which each of the above mechanisms contributes specifically to the load bearing capacity of a specimen. Differential support settlements can however significantly change the assumed contribution of each mechanism. It is analyzed to what extent two-span specimens of which reinforcement is determined with LE-FEM are capable to resist differential support settlements redistribute internal forces.

In total two specimens with a distinctive geometry are considered of which the redistribution capacity due to differential support settlements is analyzed. For each specimen two reinforcement configurations are taken into account, one which is based on a relative high concentrated top load of 550 kN and one which is based on a smaller concentrated top load of 200 kN. These loads have been chosen such that in the linear elastic finite element analyses nowhere in the considered two-span specimens the concrete compressive strength f_{cd} is exceeded, and no compressive reinforcement is required. As a consequence the non-linear analysis results are not influenced by disfunctioning of compression reinforcement, as was observed during analyses of single-span specimens in chapter 7.

The overall geometry is based on the same principles as the single-span specimens and will therefore not be discussed in detail again. A distributed introduction of reaction forces at the supports is applied to exclude immediate concrete crushing in ATENA or unrealistic peak stresses during the reinforcement design with LE-FEM. Supports at the ends of a specimens have a width of 100 mm, the width of the middle support is equal to 200 mm. Specimens are loaded at both midspans by an identical load which are introduced over a width of 200 mm. The centre lines of the loads are positioned exactly at the midpoint between the centre lines of the supports. The overall geometry of a two-span specimen can be seen in figure 8.3. The specific geometrical properties of the considered specimens are shown in table 8.3.

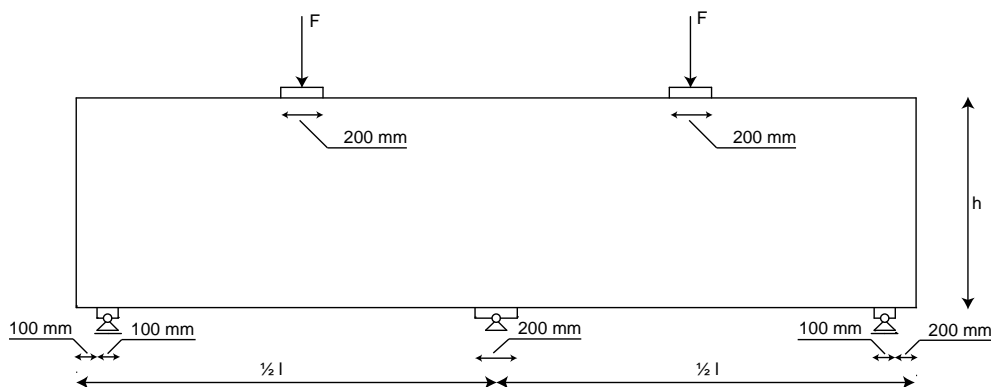


Figure 8.3: Overall geometry of the considered two-span specimens.

Specimen	Length l [mm]	Depth h [mm]	Width t [mm]	Design load [kN]
S-6-1	4000	1000	200	550
S-6-2	4000	1000	200	200
S-7-1	6000	1000	200	550
S-7-2	6000	1000	200	200

Table 8.3: Geometrical properties of the considered two-span specimens.

8.3.3 Reinforcement design with LE-FEM

Reinforcement design of two-span specimens with LE-FEM is determined in a similar way as discussed in chapter 4. A basic reinforcement mesh with a bar diameter of 5 mm and a centre to centre distance of 150 mm is applied in each specimen, finished by a specific amount of additional reinforcement according to the output of the linear elastic finite element method.

To exclude numerical problems and prohibited rotation, supports are during the linear elastic analyses once again modeled by distributed springs. Contrary to the considered single-span specimens, the support stiffness of multi-span beams can have a considerable influence of the distribution of membrane forces and support reactions. The in chapter 4 derived spring stiffness of $6,6 \text{ MN/m}^2$ turned out to be such stiff, that it has no significant influence on the distribution of membrane forces.

8.3.4 Reinforcement designs

The reinforcement configuration of the considered two-span specimens can be seen in the next sections. Also the total amount and distribution of reinforcement which is required according to the linear elastic finite element method is shown. Individual reinforcement bars are positioned such that they correspond to this distribution as well as possible, although it is inevitable that some concessions had to be made.

Specimen S-6-1

The according to the linear elastic finite element method required reinforcement corresponding to a design load of 550 kN can be seen in figure 8.4.

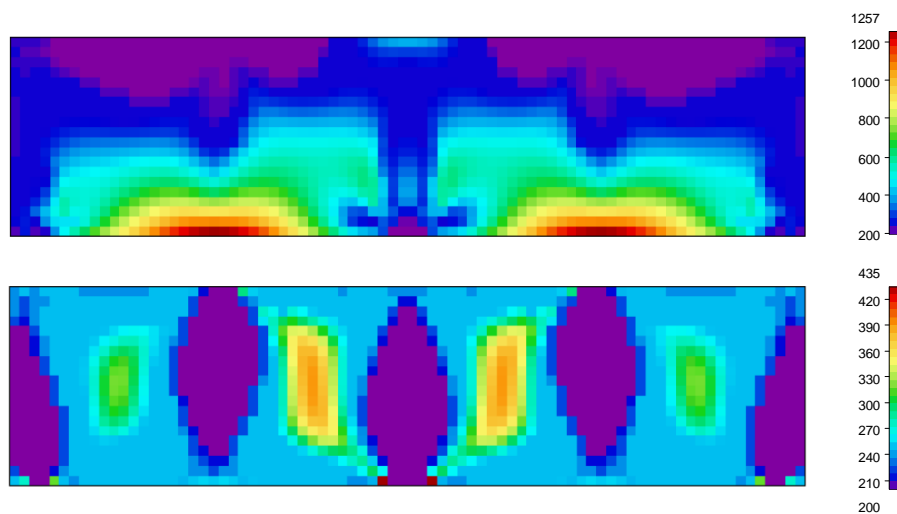


Figure 8.4: Required reinforcement for a design load of 550 kN in longitudinal direction (upper figure) and in transversal direction (lower figure). Output is given in mm^2/m .

The corresponding reinforcement drawing can be seen in figure 8.5. Due to symmetry only the left half of specimen S-6-1 is shown.

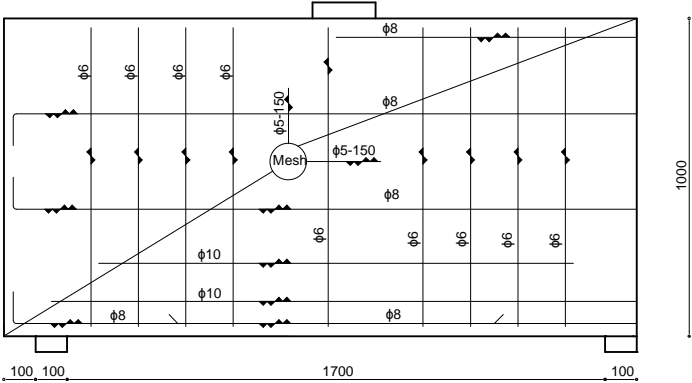


Figure 8.5: Reinforcement drawing of specimen S-6-1. Due to symmetry only the left half of the specimen is shown.

Specimen S-6-2

The according to the linear elastic finite element method required reinforcement corresponding to a design load of 200 kN can be seen in figure 8.6.

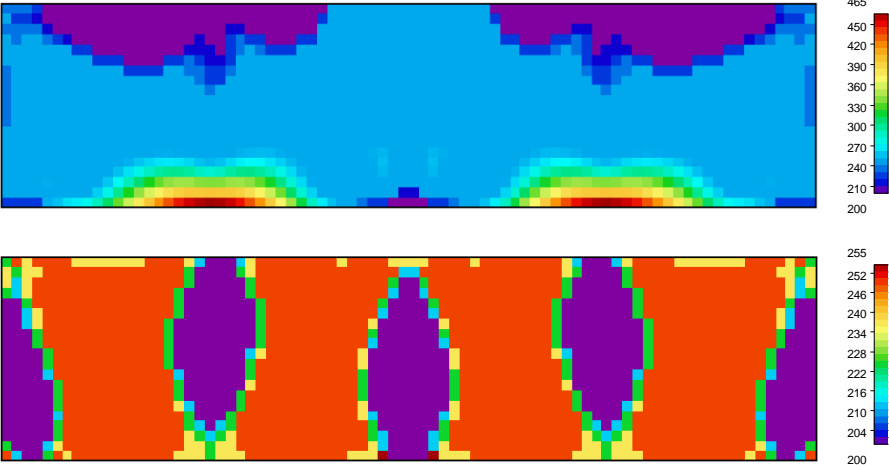


Figure 8.6: Required reinforcement for a design load of 200 kN in longitudinal direction (upper figure) and in transversal direction (lower figure). Output is given in mm²/m.

The corresponding reinforcement drawing can be seen in figure 8.7. Due to symmetry only the left half of specimen S-6-2 is shown.

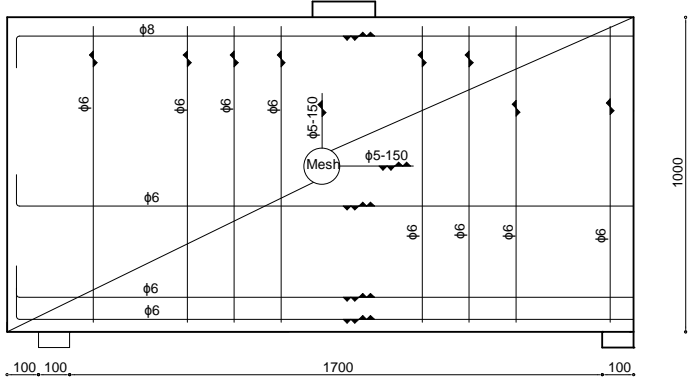


Figure 8.7: Reinforcement drawing of specimen S-6-2. Due to symmetry only the left half of the specimen is shown.

Specimen S-7-1

The according to the linear elastic finite element method required reinforcement corresponding to a design load of 550 kN can be seen in figure 8.8.

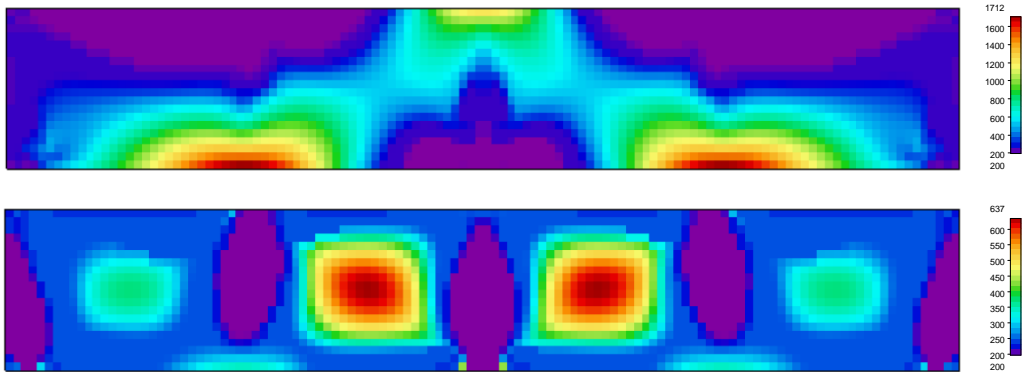


Figure 8.8: Required reinforcement for a design load of 550 kN in longitudinal direction (upper figure) and transversal direction (lower figure). Output is given in mm²/m.

The corresponding reinforcement drawing can be seen in figure 8.9. Due to symmetry only the left half of specimen S-7-1 is shown.

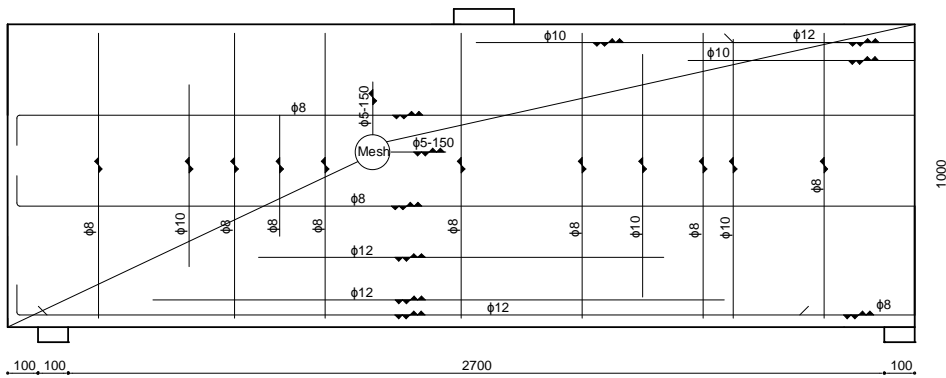


Figure 8.9: Reinforcement drawing of specimen S-7-1. Due to symmetry only the left half of the specimen is shown.

Specimen S-7-2

The according to the linear elastic finite element method required reinforcement corresponding to a design load of 200 kN can be seen in figure 8.10.

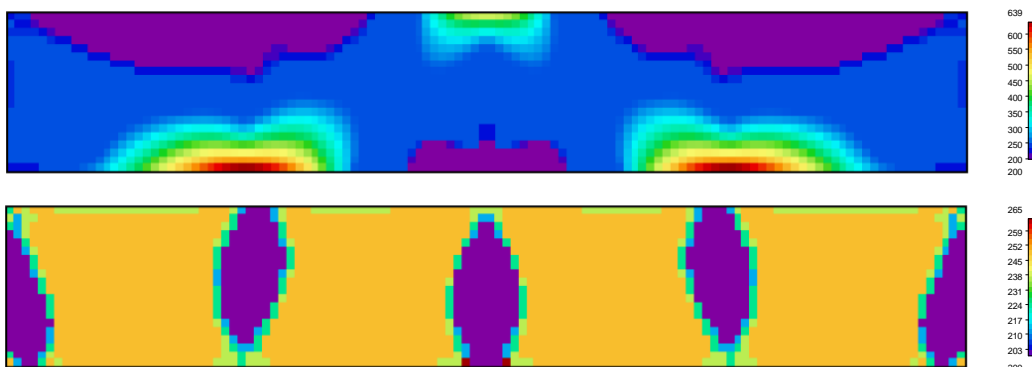


Figure 8.10: Required reinforcement for a design load of 550 kN in longitudinal direction (upper figure) and transversal direction (lower figure). Output is given in mm²/m.

The resultant forces R at the supports depend on the size of the applied external load F and the specimens' dead weight. The general qualitative size of the support reactions is expressed in figure 8.12, where the geometry of a two-span specimen is schematized to a one-dimensional element.

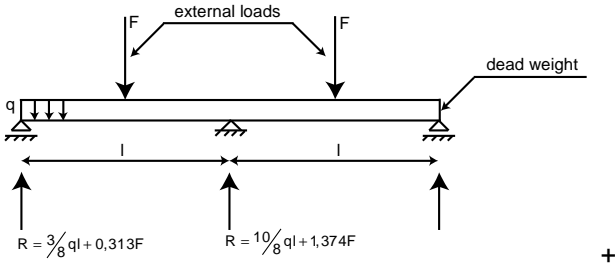


Figure 8.12: Qualitative expression of the support reactions for a two-span specimen. The span is defined as the distance between the centre lines of the supports.

It must be emphasized that due to redistribution of forces as a result of unequal support stiffnesses, the final reaction R at the support at which a spring is modeled will be lower than is assumed during the calculation of the spring stiffness, resulting in a somewhat smaller support settlement during the non-linear analyses.

The cross-sectional area of the spring, in equation 8.2 expressed by the variable A , is set equal to the surface of the supports. For the length l of the spring an arbitrary value of 500 mm has been chosen. To exclude that an arbitrarily chosen spring length would have a considerable influence on the resistance to failure, the resistance to failure of specimen S-6-1 has also been verified with a spring length of respectively 200 and 1000 mm. Analysis results showed a scatter of only 2%.

In table 8.4 an overview can be seen of the applied spring stiffnesses in the several non-linear analyses.

Support settlement [mm]	Location settlement	Spring stiffness per specimen [N/mm ²]			
		S-6-1	S-6-2	S-7-1	S-7-2
5	end	881	346	894	364
5	middle	1923	720	1941	738
10	end	440	173	447	182
10	middle	961	360	970	369
20	end	220	87	224	91
20	middle	481	180	485	185

Table 8.4: Applied spring stiffnesses to model differential support settlements.

Analysis results

All non-linear analyses in which differential support settlements are taken into account show similar results. In each analysis a regression of the resistance to failure is observed, even if only a relative small support settlement of 5 mm is taken into account. In table 8.5 an overview can be seen of the resistances to failure which follow from the non-linear analyses. Next to it the found resistance is expressed as a percentage of the design load.

Support settlement [mm]	Location settlement	Resistance per specimen [kN]							
		S-6-1		S-6-2		S-7-1		S-7-2	
-	-	660	1,2	430	2,15	563	1,02	359	1,80
5	outer	472	0,86	317	1,59	487	0,89	311	1,56
10	outer	304	0,55	243	1,22	429	0,78	260	1,3
20	outer	297	0,54	182	0,91	369	0,67	182	0,91
5	middle	597	1,09	333	1,66	506	0,92	347	1,74
10	middle	516	0,94	236	1,18	502	0,91	296	1,48
20	middle	454	0,82	191	0,96	442	0,80	203	1,02

Table 8.5: Resistances to failure which follow from the non-linear analyses. The first row with analysis results relates to an analysis in which no support settlements are taken into account.

Table 8.5 shows that especially the specimen of which reinforcement is based on a design load of 550 kN show less capacity to overcome differential support settlements. Except the analysis of specimen S-6-1 in which a deflection of the middle support of 5 mm is taken into account, all analyses show a regression of the resistance to failure to a value lower than the original design load. This is primarily caused by the fact that concrete, which strength turns out to be normative, in some areas is already almost loaded up to its design strength f_{cd} when a design load of 550 kN is applied. The capacity left to redistribute membrane forces due to differential support settlements is therefore very limited.

In figure 8.13 the load-displacement diagrams which follow from non-linear analyses of specimen S-6-1 and S-7-1 can be seen. Due to its more flexural behavior the more slender specimen S-7-1 requires a larger top displacement before failure is initiated. Although specimen S-7-1 behaves less stiff, no considerable reduced sensitivity to differential support settlements is observed.

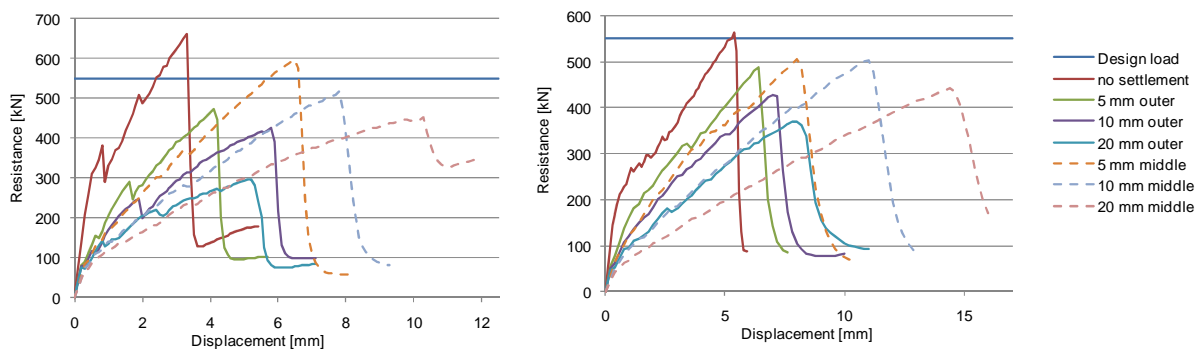


Figure 8.13: Load-displacement diagrams which follow from non-linear analyses of specimen S-6-1 (left diagram) and S-7-1 (right diagram). For clarity, graphs which belong to analyses in which settlement of the middle support is analyzed are indicated by a dashed line.

Since non-linear analyses are primarily performed to analyze the effect of differential support settlements on the resistance to failure, analyses were interrupted after the normative failure mode appeared. Thus, the ends of the graphs in figure 8.13 do not mean that the resistance to failure of a specimen has completely been reduced to zero. After the normative failure mechanism has appeared, still a certain load bearing capacity is monitored after continuous prescribed displacement, primarily due to yielding of the reinforcement.

The structural response which follows from the non-linear analyses of specimens in which no differential settlements are taken into account seems to follow the schematized structural mechanisms which were shown in figure 8.2. Flexural cracks develop within a view load steps, both at midspan and above the middle support. In subsequent load steps diagonal shear cracks develop, first between middle support and the loading point, later on also between the loading point and the outer support. Specimen S-6-1 shows a sudden development of shear cracks which involves a small regression in the monitored resistance, visible in the load-displacement diagram in figure 8.13. Specimen S-7-1

shows a more uniform development of shear cracks. Until failure the amount and width of shear cracks increases. Failure is finally caused by shear failure of the concrete compressive strut between the loading point and the middle support. An global overview of crack development can be seen in figure 8.14 and 8.15. Besides, the development of principal compressive stresses is plotted.

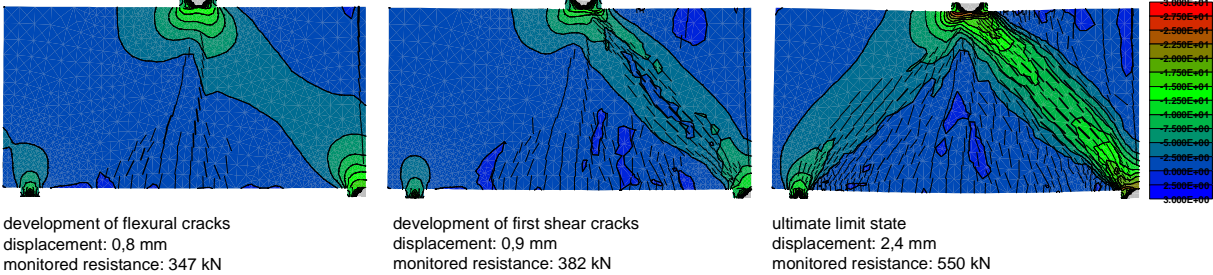


Figure 8.14: Development of cracks in specimen S-6-1 in case no differential support settlements are taken into account. Shown displacements are magnified by a factor 10, output is in N/mm^2 .

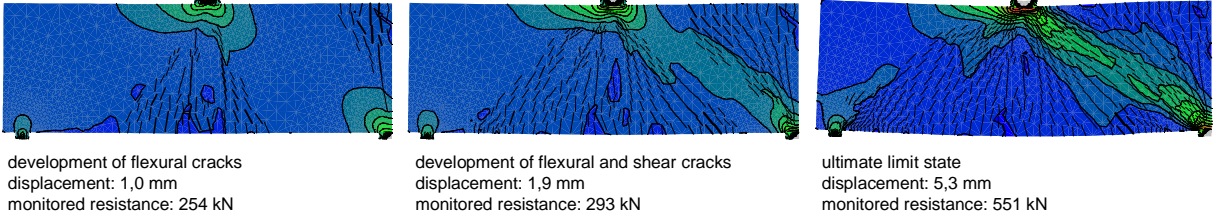


Figure 8.15: Development of cracks in specimen S-7-1 case no differential support settlements are taken into account. Shown displacements are magnified by a factor 10. A same scale of stresses is applied as in figure X.X. Output is in N/mm^2 .

In case differential support settlements are taken into account in the non-linear analyses, a considerable change in the crack pattern can be observed which alludes to redistribution of forces. The redistribution capacity of specimen S-6-1 and S-7-1 is however too limited to maintain the required load-bearing capacity. Due to settlement of the outer support more load is transferred by the top reinforcement above the middle support. As a consequence the top reinforcement reaches its plastic phase and starts to yield, resulting in a considerable increase in the width of cracks and premature failure. Figure 8.16 shows the crack pattern of specimen S-6-1 and S-7-1 for a settlement of the outer support of 5 mm, at the increment before failure appears. For comparison, also the development of cracks is shown when an approximately similar resistance is monitored in case no support settlements are taken into account.

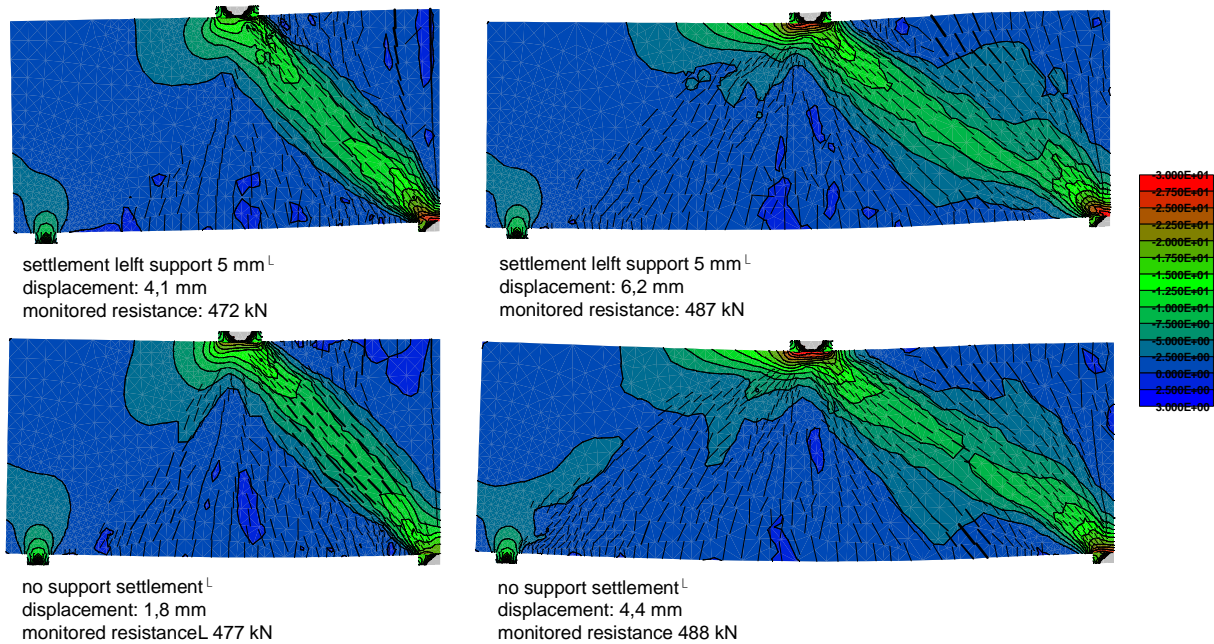


Figure 8.16: Crack development in specimen S-6-1 and S-7-1 with differential settlement of the outer support of 5 mm (upper figures) and without (bottom figures). Shown displacements are magnified by a factor 10, output is in N/mm².

Figure 8.17 shows the redistribution of load transfer to the supports up to the moment of failure in case a differential support settlement of the outer support of 5 mm is taken into account. The diagrams show clearly that in case of a differential settlement of the outer support, relatively more load is transferred to the middle support. Disturbances in the diagrams are caused by a regression of the monitored resistances due to cracking of the concrete.

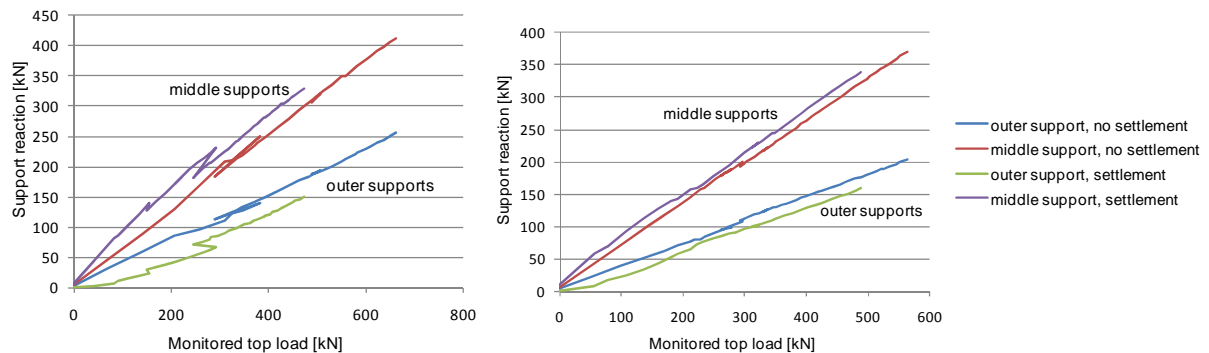
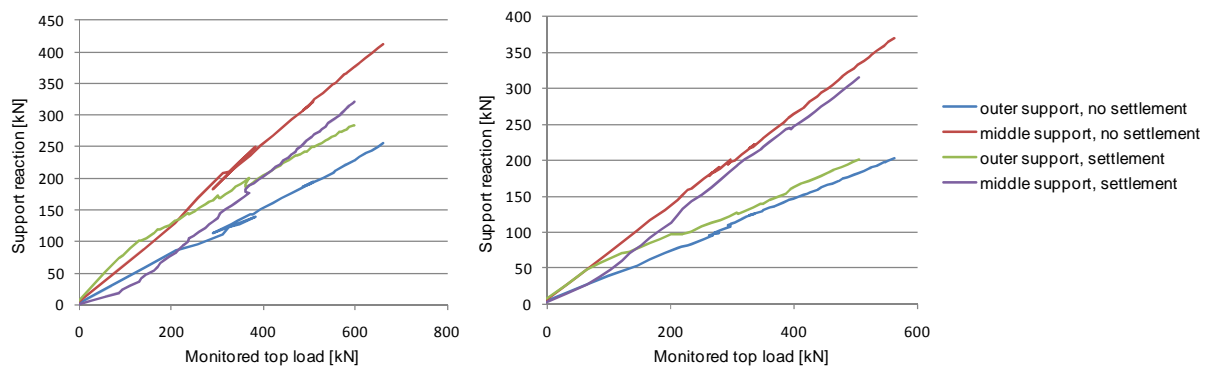
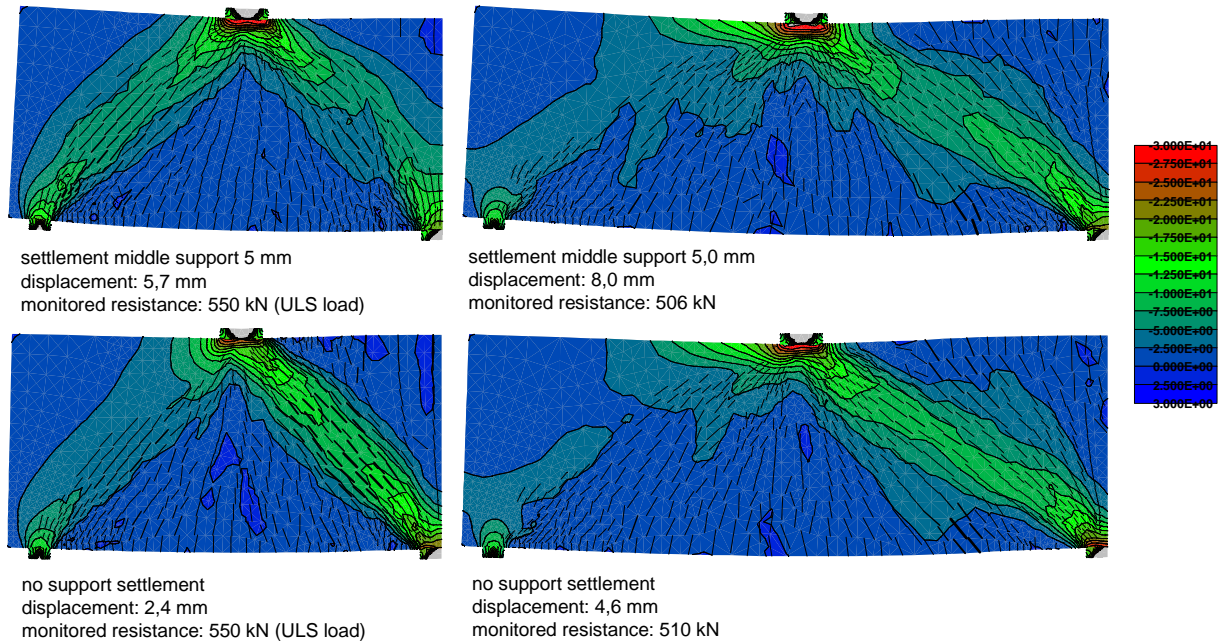


Figure 8.17 Redistribution of load transfer to the supports in specimen S-6-1 (left diagram) and S-7-1 (right diagram) in case a differential support settlement of 5 mm at the outer support is taken into account.

Differential settlement of the middle support results in an increase in the load transfer to the outer supports. The amount and width of cracks above the middle support decrease, since fewer load is transferred by the top reinforcement. Conversely, a considerable increase of the amount and width of flexural cracks at midspan and shear cracks in the compression strut between the loading point an outer support can be observed. Figure 8.18 gives an impression of the crack development. For comparison, also the development of cracks is shown when an approximately similar resistance is monitored in case no support settlements are taken into account.



Due to differential settlement of the middle support a change in the normative failure mode can be observed. Most of the load is transferred by the bottom reinforcement, which starts to yield. An increase in the width of cracks and flexural deformation can be observed. Flexural deformation finally results in compressive failure of the concrete in the compressive zone at midspan, a failure mode similar to the one discussed in chapter 7.

Specimen S-6-2 and S-7-2, which reinforcement is determined on a design load of 200 kN, show a higher redistribution capacity before the load bearing capacity reduces to a value lower than the original design load. This can be explained by the fact that at a design load of 200 kN by no means the normative concrete compressive strength f_{cd} is reached. In case of small differential settlements sufficient capacity is left to resist the design load, although this involves a considerable increase in the width of cracks.

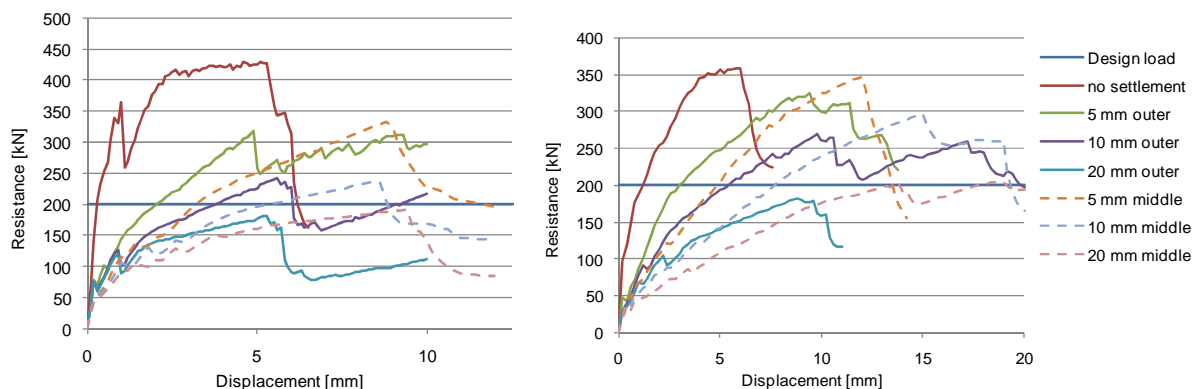


Figure 8.20: Load-displacement diagrams which follow from non-linear analyses of specimen 11-2 (left diagram) and 12-2 (right diagram). To be clear, graphs which belong to analyses in which settlement of the middle support is analyzed are indicated by a dashed line.

Redistribution of internal forces and crack development in analyses of specimen S-6-2 and S-7-2 in which differential settlements are taken into account show great similarities with the already discussed specimens S-6-1 and S-7-1. Crack development is somewhat more concentrated at the midspan and above the middle support, where yielding of the reinforcement is observed. Exceeding of the maximum yield strain of reinforcement which is located above the supports characterizes the failure mode of specimens in which differential settlement of the outer support is taken into account. The failure mode which is found by specimens where differential settlement of the middle support is considered is characterized by compressive failure of concrete in the concrete compressive zone at midspan.

Code provisions

Geotechnical design codes provide requirements in which limiting values for settlements of foundations are defined. The Dutch national annex of Eurocode EN1997-1, in which the geotechnical design provisions are stated, refers to relevant clauses of the former Dutch code NEN 6740 with respect to allowed differential settlements. According to NEN 6740 in the serviceability limit state a maximum differential settlement equal to a value of $1/300$ times the distance between the centerlines of the supports is allowed. This value must be seen as an upper bound, since more stringent rules may apply if the supported structure is very sensitive to differential settlements. For the considered variants of specimen S-6, which have a distance of 1850 mm between the centerlines of the middle and outer support, a differential settlement of 6,2 mm should be possible. The considered variants of specimen S-7, of which the distance between the centerlines is equal to 2850 mm, should be able to resist an differential settlement of 9,5 mm.

Although this analysis of differential support settlement focuses primarily on the ultimate limit state, while provisions in NEN 6740 relate to the serviceability limit state, a quick comparison between the above values and the analysis results in table 8.5 shows that most specimen will show a considerable decay of structural performance or even failure before a permissible differential settlement of 6,2 or 9,5 mm is reached.

Conclusions

Non-linear analyses of the four considered two-span specimen show that differential support settlements next to a considerable increase in the width of cracks immediately involve a regression of the monitored resistance to failure, often to a value which is even lower than the initial design load. In this respect it can be concluded that specimen of which reinforcement is determined with the linear elastic finite element method have very limited, or even no capacity to redistribute internal forces in

case of differential settlements. It must be emphasized that this conclusion is based on a limited set of considered specimen and that further research is required.

References

- [1] Asin, M, The behavior of reinforced continuous deep beams, Delft, The Netherlands, 1999.
- [2] NEN 6740, Geotechniek – TGB 1990 – Basiseisen en belastingen, Delft, The Netherlands, September 2006
- [3] NEN, NEN-EN 1997-1, Eurocode 7: Geotechnisch ontwerp – Deel 1: Algemene regels, Delft, The Netherlands, March 2005
- [4] Rots J.G., Hendriks M.A.N., Finite elements in Civil Engineering Applications, Delft, The Netherlands, 2002
- [5] Newman, J. et. al., Advanced Concrete Technology, Oxford, United Kingdom, 2003

9 Conclusions and recommendations

9.1 Introduction

Analyses of specimens of which reinforcement is determined according to the linear elastic finite element method (LE-FEM) have led to a number of conclusions and recommendations related to the use of this method in the design process of reinforced structures. A point by point overview of these conclusions and recommendations is given in the next two sections.

9.2 Conclusions

- Assumed linear elastic material behavior of concrete during reinforcement design with LE-FEM does not approach concrete behavior in an accurate way.

Cracked reinforced concrete loaded in compression behaves considerably stiffer than cracked reinforced concrete which is loaded in tension. As a consequence, the linear elastic, isotropic approach of concrete material behavior results in the development of load transfer mechanisms which deviate from the expected mechanisms that will develop in practice.

- No direct relation is found between the observed failure mode and the moment distribution which is no longer shifted to prevent failure as a result of possible appearance of inclined bending cracks in the ultimate limit state. Concrete crushing in the concrete compressive zone, caused by flexural deformations, turned out to be the normative failure mode for the considered specimens.

In the considered single-span specimens of which reinforcement was determined with LE-FEM a relative limited amount of longitudinal reinforcement had to reach the supports. The presence of transversal bars and bars of the applied reinforcement mesh which cross a possible inclined bending crack reduce the direct influence of the development of such a crack considerably.

- Especially heavily loaded specimens which are subjected to bending and in which according to LE-FEM compression reinforcement is required in the concrete compressive zone, can be considered to be unsafe. Failure occurs at monitored loads which in the worst case are 25% lower than the assumed design load.

Premature failure was primarily caused by the relative conservative shape of the applied stress-strain relation in the non-linear analyses and the limited development of stresses in the compression reinforcement, while concrete at the same moment already reached its ultimate compressive strength. It must be emphasized that generally, independent of the applied reinforcement design method, the compressive stresses in concrete and reinforcement do not develop at the same rate. This is indicated in figure 9.1.

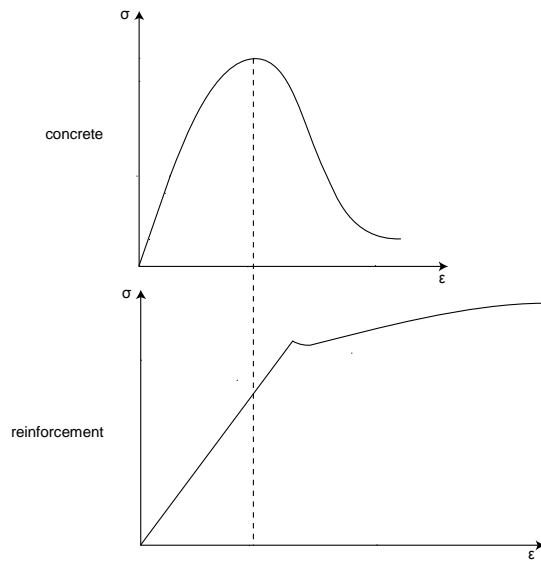


Figure 9.1: Global development of maximum compressive stresses in concrete and hot-rolled reinforcement, according to the behavior which will follow from laboratory tests. Before compressive reinforcement will be fully active, the concrete compressive strength is already decreasing due to the development of macro cracks.

- Execution of a full probabilistic analysis results in even lower failure loads compared to the ones which will be found when the popular partial safety factor methods of the codes are applied, even when all these types of safety assessment are based on a similar reliability index of 3,8. Compared to the partial safety factor method which is discussed in Eurocode EN1992-1-1, the full probabilistic analysis result in failure loads which can be up to 10% lower, although this is strongly related to the assumed coefficient of variation of the applied load.
- LE-FEM overestimates the concrete strength of structures which are loaded by a top load and fully supported at their base, since eccentricities are left out of consideration.

According to Eurocode EN1992-1-1 §6.1 (4) for cross-sections with symmetrical reinforcement loaded by a compression force it is necessary to assume a minimum eccentricity e_0 equal to $h/30$ but not less than 20 mm, where h is the depth of the section. Since LE-FEM is only capable to analyze in-plane stress fields, it takes no eccentricities or second order effects into account and allows structures to be loaded up to their full design strength f_{cd} , without requiring additional reinforcement. This is illustrated in figure 9.2.

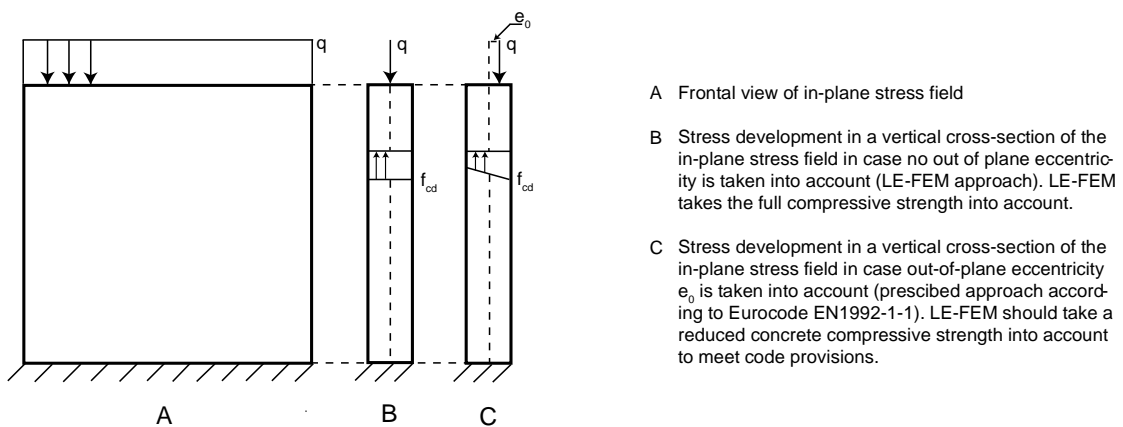


Figure 9.2: Stress development in a vertical cross-section of an in-plane stress field.

- Reinforcement designs according to LE-FEM of the considered single-span specimens do not meet the requirements related to crack control in the serviceability limit state. It is not possible to verify the stress development in the distributed reinforcement bars without the application of advanced (non-linear) methods, since there is no linear relation between the applied load and stress development in the distributed reinforcement bars which are required according to LE-FEM. In common design methods, like the beam theory or strut and tie method, it's less complicated to verify the stresses in the SLS, since these methods assume that longitudinal reinforcement is concentrated in a specific tension zone.
- Considered specimens seem to be less sensitive for the development of shrinkage cracks. Redistribution capacity of two-span specimens which during the design process are already loaded up to their limit strength f_{cd} turned out to be negligible.

9.3 Recommendations

- Although no direct relation is found between the observed failure mode and the limited amount of longitudinal reinforcement bars which reach the supports, it is still recommended to extend all bars such that they are properly anchored near the supports to limit the development of local cracks.
- Also stirrups and other vertically positioned reinforcement bars should be extended such that they enclose longitudinal reinforcement at the bottom or top of a structure, and must be anchored properly.
- To meet requirements related to crack control in the serviceability limit state, the required amount of bottom reinforcement in the tension zone of structures which are subjected to bending should be multiplied by a specific factor, larger than 1. Further research is required to quantify this factor.
- To take prescribed eccentricities according to Eurocode EN1992-1-1 §6.1 (4) into account during the design of structures which have symmetrical reinforcement and are loaded under compression, a reduced concrete compressive strength f_{cd} should be taken into account during the reinforcement design process with LE-FEM. Otherwise, specific code requirements are not met. Although it is not required by code provisions, this approach is also recommended for the design of structures which are subjected to flexural deformations and possess a local concrete compressive zone where high, concentrated compressive stress appears. Further research is required to quantify this reduction factor.

Appendix A – Results survey

A.1 Introduction

To get an impression to what extent linear elastic analyses, and more specific the linear elastic finite element method to determine required reinforcement, are already applied in engineering practice for the design of reinforced concrete walls, a small survey was conducted among ten consulting engineering firms and other authorities which are active in the field of commercial and building industry. The results of this survey are discussed in the next section.

A.2 Results of the survey

Practically all interviewees of companies which are involved in the design of reinforced concrete structures indicated that linear elastic finite element analyses are applied within their company to determine the stress distribution in concrete structures, primarily when hand calculations are insufficient to determine the distribution of membrane forces adequately.

A majority takes the view that linear elastic analyses in which isotropic material behavior is assumed are adequate enough to approach the actual behavior of reinforced concrete. This is illustrated in figure A.1, where the answers are shown on the multiple-choice question:

Do you take the view that the approach of reinforced concrete as a linear elastic, isotropic material, as is assumed in the finite element analyses, is an accurate approach of the actual behavior?

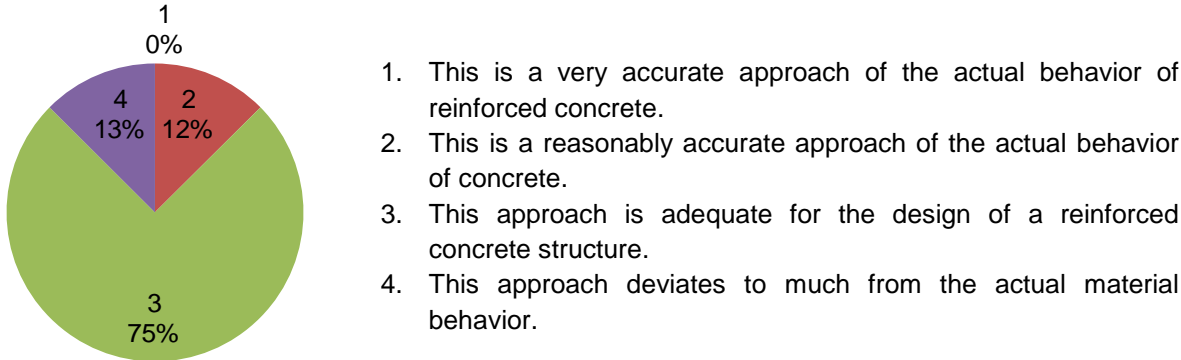
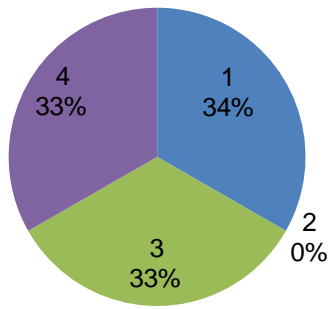


Figure A.1: Approach of reinforced concrete as a linear elastic isotropic material.

Although linear elastic analyses are applied frequently in practice to determine the distribution of membrane forces in concrete walls, the design method to derive the required amount of reinforcement automatically from the determined membrane forces is applied less frequently. Figure A.2 shows the answers on the question:

Do you personally use, or are there colleagues within your company who use the mentioned method to determine the required reinforcement automatically and/or are there calculations verified of third parties in which this method is applied?



1. Calculations which are based on this method are both applied as well as verified.
2. Calculations which are based on this method are only applied, but never verified.
3. Calculations which are based on this method are never applied, but verified.
4. Calculations which are based on this method are never applied and verified.

Figure A.2: Use of the method to determine the required reinforcement directly from the membrane forces in practice.

Interviewees which indicated that within their company calculations are made or verified in which the discussed method is applied, unanimously declared that additional checks are applied. These additional checks vary from a verification of possible incorrect determined peak stresses to the actual verification of cross-sections based on code checks.

The response to the question if it can be stated that the maximum allowed steel stress σ_s in the serviceability state (SLS) can be expressed by equation A.1, as is assumed in chapter 4, was less univocal.

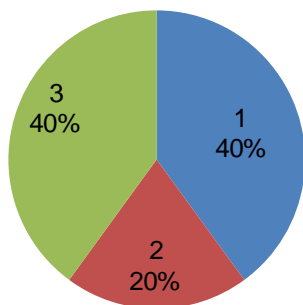
$$\sigma_s = \frac{f_{yd}}{\gamma} \quad \text{A.1}$$

Where:

f_{yd} is the design yield strength of reinforcement steel.

γ is the mean partial load factor which is applied for external loads.

The response to this question can be seen in figure A.3

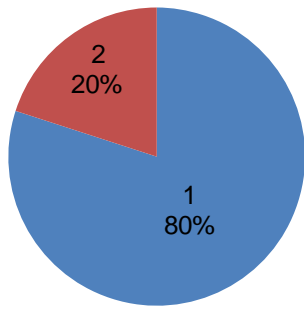


1. This is a suitable guideline for the maximum steel stress in the SLS.
2. This is not a suitable guideline for the maximum steel stress in the SLS.
3. Else.

Figure A.3: Response to the question the maximum steel stress in the ULS can be determined according to equation A.1.

A frequently mentioned remark about the maximum allowable steel stress in the serviceability limit state which follows from equation A.1 is that not only the size of the stresses in the serviceability limit state determine if the crack width requirements are satisfied, but that also the assumed exposure class, bar diameter and bar spacing.

Finally it was asked if the term "linear elastic finite element method" could be considered as a correct name for the considered method. In figure A.4 it can be seen that a majority agree with this name.



1. This can be considered as a correct name.
2. This cannot be seen as a correct name.

Figure A.4 Response to the question if the term "linear elastic finite element method" can be considered as a correct name for the considered reinforcement design method.

Interviewees which did not agree with this nomenclature put the argument forward that this term can lead to confusion, since this method can only be applied in a limited field of applications.

Appendix B - Reinforcement drawings

B.1 Introduction

This appendix contains the reinforcement drawings of the specimen which are not discussed in chapter 4. For each specimen the required reinforcement and the actual reinforcement drawing are shown. In these drawings all individual bars are drawn, except for the bars of the reinforcement mesh. It must be emphasized that the output of the linear elastic finite element method is given for one single side face of the specimen only, and should be applied at both faces.

B.2 Specimen S-1-1

Dimensions: 2000 x 1000 x 200 mm
 Load: concentrated load, equal to 651 kN

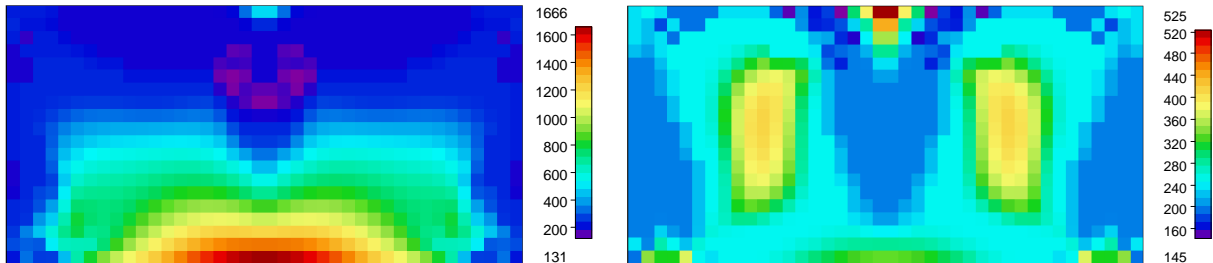


Figure B.1: Required reinforcement in longitudinal (left figure) and transversal (right figure) direction. Output is in mm²/m.

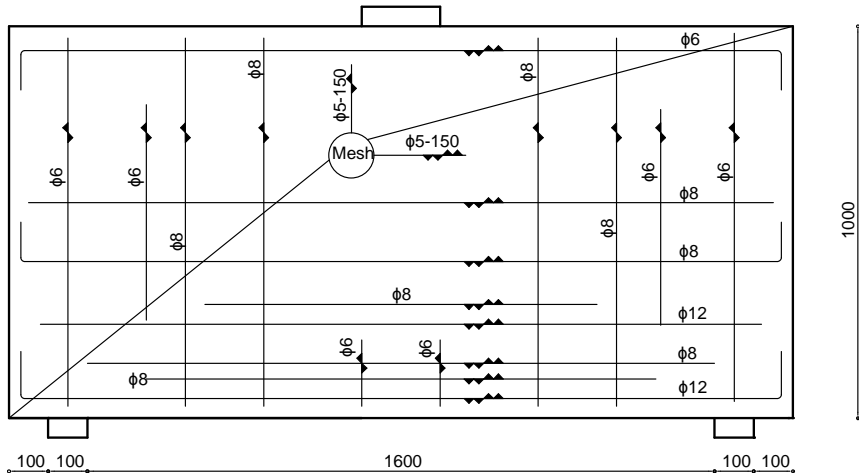


Figure B.2: Reinforcement drawing of specimen S-1-1.

B.3 Specimen S-1-2

Dimensions: 2000 x 1000 x 200 mm
 Load: concentrated load, equal to 326 kN

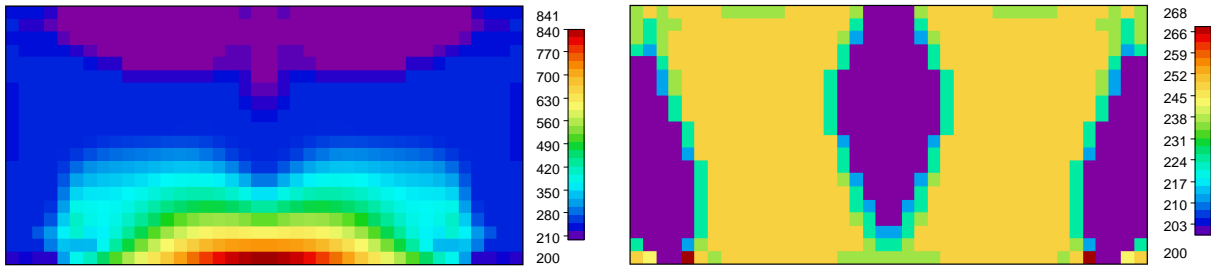


Figure B.3: Required reinforcement in longitudinal (left figure) and transversal (right figure) direction. Output is in mm^2/m .

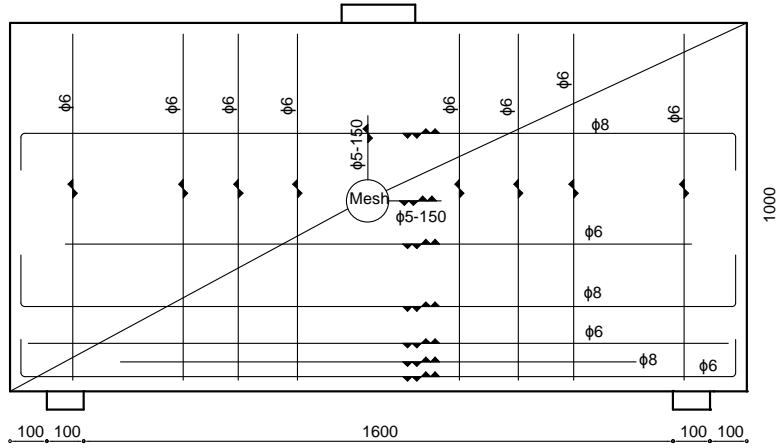


Figure B.4: Reinforcement drawing of specimen S-1-2.

B.4 Specimen S-1-3

Dimensions: 2000 x 1000 x 200 mm

Load: concentrated load, equal to 163 kN

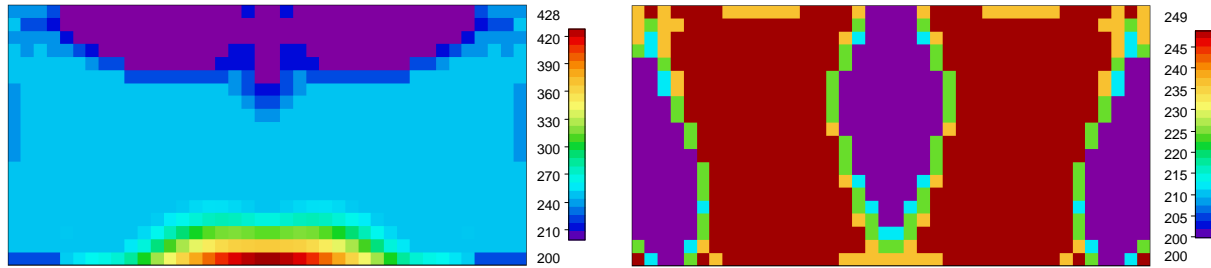


Figure B.5: Required reinforcement in longitudinal (left figure) and transversal (right figure) direction. Output is in mm^2/m .

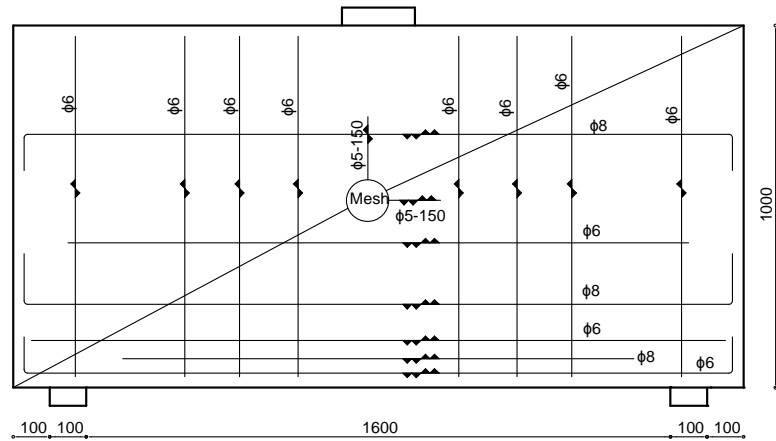


Figure B.6: Reinforcement drawing of specimen S-1-3.

B.5 Specimen S-1-4

Dimensions: 2000 x 1000 x 200 mm
 Load: concentrated load, equal to 651 kN

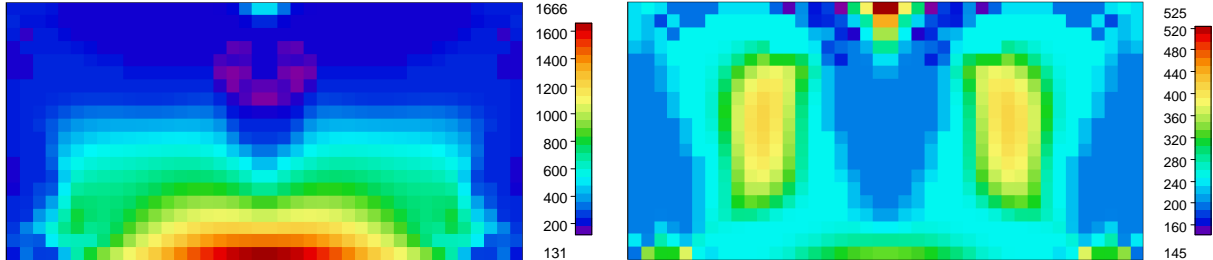


Figure B.7: Required reinforcement in longitudinal (left figure) and transversal (right figure) direction. Output is in mm²/m.

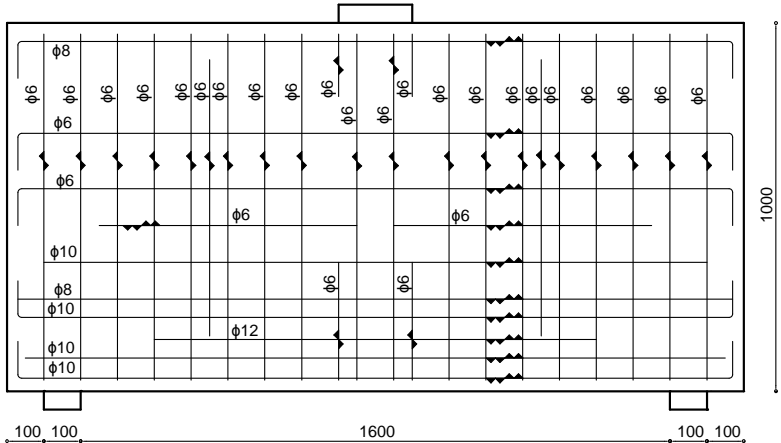


Figure B.8: Reinforcement drawing of specimen S-1-4.

B.6 Specimen S-1-5

Dimensions: 2000 x 1000 x 200 mm
 Load: distributed load, equal to 382 kN/m

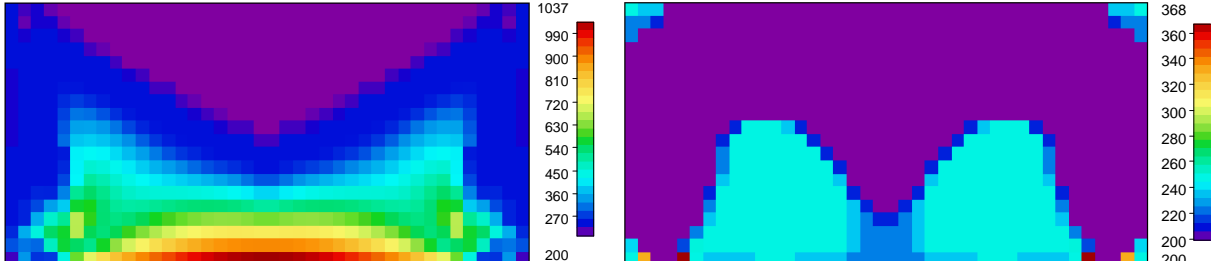


Figure B.9: Required reinforcement in longitudinal (left figure) and transversal (right figure) direction. Output is in mm²/m.

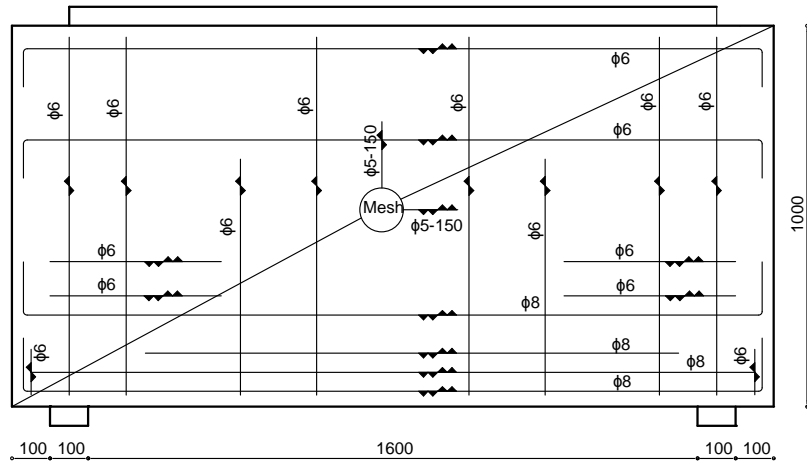


Figure B.10: Reinforcement drawing of specimen S-1-5.

B.7 Specimen S-2-2

Dimensions: 3000 x 1000 x 200 mm

Load: concentrated load, equal to 323 kN

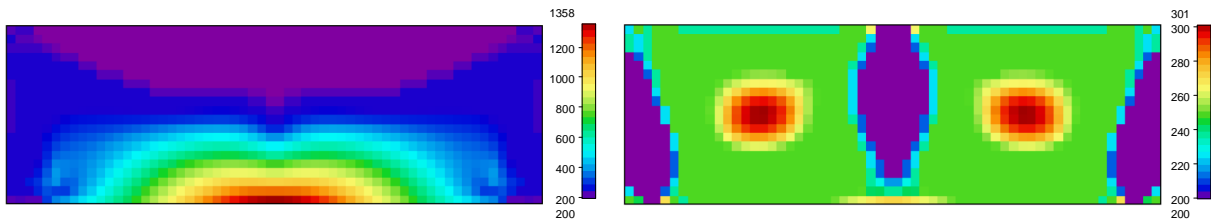


Figure B.11: Required reinforcement in longitudinal (left figure) and transversal (right figure) direction. Output is in mm^2/m .

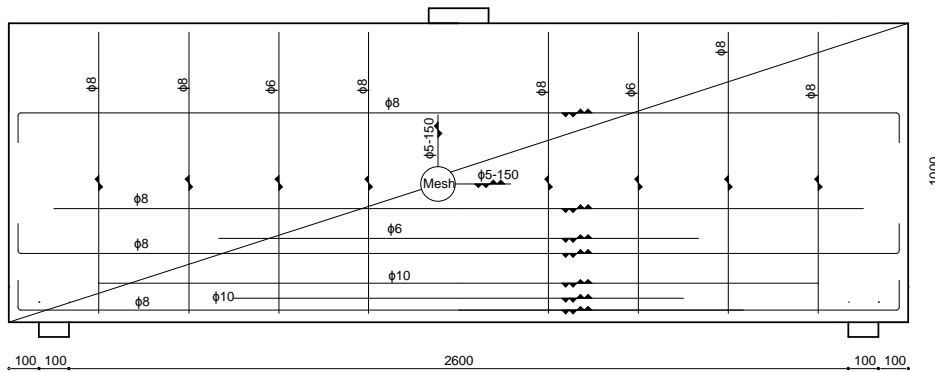


Figure B.12: Reinforcement drawing of specimen S-2-2.

B.8 Specimen S-2-4

Dimensions: 3000 x 1000 x 200 mm

Load: concentrated load, equal to 646 kN

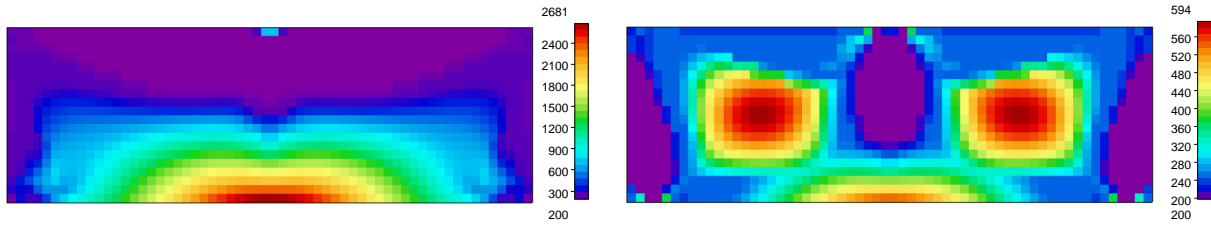


Figure B.13: Required reinforcement in longitudinal (left figure) and transversal (right figure) direction. Output is in mm^2/m .

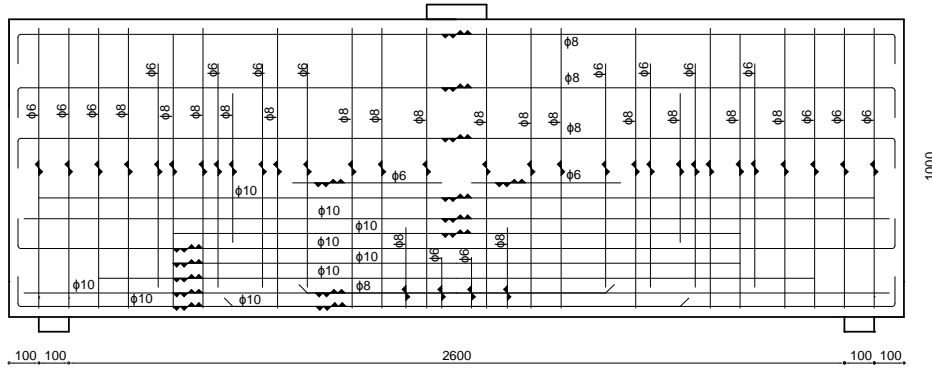


Figure B.14: Reinforcement drawing of specimen S-2-4.

B.9 Specimen S-3-1

Dimensions: 4000 x 1000 x 200 mm

Load: concentrated load, equal to 640 kN

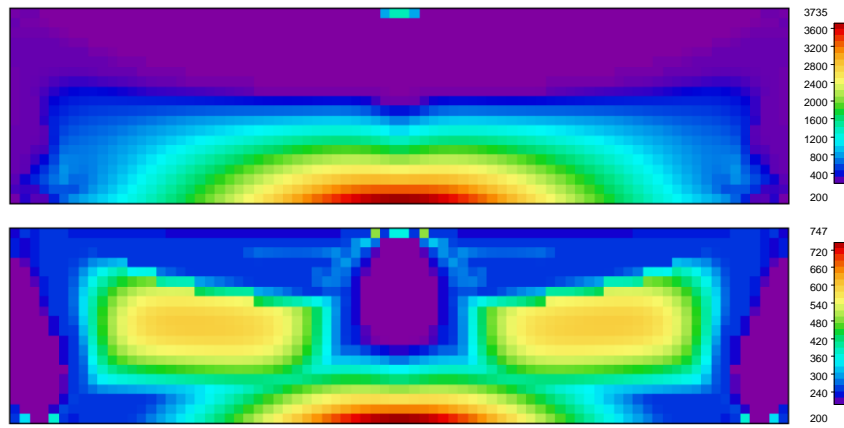


Figure B.15: Required reinforcement in longitudinal (left figure) and transversal (right figure) direction. Output is in mm^2/m .

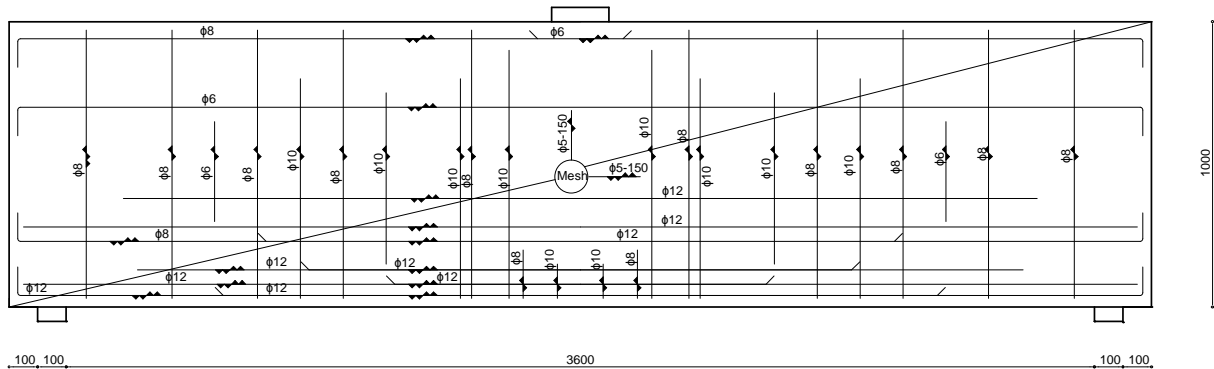


Figure B.16: Reinforcement drawing of specimen S-3-1.

B.10 Specimen S-3-2

Dimensions: 4000 x 1000 x 200 mm
 Load: concentrated load, equal to 320 kN

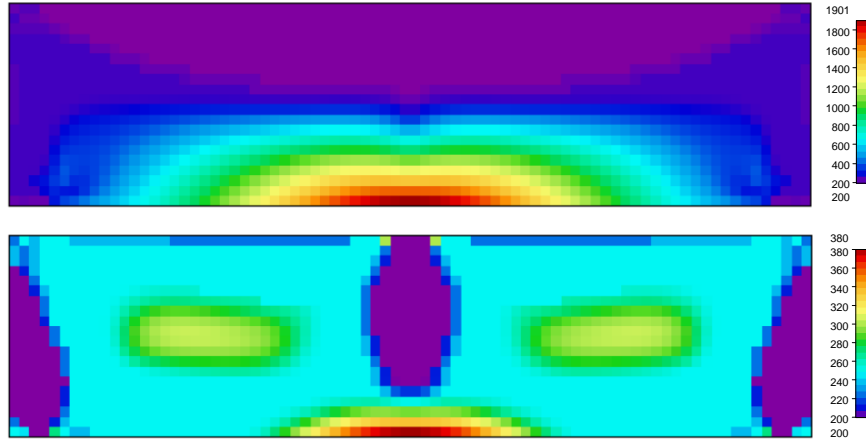


Figure B.17: Required reinforcement in longitudinal (left figure) and transversal (right figure) direction. Output is in mm^2/m .

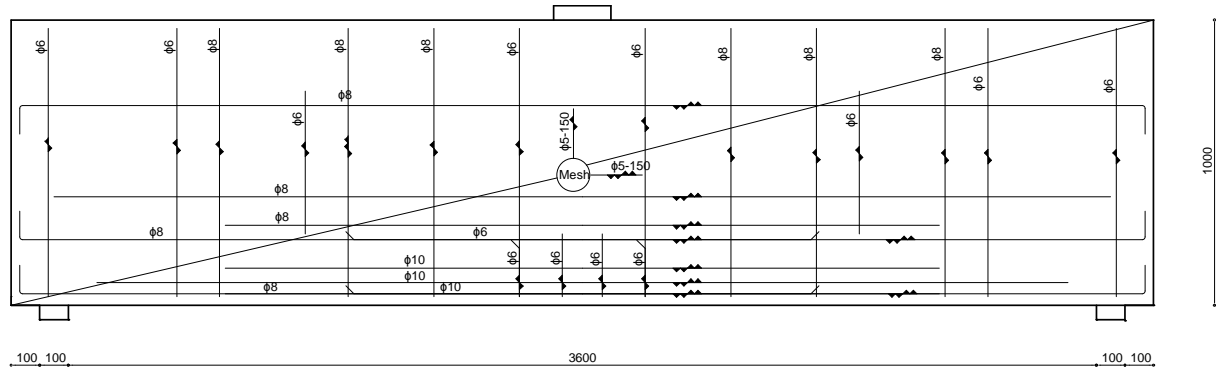


Figure B.18: Reinforcement drawing of specimen S-3-2.

B.11 Specimen S-3-3

Dimensions: 4000 x 1000 x 200 mm
 Load: concentrated load, equal to 160 kN

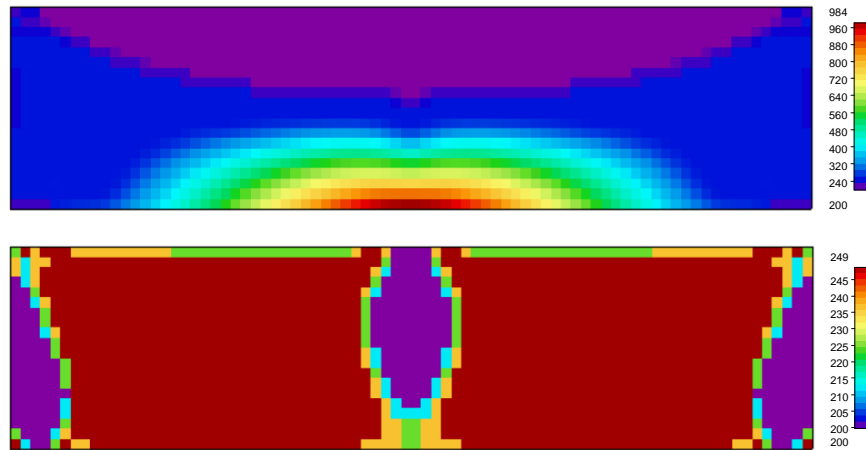


Figure B.19: Required reinforcement in longitudinal (left figure) and transversal (right figure) direction. Output is in mm^2/m .

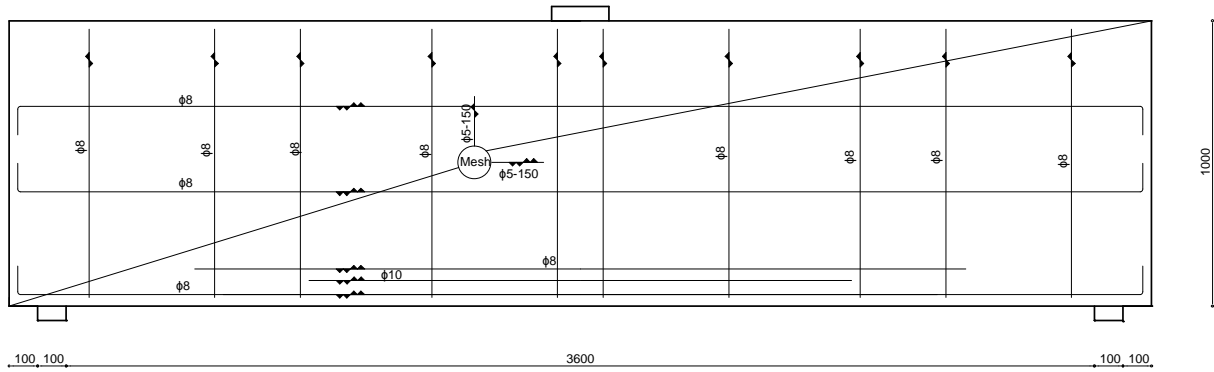


Figure B.20: Reinforcement drawing of specimen S-3-3.

B.12 Specimen S-3-4

Dimensions: 4000 x 1000 x 200 mm

Load: concentrated load, equal to 640 kN

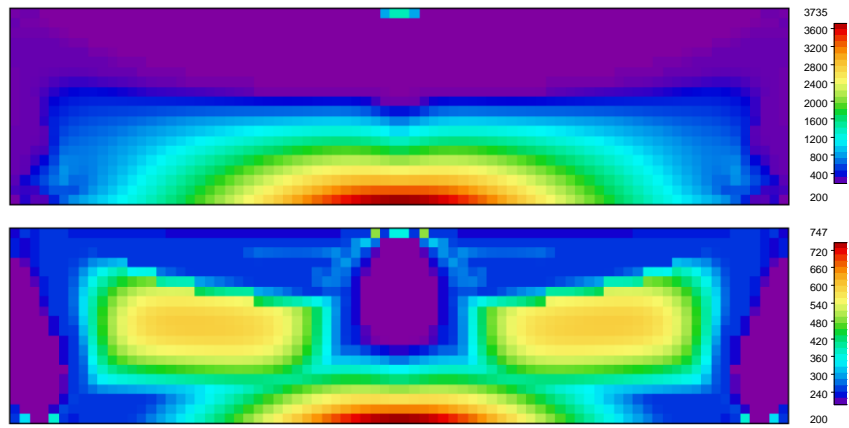


Figure B.21: Required reinforcement in longitudinal (left figure) and transversal (right figure) direction. Output is in mm^2/m .

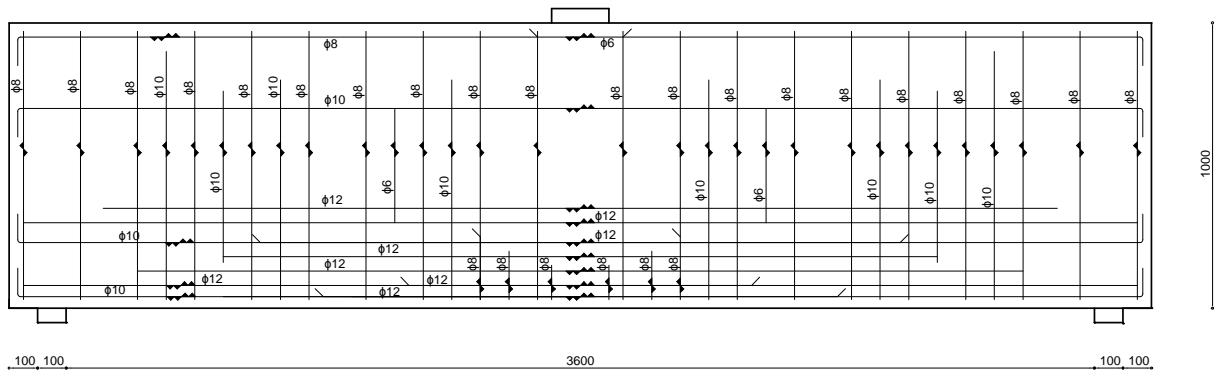


Figure B.22: Reinforcement drawing of specimen S-3-4.

B.13 Specimen S-3-5

Dimensions: 4000 x 1000 x 200 mm

Load: distributed load, equal to 172 kN/m

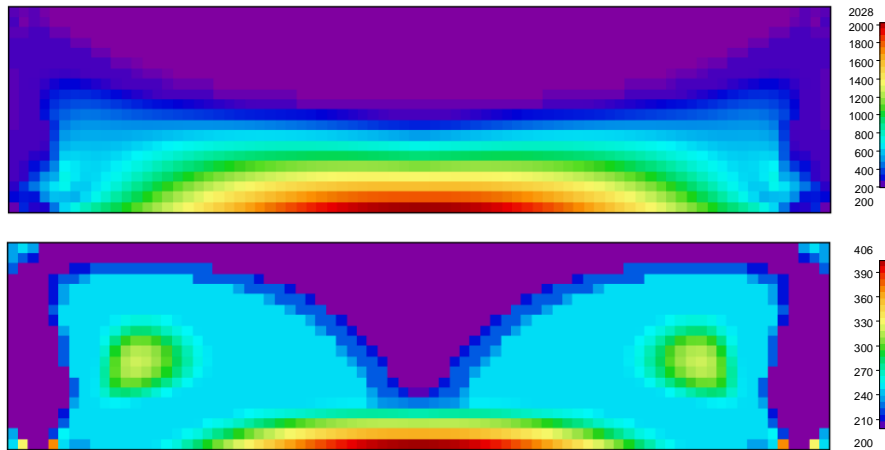


Figure B.23: Required reinforcement in longitudinal (left figure) and transversal (right figure) direction. Output is in mm^2/m .

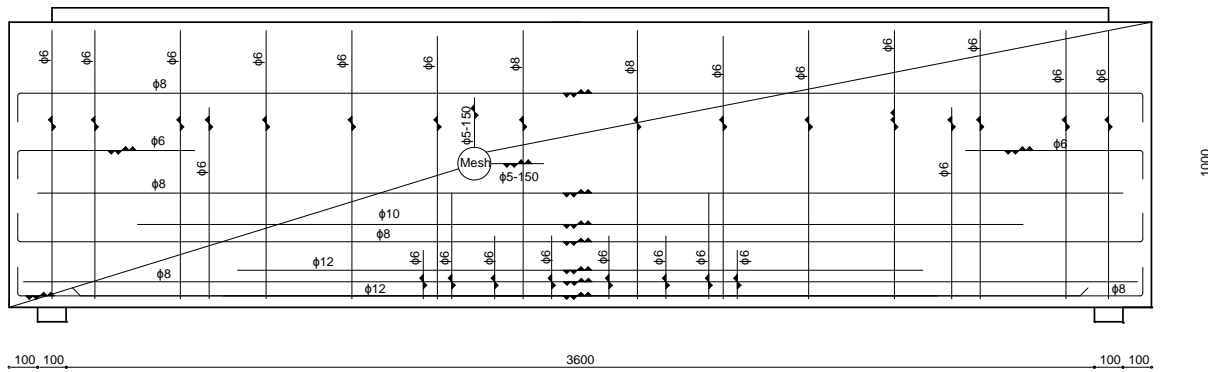


Figure B.24: Reinforcement drawing of specimen S-3-5.

B.14 Specimen S-4-1

Dimensions: 6000 x 1000 x 200 mm

Load: concentrated load, equal to 628 kN

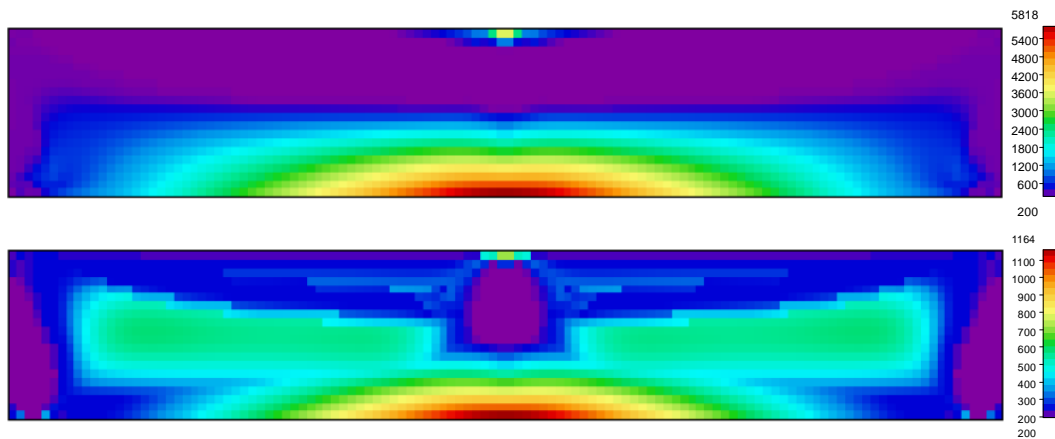


Figure B.25: Required reinforcement in longitudinal (left figure) and transversal (right figure) direction. Output is in mm^2/m .

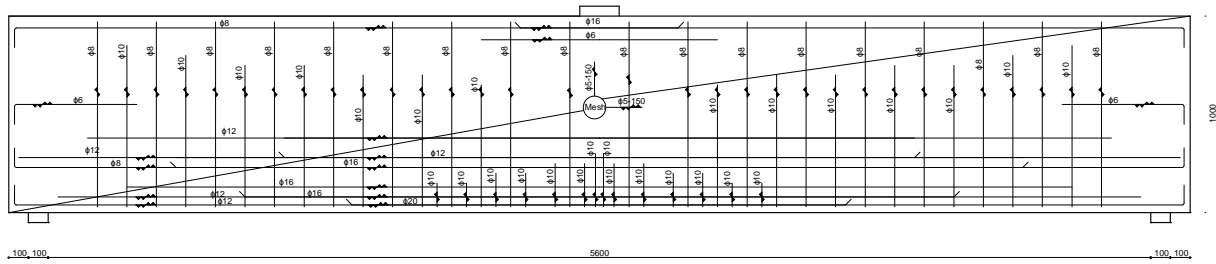


Figure B.26: Reinforcement drawing of specimen S-4-1.

B.15 Specimen S-4-2

Dimensions: 6000 x 1000 x 200 mm

Load: concentrated load, equal to 314 kN

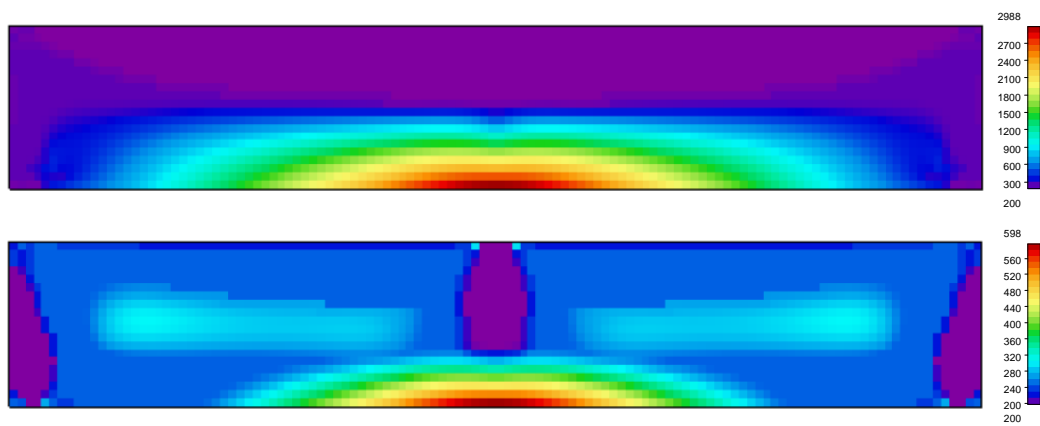


Figure B.27: Required reinforcement in longitudinal (left figure) and transversal (right figure) direction. Output is in mm^2/m .

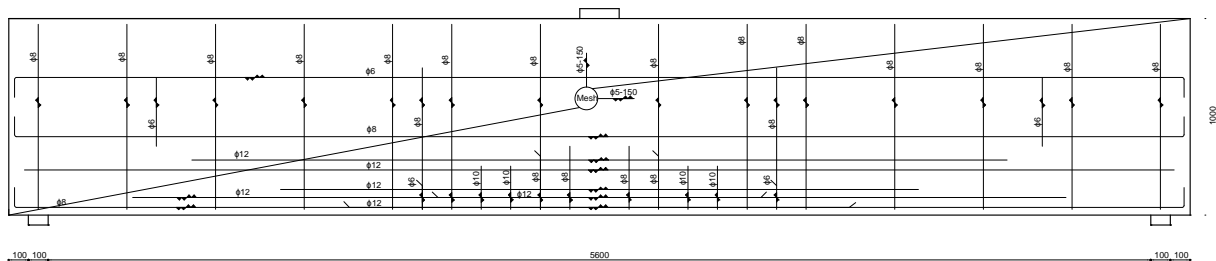


Figure B.28: Reinforcement drawing of specimen S-4-2.

B.16 Specimen S-4-3

Dimensions: 6000 x 1000 x 200 mm

Load: concentrated load, equal to 157 kN

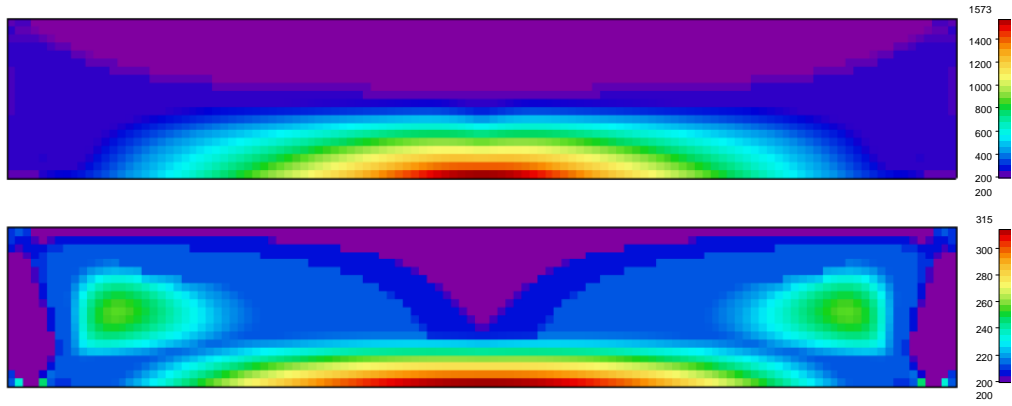


Figure B.29: Required reinforcement in longitudinal (left figure) and transversal (right figure) direction. Output is in mm^2/m .

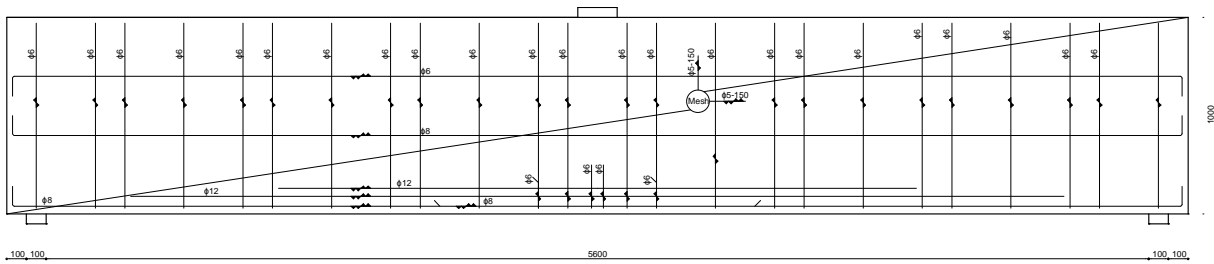


Figure B.30: Reinforcement drawing of specimen S-4-3.

B.17 Specimen S-4-4

Dimensions: 6000 x 1000 x 200 mm

Load: concentrated load, equal to 628 kN

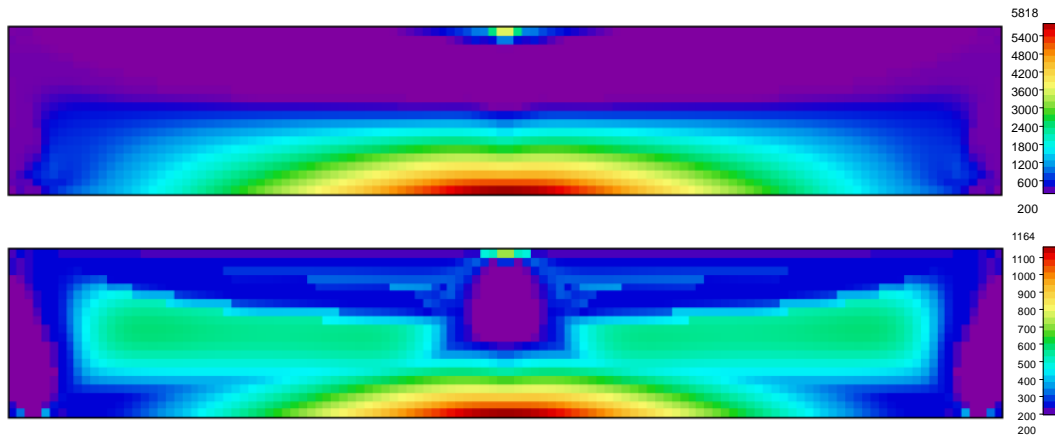


Figure B.31: Required reinforcement in longitudinal (left figure) and transversal (right figure) direction. Output is in mm^2/m .

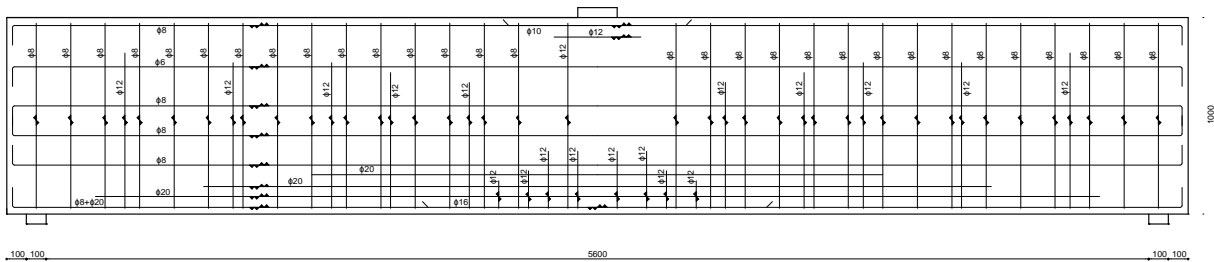


Figure B.32: Reinforcement drawing of specimen S-4-4.

B.18 Specimen S-4-5

Dimensions: 6000 x 1000 x 200 mm
 Load: distributed load, equal to 110 kN/m

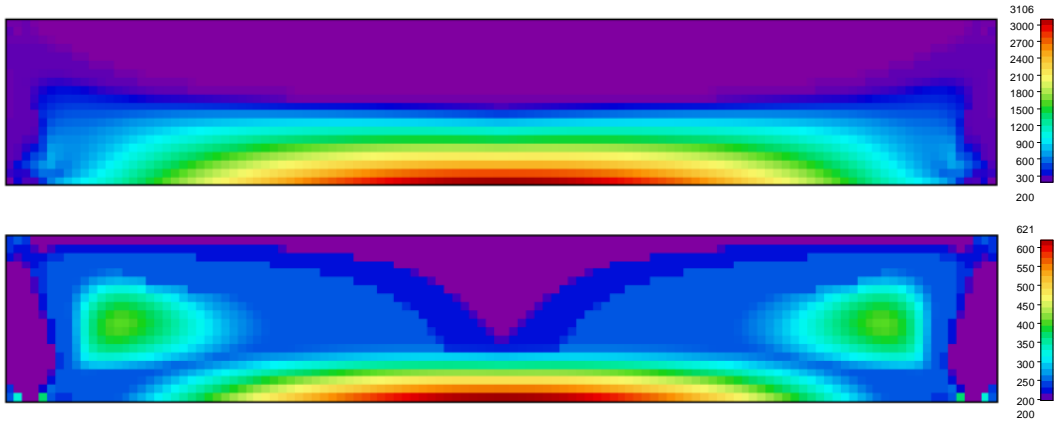


Figure B.33: Required reinforcement in longitudinal (left figure) and transversal (right figure) direction. Output is in mm²/m.

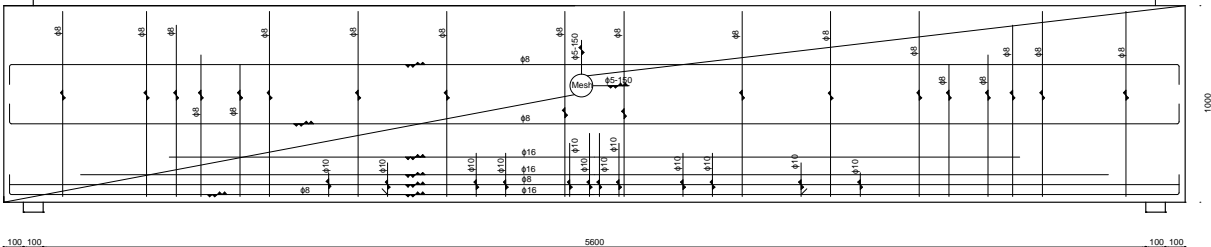


Figure B.34: Reinforcement drawing of specimen S-4-5.

B.19 Specimen S-5-1

Dimensions: 2000 x 2000 x 200 mm
 Load: concentrated load, equal to 696 kN

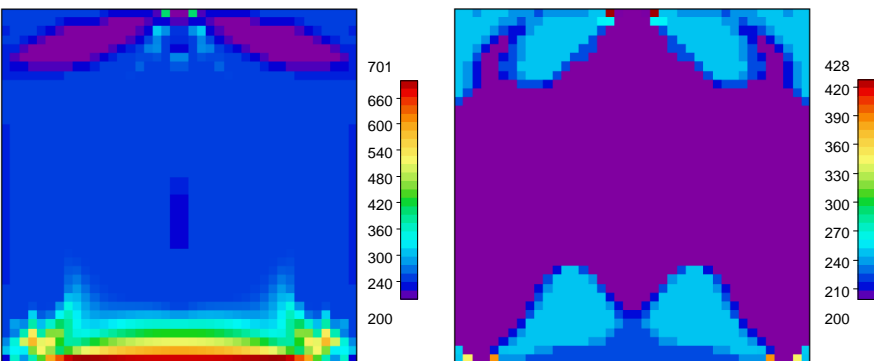


Figure B.35: Required reinforcement in longitudinal (left figure) and transversal (right figure) direction. Output is in mm²/m.

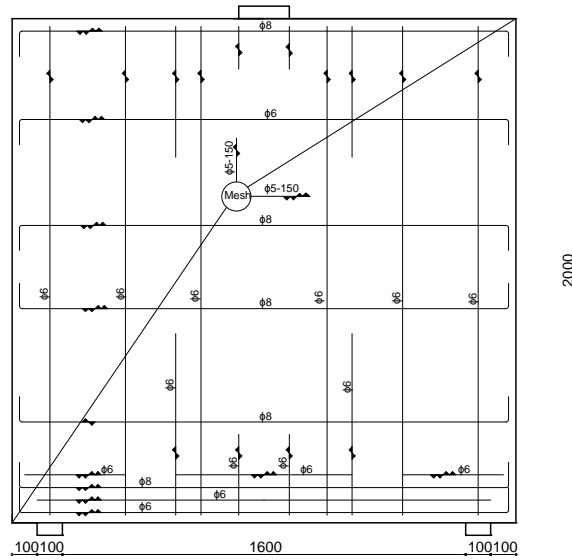


Figure B.36: Reinforcement drawing of specimen S-5-1.

B.20 Specimen S-5-2

Dimensions: 2000 x 2000 x 200 mm

Load: concentrated load, equal to 348 kN

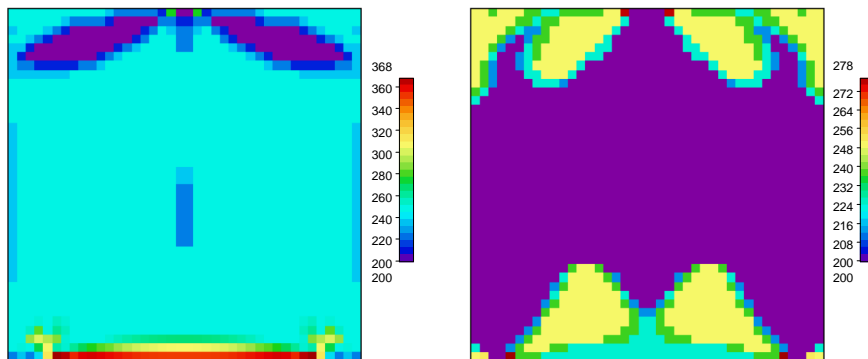


Figure B.37: Required reinforcement in longitudinal (left figure) and transversal (right figure) direction. Output is in mm^2/m .

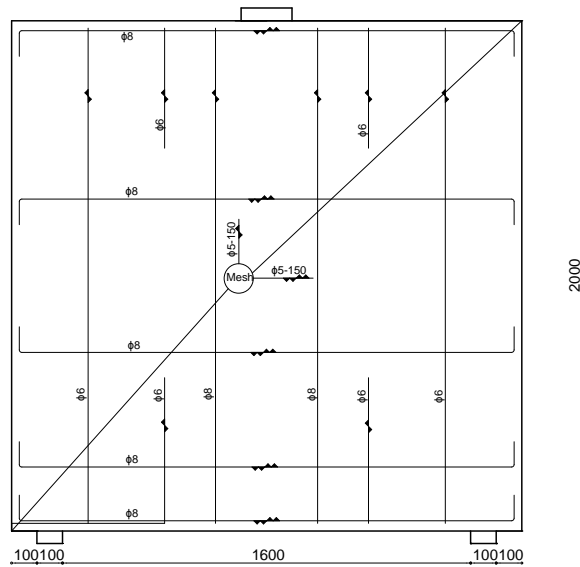


Figure B.38: Reinforcement drawing of specimen S-5-2.

B.21 Specimen S-5-3

Dimensions: 2000 x 2000 x 200 mm
 Load: concentrated load, equal to 174 kN

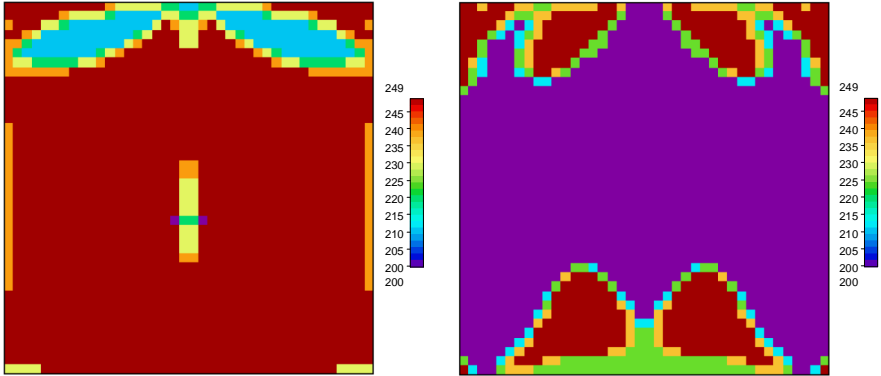


Figure B.39: Required reinforcement in longitudinal (left figure) and transversal (right figure) direction. Output is in mm²/m.

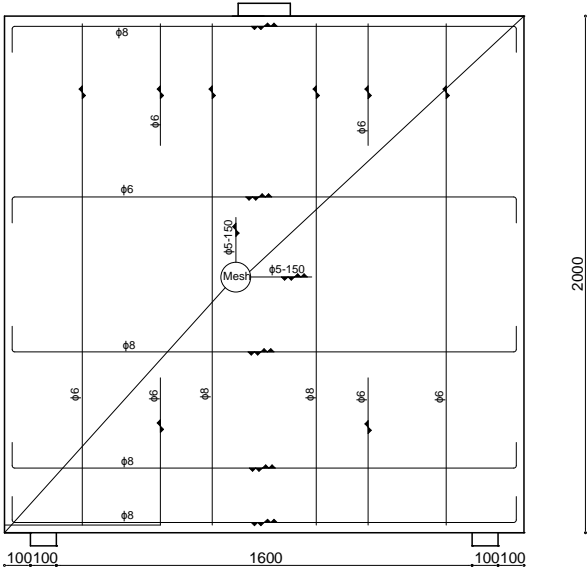


Figure B.40: Reinforcement drawing of specimen S-5-3.

B.22 Specimen S-5-4

Dimensions: 2000 x 2000 x 200 mm
 Load: concentrated load, equal to 696 kN

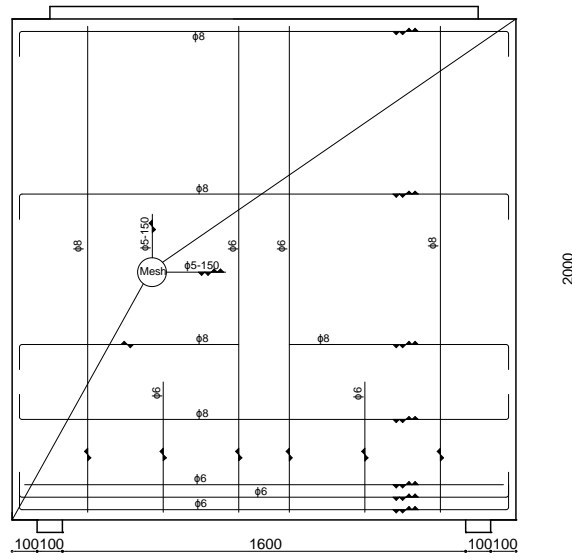


Figure B.44: Reinforcement drawing of specimen S-5-5.

Appendix C - Maple code

This appendix contains the applied input in the computer algebra system Maple, a computer program which has been used several times to solve mathematical problems. To keep this appendix concise, only the input is shown. The output will be generated automatically when the code below is entered in Maple. Version 12.0 of Maple is used.

In section 4.4.3 of chapter 4 the stresses in individual horizontal bars in the serviceability limit state are verified for specimens of which the span is not less than three times the overall section depth. To determine these stresses equation C.1 and C.2 have to be solved, in which ϵ_c and x_u are two unknown variables.

$$\sum_{i=1}^n \left[\left(\frac{h - h_{bar,i}}{x_u} - 1 \right) \epsilon_c E_s A_{s,i} \right] + \frac{1}{2} \epsilon_c E_c x_u t = 0 \quad (C.1)$$

$$\sum_{i=1}^n \left[\left(\frac{h - h_{bar,i}}{x_u} - 1 \right) \epsilon_c E_s A_{s,i} h_{bar,i} \right] + \frac{1}{2} \epsilon_c E_c x_u t \left(h - \frac{1}{3} x_u \right) = M \quad (C.2)$$

The Maple code which is shown below is based on the geometry of specimen S-4-1. However, the applied code for the other considered specimens is based on the same principles.

```
> restart;
> h:=1000;
> t:=200;
> fcd:=20;
> ec3:=1.75/1000;
> Ec:=fcd/ec3;
> Es:=200000;
> M:=449;
> n:=20;
> hbar:=Vector([940,940,935,785,700,635,485,380,335,280,230,230,185,130,130,80,80,40,40,35]);
> dbar:=Vector([6,8,5,5,6,5,5,12,5,12,8,12,5,12,12,12,12,12,8,5]);
> nbar:=Vector([2,2,2,2,2,2,2,2,2,2,2,2,2,2,2,2,2,2,2]);
> Ns:=(add((((h-hbar[k])/xu-1).ec.Es.((dbar[k].0.5)^2.π.nbar[k]),k=1..n))/1000;
> Nc:=(Ec.ec.t.xu.0.5)/1000;
> Ms:=(add((((h-hbar[k])/xu-1).ec.Es.((dbar[k].0.5)^2.π.nbar[k]).(hbar[k]/1000),k=1..n))/1000;
> Mc:=(Nc.(h-((1/3).xu)))/1000;
> eq1:=Ns+Nc=0;
> eq2:=Ms+Mc=M;
> solution:=solve({eq1,eq2},{xu,ec});
> assign(solution[1]);
> xu;
> ec;
```